Smart dressings based on bacterial cellulose for chronic wounds healing and monitoring

Manni Yang

Supervisor: Professor Kwang-leong Choy

Submitted in part fulfilment of the requirements for the degree of

Doctor of Philosophy

of

University College London

Department of Chemistry

Institute for Materials Discovery

University College London

April, 2021

I, Manni Yang, confirm that the work presented in this thesis is my own. Where information has been derived from other sources, I confirm that this has been indicated in the work.

Abstract

In recent years, there has been an upward trend for novel biomass based green materials for dressing chronic wounds, which can assist in wound healing and monitoring. This research focuses on candidate components for smart chronic wound dressings based on bacterial cellulose (BC), which is comprised of two parts: antimicrobial BC nanocomposites for wound dressing, and a BC-derived pH sensor for monitoring chronic wounds. This research demonstrates a novel ability to utilise BC and BC-derived nanocomposites in potential applications for smart wound dressings.

In the chapter regarding BC production, samples grown in static from four different *Acetobacter* bacterial strains are characterized and compared for the first time. SEM and BET results demonstrate a large surface area (>100 m^2/g) and XRD analysis reveals high crystallinity ($>60\%$). *In vitro* cell tests indicate potential biocompatibility. In the BC based pH sensor chapter, a pyrolyzed BC (p-BC) aerogel was incorporated with polyaniline (PANI) and polydimethylsiloxane (PDMS), exhibiting near-Nernst pH sensitivity (50.4 mV/pH). In the chapter on antimicrobial BC nanocomposites, the inorganic BC/silver nanoparticle (BC/AgNP) and organic BC/lysozyme, BC/eggshell membrane (BC/ESM), BC/methylglyoxal (BC/MGO) nanocomposites were fabricated and characterized, with BC/ESM and BC/MGO nanocomposites proposed for the first time. The antimicrobial properties were tested *via* a disk diffusion method, with BC/MGO exhibiting the greatest antimicrobial activity, with diameters of inhibition zone (DIZ) up to 17.1 ± 0.6 mm against *S. aureus* and 15.5 ± 0.5 mm against *E. coli*. Tensile tests show the nanocomposites still retain the high tensile strength of plain BC (>2 MPa).

These results indicate that BC and BC-derived nanocomposites are promising candidate materials for smart wound dressings. The future work will focus on more detailed *in vitro* biocompatibility tests and *in vivo* wound healing assays.

Acknowledgment

List of Publications

[1] **Yang, M**. and Choy, K.L., 2021. A nature-derived, flexible and three dimensional (3D) nano-composite for chronic wounds pH monitoring. *Materials Letters*, *288*, p.129335.

[2] **Yang, M**., Ward, J. and Choy, K.L., 2020. Nature-Inspired Bacterial Cellulose/Methylglyoxal (BC/MGO) Nanocomposite for Broad-Spectrum Antimicrobial Wound Dressing. *Macromolecular bioscience*, *20*(8), p.2000070.

Conference

Poster presentation on Materials Research Society annual conference, November 2019, Boston, USA.

List of Figures

List of Tables

Abbreviations

BC - bacterial cellulose

3D - three dimensional

ECM - extracellular matrix

MMP9 - metalloproteinase-9

p-BC - pyrolyzed bacterial cellulose

DFU - diabetic foot ulcers

VLU - venous stasis

PDMS – polydimethylsiloxane

PU – polyurethane

O.D - optical density

PMMA - poly(methyl methacrylate)

PANI – polyaniline

PEG - poly(ethylene glycol)

MMT – Montmorillonite

PI - povidone-iodine

PHMB – polyhexanide

TCH - tetracycline hydrochloride

FA - fusidic acid

BLF - bovine lactoferrin

SA - sodium alginate

AgNP - silver nanoparticle

FESEM - field-emission scanning electron microscopy

SEM - scanning electron microscopy

EDX - energy-dispersive X-ray spectroscopy

BET - Brunauer–Emmett–Teller

AFM - atomic force microscopy

FTIR - Fourier transform infrared spectroscopy

XRD - X-ray diffraction

WHC - water-holding capacity

BC/MGO – bacterial cellulose/methylglyoxal

BC/ESM – bacterial cellulose/eggshell membrane

PDA – polydopamine

PBS - phosphate buffer solution

HDF - human dermal fibroblasts

G. xylinus - *Gluconacetobacter xylinus*

K. xylinus - *Komagataeibacter xylinus*

M. luteus - *Micrococcus luteus*

P. aeruginosa - *Pseudomonas aeruginosa*

S. aureus - *Staphylococcus aureus*

E. coli - Escherichia coli

LB - Luria-Bertani

AgNO3 - silver nitrate

SC – soft carbon

HC – hard carbon

GC – graphite carbon

MRSA - multi-antibiotic-resistant *S. aureus*

PMNs - polymorphonuclear leukocytes

Impact Statement

Since the 21st century, non-healing or hard-to-heal chronic wounds have been a social burden to human health and society. In clinical settings, long-term suffering creates an urgent need for advanced smart dressings which can accelerate healing and effectively monitor wounds. Since antibiotics are susceptible to multi-resistant pathogens and novel silver or nano-particle based wound dressings may have adverse side effects, naturally derived bio-mass based materials are attractive for treatment and monitoring of infectious wounds. For over half a century, research on chronic wound dressings or smart wound dressings (particularly those fabricated by natural materials) show great potential for benefiting the health, prosperity and well-being of society. However, there still remains an urgent challenge to meet the growing need for safe and environmentally sustainable technologies for wound healing. Our research on nature-derived biomaterials gives a versatile and tuneable platform for designing a new generation of bio-mass based composites for smart chronic wound dressings that promote healing and facilitate monitoring during clinical treatment. Additionally, the inherent high biocompatibility and degradability of natural bio-composites provides opportunity for further applications as temporary skin substitutes or tissue scaffolds.

The aims and objectives of our research are and will remain fundamental to achieving this impact.

Contents

Chapter 1 Introduction

1. Introduction

1.1 Overview

Wound healing is a dynamic, complicated process involving the replacement of damaged structures with new cells and tissues. Unlike normal wounds which heal in a short time, chronic wounds require extensive therapy and monitoring of the healing process due to the overexpression of ECM (extracellular matrix) proteases (such as metalloproteinase-9 (MMP9))[1]. This may be attributed to certain bacteria and their biofilms which delay the healing process and lead to serious infections that can spread to the bones or cause systemic septicaemia which significantly threatens the patients' health[2]. Therefore, to minimise this risk, smart dressings, which refer to the use of biochemical cues to generate a readable output for diagnostic or theragnostic value via biosensor incorporation into or near dressings[3], have the potential to not only assist in wound healing but also monitor the healing process. As defined in green chemistry, "green" refers to the products and processes that reduce or eliminate the generation of hazardous substances[4]. Therefore, wound dressings and sensors based on naturally derived green materials and fabrication methods are required to avoid possible potential hazards to human health. Bacterial cellulose (BC), also known as bacterial nanocellulose, is a natural green material that is a suitable candidate for non-healing chronic wounds, with high water-holding capacity, biocompatibility, and strong mechanical properties. By taking advantage of the unique three-dimensional (3D) nano-structure of BC, antimicrobial wound dressings and pH sensors were fabricated in this project where the inherent material properties of BC grown from different bacterial strains were additionally investigated. The hypothesis of this project is that BC can be used as candidate components or materials in application of smart

dressings for chronic wounds to achieve the designated sensing or dressing functions by utilizing its unique nano-network structure and incorporating with other materials *via* green fabrication methods. Therefore, the research objectives were:

1)   Growth of BC from four different bacterial strains in different culture mediums in static and comparison of the material properties among the resultant BC pellicles in terms of; surface morphology, water-holding capacity, chemical structure and thermal stability. Investigation of *in vitro* biocompatibility of human fibroblasts on BC of variable thickness.

2)   Fabrication of BC based antimicrobial nanocomposites with inorganic materials and organic agents, and characterisation of material properties, chemical structure, and antimicrobial activity.

3)   Fabrication of pyrolyzed BC (p-BC) aerogels for wound pH sensing applications, during which the material properties, electrical conductivity, pH sensitivity in commercial buffer solution and *in vitro* wound simulating fluid were investigated.

1.2 Chronic wounds

Chronic wounds are wounds which do not progress through a normal orderly and timely repair process, where the repair process fails to respond and restore functional integrity after three months[5].

Chronic ulcers are a societal burden due to the long-term and serious suffering caused to patients, which are estimated to affect approximately 1-2% of the population[6]. Chronic ulcers are most prevalent in elderly and diabetic patients. However, owing to countrywide variations in politics and limited investment in research funding[7] in combination with lack of public awareness, there is slow progress in targeting chronic

wound healing conditions[8]. In medical settings, there is a lack of available therapies for non-healing wounds and extra-cellular matrix as well as scar formation. This is due to limited understanding of the molecular basis of tissue repair and the lack of appropriate animal models for the precise replication of human conditions[7]. Therefore, there is an increasingly urgent need to improve treatments via enhancement of the inherent regenerative properties of tissues. Normal wound healing from skin injuries involve extensive communication between the different skin compartments and the underlying extracellular matrix. Chronic wounds are barrier defects which are incapable of regaining structural and functional integrity on an appropriate timescale.
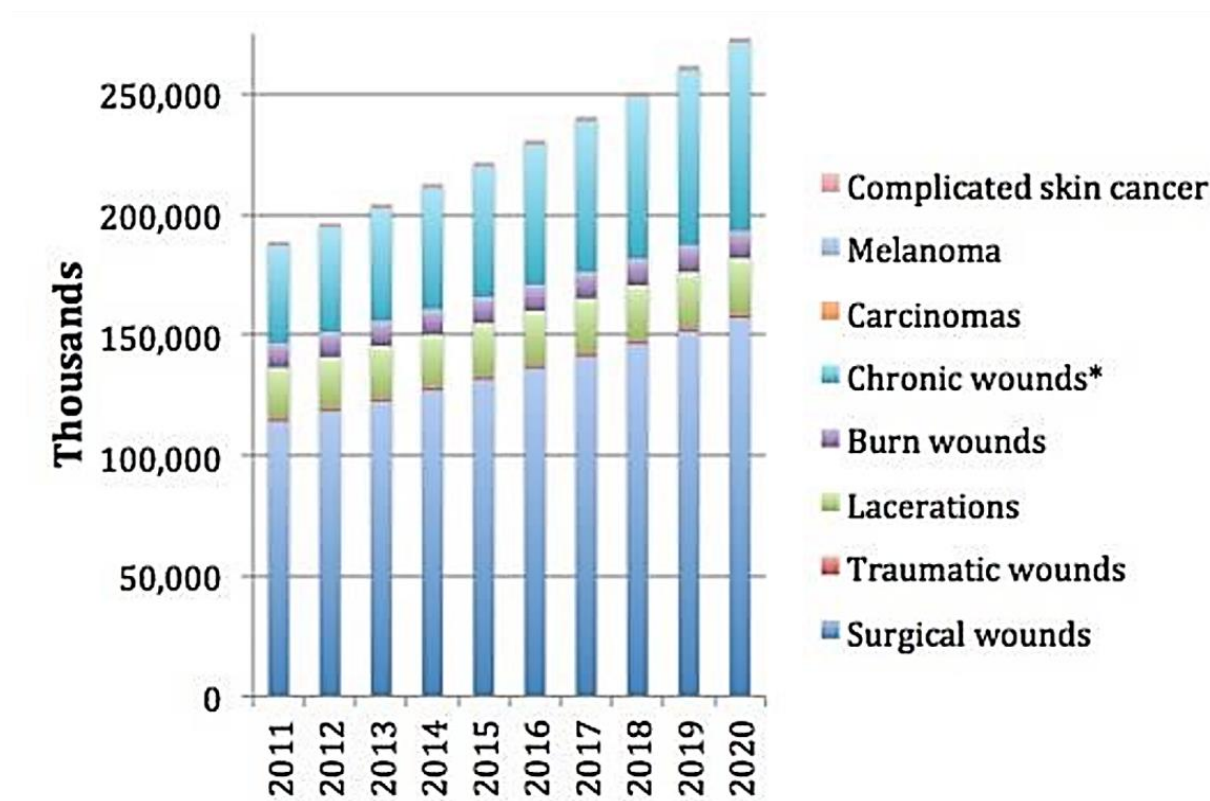
Figure 1.1 The increased prevalence of different wound types globally from 2011 to 2020[9]

The prevalence of all types of wounds are increasing exponentially, with chronic wounds increasing at the second largest rate, as shown in figure 1.1. Chronic wounds

have an associated economic burden, whereby medical care costs and productivity losses are increasing every year worldwide[10]. In developed countries, more than 1-3% of total healthcare expenditure is taken up by the costs associated with caring for chronic wounds[11][12]. Due to an aging population, chronic wounds caused by diabetes are on the rise, inducing significant societal economic impact.

1.2.1   The wound healing process

The normal cutaneous wound healing process following skin injury involves extensive communication of different compartments of skin and their extracellular matrix (ECM), where restoration of a new functional epidermal barrier occurs efficiently [8]. During this process, the epidermis, dermis, local vascular structures and immune systems play a coordinated role in the stages of wound healing [13][14]. Figure 1.2 illustrates the healing stages of a normal wound. In the first stage, following tissue injury, hemostasis occurs as the initial response where the wound is being closed by clotting. When hemostasis starts, the blood leaks out of the body and blood flow is restricted when blood vessels constrict. After that, the exposed collagen and skin elements in ECM start to contact with platelets in order to seal the broken wall of blood vessels, which results in the release of clotting factors, essential growth factors and cytokines. Then the coagulation begins and the threads of fibrins are reinforced with the platelets which act like a molecular binding agent. As a result, the platelets adhere to the sub-endothelium surface. After that, the first fibrin strains start to adhere and mesh, when the blood is transformed from liquid to gel status and blood cells are trapped in wound area by clotting or thrombus[15]. In the next stage, inflammation occurs at the site of polymorphonuclear leukocytes (PMNs) influx when the injured blood vessels leak

transudate which causes localized swelling. Phagocytosis begins when neutrophils enter the wound site, thus foreign materials, bacteria and damaged tissue are removed. After that, monocytes quickly differentiate into macrophages,, where leukocyte effectors continue phagocytosis and mark the transition of the inflammatory phase into the proliferative phase of healing by releasing an array of growth, angiogenic and inflammatory factors. Late inflammatory response comes into effect after the early inflammatory response. Endothelial cell migration and proliferation occur when microvascular endothelial cells are activated by pro-angiogenic factors [16]. The interactions between cell to cell, cell to ECM, and cell to growth factor are orchestrated during angiogenesis. In chronic wounds, this process is interrupted and there is an imbalance between pro-and anti-angiogenic factors. While in the normal wound healing process, inflammatory cells such as macrophages are involved in angiogenesis because they secrete mediators including pro- and anti-angiogenic factors.

In the next stage, after the wound site is cleaned, the fibroblasts migrate and deposit new ECM indicating the proliferative phase. During this phase, numerous chemotactic signals and growth factors are released at the wound site, indicating the start of fibroblast migration producing matrix proteins which support cell migration. After cellular replication and migration which only occur in the early proliferative phase of fibroblasts, collagen synthesis begins in the late stage by collagen cross-linking involving hydroxylation and glycosylation of lysine residues and proline, responsible for vascular integrity and the strength of new capillary beds. A new network of blood vessels is built for the granulation tissue to receive sufficient nutrients and oxygen. Fibroblasts start attaching to the collagen and fibronectin in the ECM. The contract of wounds is caused by myofibroblasts *via* griping and pulling wound edges together

through the same mechanism as smooth muscle cells. Epithelial cells resurface the injury in the final phase of proliferation stage[15].

In the final stage of wound healing, remodelling occurs when the collagen is degraded and broken into pieces to be further digested by proteases *via* collagenase enzymes. Weeks later, the collagen levels peak and remodelling continues for several months influencing the scar formation process of a healed wound [17].
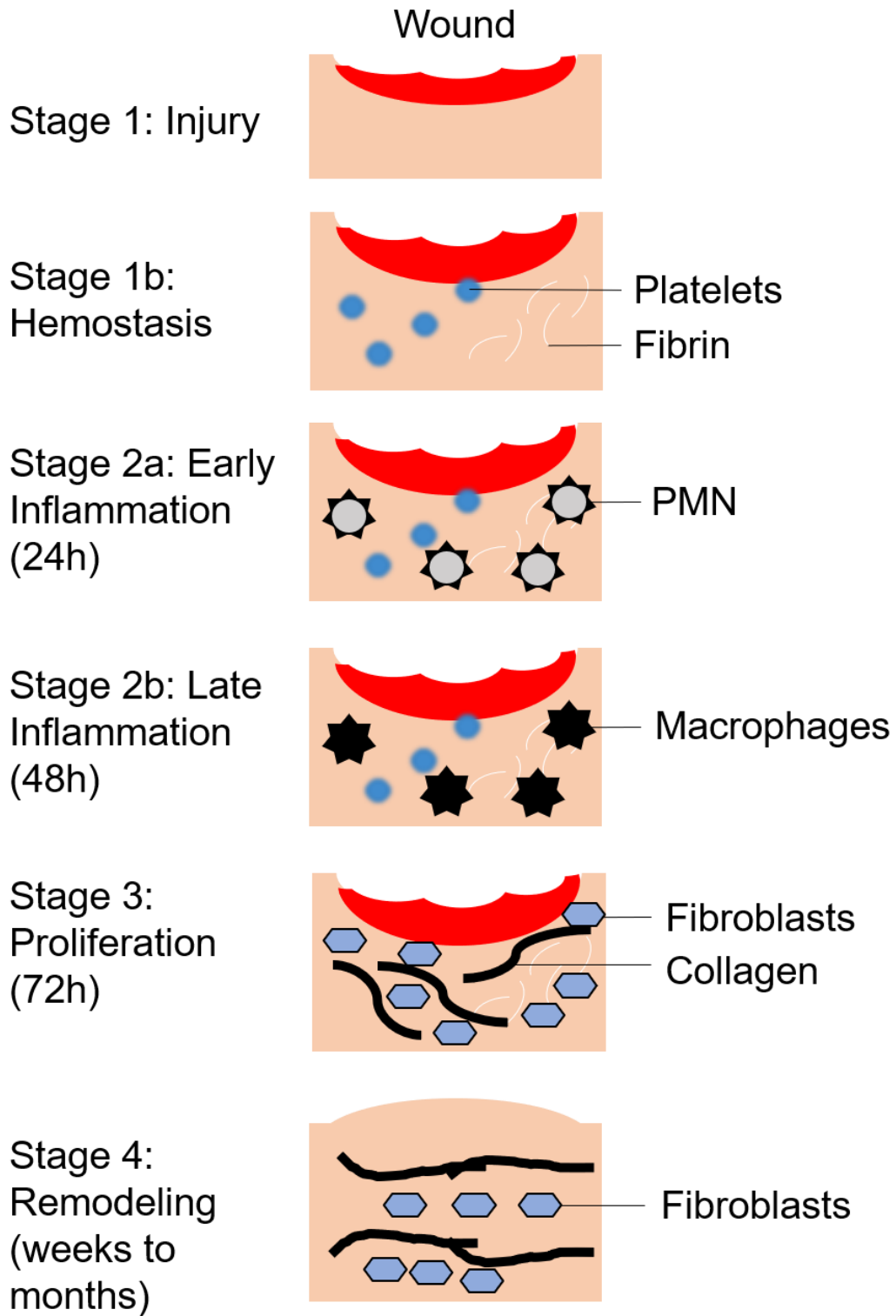
Figure 1.2 Stages of wound healing (adapted from a publication by Banerjee et.al[17]).

1.2.2 Typical chronic wound types

Acute wounds such as cuts, surgical site incisions and abrasions, can recover within a short period of time without the aid of antimicrobial intervention. However, as characterized by the failure to wound closure in a timely and predictable manner, chronic wounds are regarded as clinically infected when the microbial load exceeds 1×10^6 colony per gram of tissues[18]. Typically, the microbes in chronic wounds infections are in a biofilm state[19][20][21]. Biofilm related diseases are persistent infections which developed slowly and rarely solved by immune defences[22]. In a study by James et.al [23], biofilms have been demonstrated in around 60% of chronic wounds, which are almost ten-fold higher than acute wounds. The existence of biofilms in chronic wounds can affect host cellular, immune and inflammatory elements such as cytokines, neutrophils, macrophages, and metalloproteases[24][25]. In the chronic wounds area, two or more species of pathogenic bacteria normally occupy the infection site including aerobic *Staphylococcus aureus* (*S. aureus*) , *Pseudomonas aeruginosa* (*P. aeruginosa*), and *streptococci* which are the primary causes of infections. Other anaerobic bacteria found in wound infections include *Klebsiella pneumoniae*, *Enterococcus* spp, *Enterobacter* spp, *Acinetobacter baumanii* (ESKAPE pathogens), *Staphylococci*, and *Proteus* species[26]. In addition, several types of endogenous fungi including Malasezzia, Curvularia, and Candida also constitute an important part in chronic wounds microbial burden[27]. The progress and outcome of chronic wounds healing are known to be affected by the interactions between bacterial species, bacterial and fungal species in the wounds microbial environment. Particularly, higher inflammatory responses are linked with co-infection of *P.*

aeruginosa and *S. aureus*, leading to the increased antimicrobial tolerance, thus contributing to the non-healing state of chronic wounds[25].

According to various underlying causes, chronic non-healing wounds have three main categories: diabetic foot ulcers, venous leg ulcers, and pressure ulcers. Other types of chronic wounds such as arterial ulcers, are also common. Images of typical chronic wounds are shown below in figure 1.3. The main causes of chronic wounds are vascular insufficiency, diabetes mellitus, and local-pressure effects from complications by diabesity. However, other causes such as compromised nutritional or immunological status, advanced age and chronic mechanical stress can also lead to chronic non-healing wounds[8].

Venous ulcers are the most common chronic wound. They are typically located on the lower extremity and have a shallow shape. The features of a typical venous ulcer are edema, hemosiderin staining and lipodermatosclerosis. They are usually assessed by their arterial status using the ankle-branchial index or toe-branchial index. Other assessment methods including angiography, lower extremity arterial duplex ultrasonography and segment limb pressure can be used. Pressure ulcers are typically located over bony prominences and often in a superficial to deep shape. Types of assessment include computed tomography, magnetic resonance imaging and radiography. Diabetic foot ulcers are normally located on the plantar of foot, in a superficial to deep shape. As with venous ulcers, they are usually assed *via* the ankle-brachial index or toe-brachial index, a bone scan, lower extremity arterial duplex ultrasonography or magnetic resonance imaging[28].

Figure 1.3 Images of typical types of chronic wounds: (a) venous leg ulcer, (b) arterial ulcer, (c) diabetic foot ulcer, (d) pressure ulcer (figure adapted from publication by Eming et.al[8]).

1.2.3 Chronic wound healing

The normal wound healing process involves three progressive stages. Early stages of wound healing include haemostasis and activation of keratinocytes and inflammatory cells. This is followed by proliferation and migration of keratinocytes, proliferation of fibroblasts, matrix deposition, and angiogenesis. The final stage of healing consists of remodelling of the ECM, leaving scars and restoring a protective barrier. However, it the chronic wound healing process has a more complicated mechanism, involving various types of cells locally at the site of the wound as well as systemically. Furthermore, the use of animal models which are not precisely correlated to human tissues contribute to the difficulty of finding healing therapies. As figure 1.4 shows, chronic wounds have hyper-proliferative and non-migratory epidermis, unresolved inflammatory cells, biofilm formation and infection. The overexpression of proteases interferes with essential repair mechanisms. Fibroblasts are senescent. Therefore, in chronic wounds, the angiogenesis, stem cell recruitment and activation and ECM remodelling are all greatly reduced compared to normal wounds.
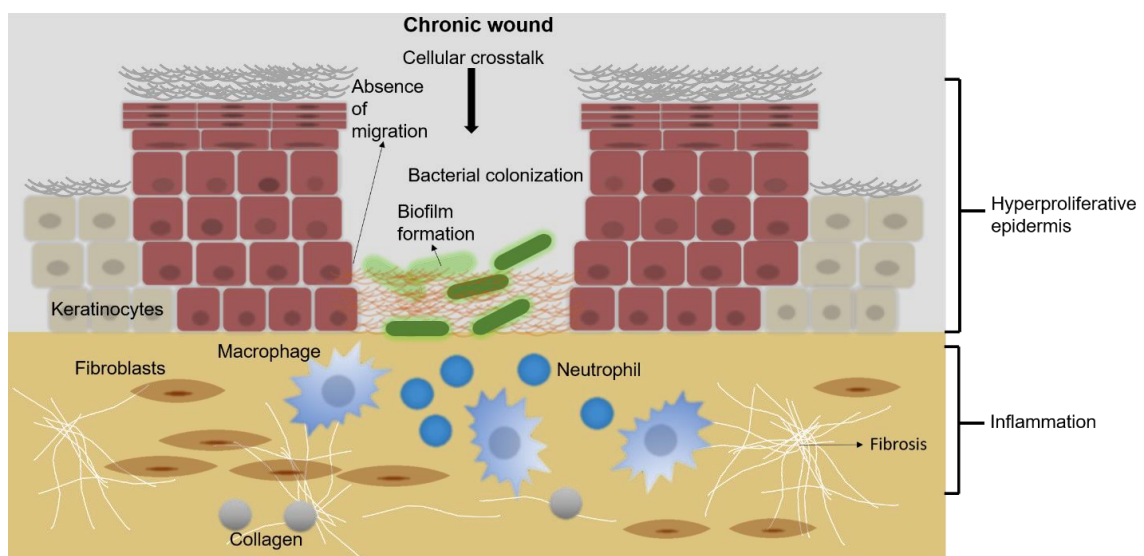
Figure 1.4 Illustration of molecular pathology of chronic wounds: molecular and cellular mechanisms impaired in chronic wound healing (adapted from publication by Eming et.al[8]).

Local care of chronic wounds involves debridement and proper wound dressings. These steps are essential to prepare the wound bed to accept a skin graft or flap, or for closure. Table 1.1 shows local treatments for chronic problems such as odour, bleeding, itching, excess exudate, pain and infection[29]. These treatments are for the most common chronic wounds types such as diabetic foot ulcers, venous leg ulcers and pressure ulcers. The frequency of most of these treatments are required in a daily basis[29].

Table 1.1 Typical chronic problems and their treatments[29].

Chronic problems	Treatments
Odour	Intervals of mechanical debridement to decrease the microbial burden on the wound surface, with topical antimicrobial therapy like metronidazole[30], and/or with odour absorbing dressing with soaks of acetic acid or Darkin solution.
Bleeding	Non-adherent dressing is placed on the wound to reduce the bleeding, with a second layer of alginate dressing. Malignant wounds can be controlled with topical hemostatic agents or sucralfate[31], and gentle pressure of elastic bandages, with focal points of bleeding treated with silver nitrate, hand-held cautery, or local anesthetic with epinephrine.
Pruritis/itching	Keep the skin moisturized and protected, topical corticosteroid creams can be added if necessary.
Exudate	Place an absorptive dressing over the nonadherent dressing to control the drainage and reduce periwound maceration.
Pain	The World Health Organization analgesic ladder; supplemental doses of a short-acting agent

Some typical markers and wound healing approaches are shown below in table 1.2:

Table 1.2 Summary of markers and wound monitoring approaches.

Category	Marker	Approach	Test Condition
Infection	Pyocyanin	Square wave voltammetry	Broth culture[20]
	Uric acid	Square wave voltammetry	Blood and blister fluid[21]
	Temperature	Wireless carbon nanotube temperature sensors	*In vivo* calf model[22]
	Disc displacement[23]	Picrosirius red staining, atomic force microscopy (AFM), transmission electron microscopy (TEM), Fourier-transformed infrared microspectroscopy (FTIRM) and circular dichroism	*In vivo* female rat model
Healing markers	pH(infection, healing marker)[24]	indicator dyes/inductance change from pH sensitive hydrogel with wireless transponder	buffer solutions

pH and partial pressure of oxygen[25]	Luminescence life-time imaging sensors with digital photography	Chronic wound in clinical

1.2.4 Current wound dressings

Most of current commercial wound dressings are developed to provide protection from bacterial infections and assist in the wound healing process themselves by incorporating antibiotics, antiseptics or silver. As table 1.3 show below, different categories of wound dressings are in use for different types of wounds. The main advantages and disadvantages of each commercial dressing type are discussed as well.

Table 1.3 Summary of currently available wound dressings (adapted from publication by Han et.al[26]).

Type of dressing	Commercial products	Applications	Pros and cons
Gauze	Vaseline® Gauze, Curity™, Xeroform®	Surgical wounds and partial thickness burns	Cost effective but dry, cannot retain any moisture in wounds
Foams	Allevyn◊, 3M™ adhesive foam, Tielle™, Lyofoam®	Chronic wounds	Highly absorbent but not recommended for dry wounds

Films	Aclar®, Opsite◊, Flexigrid™, Tegaderm™, Cultifilm◊	Acute wounds, dry wounds	Retains moisture, permeable to water vapour and oxygen but only for non-exudative wounds
Alginates	Algisite◊, Sorbsan®, Tegagen™, Kaltostat®	Moderate to high exudative chronic wounds	Highly absorbent but requires a secondary dressing, not for dry wounds.

Hydrogels	XCell®, Restore™, Carrasyn®, Curagel™, Purilon®, Nu-gel™	Dry wounds	Rehydrates dry wounds but can cause over-hydration
Hydrocolloids	Aquacell™, Tegasorb™, DuoDERM®, comfeel®	No-to-low exuding chronic wounds and superficial acute wounds	Reduces the frequency of dressing change, not for heavily exuded wounds
Hydrofibers	Aquacel™	Chronic wounds	Highly absorbent but not for dry wounds
Others (Tissue engineered)	Alloderm™, Biobrane®, Dermagraft®, Apligraf®, Myskin®, Transcyte®	Skin substitute, severe chronic wounds	Can address deficient growth factors and cytokines but expensive

(1) Antimicrobial chronic wound dressings

As introduced in section 1.2.2, chronic wounds are often presented with polymicrobial environment as well as various fungi, which affects the wound healing progress and leads to non-healing wound status. Therefore, one important category of chronic wound dressings is targeting antimicrobial activity which can prevent long infections in wound beds, thus accelerating the healing process. The antimicrobial agents used to functionalise wound dressings can be categorised into three main types: antibiotics, nanoparticles, and natural products. Due to the toxicity and lack of uptake by host cells, less than 1% antibiotics are used in the clinic, which includes beta-lactams, tetracyclines, quinolones, glycopeptides, aminoglycosides and sulphonamides[39][40]. The antibiotics interfere with bacteria structure or metabolic pathway by either cell wall inhibition like beta-lactams and glycopeptides[41], metabolic pathway blockage in the case of sulphonamides[42], interference on protein synthesis such as tetracyclines[43], or inhibition of nucleic acids synthesis such as quinolone group[44]. However, the use of antibiotics can also increase the number of multidrug resistant bacteria and more than 70% of bacteria in wounds display resistance at least one of the antibiotics in the clinic[45]. Nanoparticles such as silver nanoparticles, iron dioxide nanoparticles, zinc oxide nanoparticles and titanium dioxide nanoparticles, are regarded as promising alternatives to antibiotics due to the bactericidal activity against broad-spectrum bacteria strains without triggering bacterial resistance[46][47]. Nanoparticles perform the bactericidal effect by contacting the bacterial cell wall via generating reactive oxygen species (ROS) or releasing toxic metal ions[48]. Natural products such as honey, essential oils, and chitosan are incorporated into wound dressings to enhance the antimicrobial property in recent years[49][40]. The acidity, low water content, as well as

the presence of hydrogen peroxide, antimicrobial peptide bee defensin-1, phenolic acids and flavonoids of honey attributes to the antimicrobial activity[50][51]. It was believed that the acidic pH of honey can aid macrophages to kill bacteria and prevent biofilm formation[52], and low water content with high osmolarity provides an unfavourable conditions for microbes to survive and grow[53]. In addition, hydrogen peroxide can react with cell walls, lipids, and nucleic acids in bacteria, which is responsible for bacteria inhibition[54]. The antimicrobial property of essential oils can be attributed to phenolic compounds, which attacks phospholipids in cell membranes and lipids on cell walls, leading to cell lysis and loss of cellular processes[55]. The antimicrobial property of chitosan results from the electrostatic interactions between positively charged amino groups of glucosamines in chitosan and negatively charged peptidoglycans on cell walls, giving rise to internal osmotic imbalance and microorganisms inhibitions[56][40]. The antimicrobial peptides inhibit protein translation through molecular chaperone folding by interfering with effector molecules and related enzymes[57][58].

Table 1.4 summarises current novel antimicrobial materials for chronic wound dressings including natural products and nanoparticles. Novel natural product like Matrine and star-shaped peptide are employed in the wound dressing materials as well. It has been investigated that Matrine can suppress candidate related infections by controlling yeast-to-hypha conversion[42], and phenol-soluble peptide allows rapid shedding of bacteria from biofilms[45]. Inspired by nature, nanostructured bactericidal surfaces are also a promising strategy for multi-antibiotic resistant bacteria inhibitions without causing antimicrobial resistance, via contact killing mechanism. The presence of sharp nanostructures can pierce into the bacterial cell wall when they contact or rupture it, thus killing the bacteria[59][60]. This indicates a trend towards increasingly

nature-derived or bio-inspired materials research which exhibit different antimicrobial spectrum to be used potentially in chronic wounds. In addition, combating colistin-resistant, multi-drug resistant Gram-negative bacteria is still a challenge and of great significance due to increases in side effects associated with antibiotics.

Table 1.4 Current antimicrobial materials for chronic wounds dressings.

Products	Materials	Methods	Antimicrobial spectrum	Applications
Konjac glucomannan hydrogel[76]	Matrine-loaded Konjac glucomannan/fish gelatin composite hydrogel	Alkali processing and thermal treatment	*E. coli* and *S. aureus*	Antimicrobial wound dressings
Antimicrobial nanofiber mat[77]	Polycaprolactone (PCL)-coated gum arabin (GA)-polyvinyl alcohol (PVA) nanofiber mat loaded with silver nanoparticle	Electrospinning	*S. aureus*, *E. coli*, *P. aeruginosa* and *C. albicans*	Antimicrobial mat for commercial dressings
Sprayable hydrogel dressing[78]	Mathacryloyl (GelMA)-dopamine (DOPA)-conjugated polymer encapsulated with antimicrobial peptide	Chemically conjugate gelatin with dopamine motifs	*S. aureus*	Chronic wound treatment
Structurally nano-engineered antimicrobial peptide polymers [79]	Star-shaped peptide polymer nanoparticles consisting of lysine and valine residues	Synthesize by ring-opening polymerization of	*E.coli S. aureus*	Combating colistin-resistant multidrug-resistant Gram-negative pathogens.

		α-amino acid N-carboxyanhydrides		
Antimicrobial coagulase [80]	Antimicrobial peptides	Antimicrobial peptides produced by coagulate-negative staphylococcus (CoNS) species.	*S. hominis*	Specific strategy for rational microbiome therapy
Human cryopreserved viable amniotic membrane [81]	Amniotic membrane	Human term placenta tissues were procured and processed at Osiris erapeutics, Inc. (Columbia, MD) following its proprietary manufacturing procedure.	*P. aeruginosa*	Effective in wound closure and reduction of wound-related infections

L-Glutamic acid Loaded Hydrogels Through Enhanced Collagen Deposition and Angiogenesis[82]	L-glutamic acid loaded chitosan hydrogels	Preparation of L-glutamic acid loaded chitosan hydrogel *via* physical crosslinking and investigation of its potential for diabetic wound healing	E.coli and *S. aureus*[83]	Improves collagen deposition, and vascularization, and aids faster tissue regeneration
Natural and bio inspired nano-structured bactericidal surfaces[84]	Nanostructured silicon surfaces (super hydrophobic)[85]	Fabricated using the deep reaction ion etching technique	E. coli and *S. aureus*	self-cleaning and anti-bacterial surfaces in diverse applications such as microfluidics, surgical instruments, pipelines and food packaging.

Hierarchically ordered Titanium nano-patterned arrays mimicking the dragonfly wing[86]	Hydrothermally etched titanium nanowire surfaces	Aantibacterial nanoarrays fabricated on titanium surfaces using a simple hydrothermal etching process	*P. aeruginosa S. aureus*	Surfaces that have excellent prospects for biomedical applications
Nanostructured Multifunctional Surface with Antireflective and Antimicrobial Characteristics[87]	Poly(methyl methacrylate) (PMMA) film	The nanostructure was designed using the rigorous coupled-wave analysis method	E.coli	Suitable for the production of protective optical and hygienic polymer films for the displays of portable electronic devices

(2) Chronic wound sensors

a. Wound sensor substrate

Wound dressing materials require high flexibility to conform to the wound without restricting patients movement[61], high gas permeability to maintain sufficient oxygen supply[62], good moisture control to keep the wound bed moist and absorb excess exudate[63]. In addition, materials in direct contact with the wound bed should be soft enough to avoid mechanical discomfort and should not interfere with the epithelisation process. Silicon elastomers such as polydimethylsiloxane (PDMS) are proposed as suitable materials for stretchable and flexible sensors. PDMS, a widely used silicon-based organic polymer, is particularly known for its excellent rheological properties, high compliance (with an elastic modulus of 1-3 MPa[64]), optical transparency (in the wavelength ranging from 240-1100 nm[65]), oxygen permeability[64] and its hydrophobicity which prevents the wound moisture being overly absorbed compared with cotton based wound dressing substrates. Most importantly, it can be reversibly or irreversibly bonded to other materials such as glass or silicon, preventing overall leakage by integrating in microfluid devices[66]. Due to its high biocompatibility and non-toxicity, PDMS is widely used in personal care, medical devices and biosensor applications[67],[68].

Porous polymeric matrices, such as polyurethane (PU)[69],[70], are promising dressing materials for wound care compared with either foam or sponge dressings which offer good absorbency fine-tuning via control of the pore size and thickness for targeted wound healing. The good mechanical properties of foam or sponge dressing products are also key to negative pressure wound therapy[71],[72]. To prevent leakage of topical

medicines, the second covering such as a hydrophobic backing is important and can also serve as a barrier against bacterial contaminations[73]. Therefore, in the research by Ethan Lee[73], PDMS was selected as a sensor substrate without the second covering, and exhibited high strength, elasticity and permeable to oxygen and water vapor[74],[75].

In the 20th century, Winter[88] found that maintaining wound moisture improves the progress of wound healing. This subsequently became a key parameter for wound dressing design especially for dry wounds. Current development of technology suggests the next significant advancement in wound care is the use of wound healing and monitoring sensors as diagnostic tools to revolutionize wound care practice. The main type of wound that would greatly benefit from sensor technology are chronic ulcers, which are especially difficult to treat and highly susceptible to infection, potentially causing long-term patient suffering. Sensor innovation in the management of these wounds has the potential to impact clinical practice, patient outcomes and economic policy[3].

Flexible wound sensors can be categorized as types of physical and chemical chronic wound sensors, including pH sensors, oxygen sensors, moisture sensors, temperature sensors, bacteria sensors, enzyme sensors and mechanical sensors.

As indicated in Figure 1.5, work by Jin Zhou et.al[89] describes a bacteria sensing system that responds by releasing an encapsulated antimicrobial from within an attached vesicle. By detecting the toxins and lipases which actively damage cell membranes, the tissue damage around infected wounds can be observed. However, this work eventually aimed to produce responsive dressings, releasing antimicrobials and an observable colour change in infected wound areas.
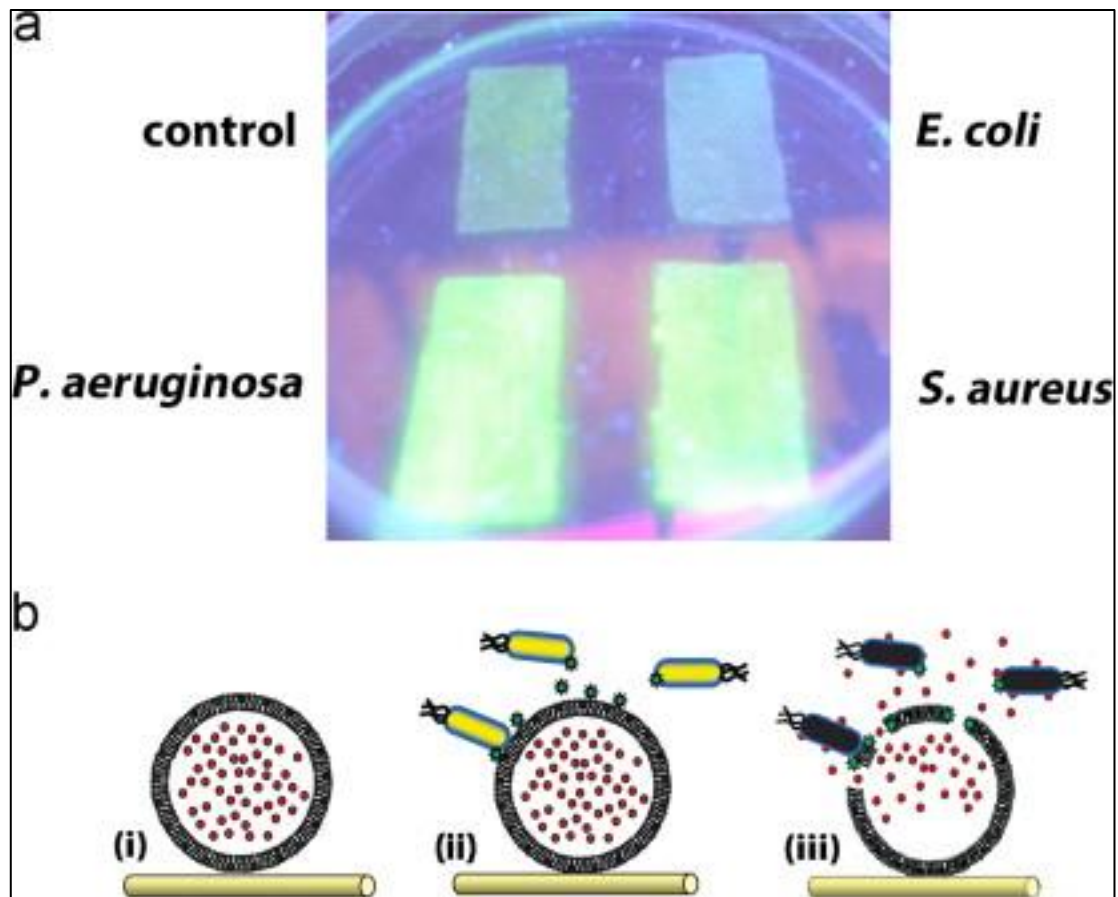
Figure 1.5 (A) Polypropylene fabric impregnated with vesicles containing carboxy-fluorescein under low UV intensity light in the presence of various bacteria. (B) The mechanism for bursting of vesicles by bacteria releasing the fluorescent dye or an antimicrobial agent: (i) vesicle prior to rupture, (ii) toxins from bacteria lyse the vesicle wall and (iii) release of vesicle contents.[89]

Research on wound healing sensors includes biosensors for monitoring changes in enzymes during the wound healing process[90] (see figure 1.6 (a)), where the biosensor comprised of two fluorescent proteins connected with a short peptide linker detects proteases enzymes, by changes in fluorescent signal. Temperature sensors are used to provide programmable delivery of local heating and electrical stimulation using systems composed of integrated single crystal silicon nanomembrane (Si NM) diode and microscale joule heating elements during the wound healing and suturing process[91](see figure 1.6 (b)). A smart bandage dressing[92] (see figure 1.6 (c))which is composed of pH and temperature sensors printed on a disposable bandage strip

that can be disposed of after use, and wireless electronics which include an inkjet printed circuit board with antenna made on a kapton tape that can be detached and reused on another bandage. There are two types of sensing mechanism used in the system: a capacitive sensor which detects the bleeding and pressure levels on the wound; a resistive sensor measuring pH levels. The detachable electronics involves a transmitter embedded with microcontroller, a capacitance to digital converter (CDC), and an LED to signal the status of the bandage and battery power. The sensor capacitance is compared to a reference capacitance in the CDC, and the CDC outputs logic high when the sensor capacitance is greater than the reference capacitance caused by bleeding or external pressure. Then the change of resistance in sensor is converted into voltage change through another port of the microcontroller. The bottom electrode which are made of carbon ink by a screen printing method, reacts with hydronium ions in the case of an acid or hydroxide ions in the case of the alkaline, resulting in the change of conductivity. Carbon acts as a conductor with free electrons as the charge carriers. The adsorption of hydrogen ions in the case of acid leads to the reduction of concentration of electrons on the surface of the electrode, while the effect of hydroxide ions is opposite. The bandage can communicate wirelessly to a patient's smart phone which can then connect to remote health monitoring over the mobile network or the internet.
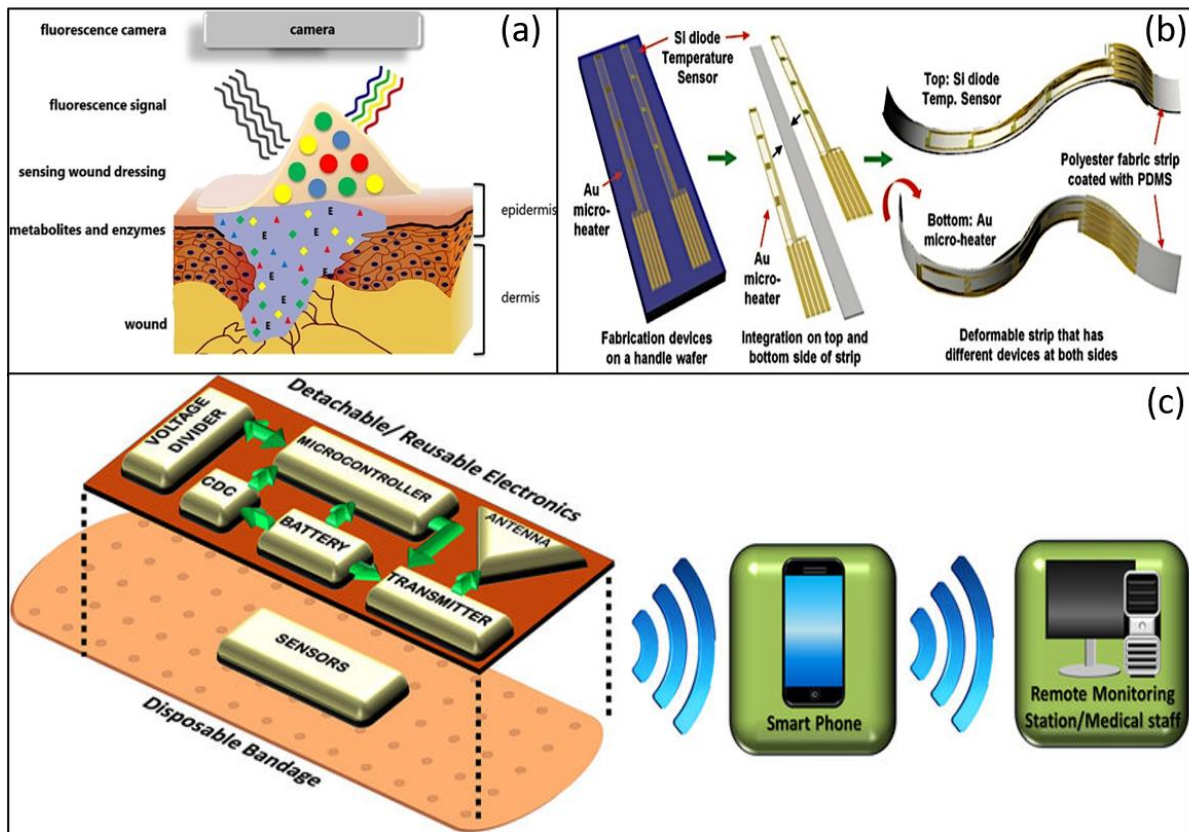
Figure 1.6 (a) Biosensors that monitor enzymatic wounds by sensing the neutrophil elastase concentration via changes in fluorescent signal[90]. (b) Ultrathin suture strip with integrated temperature sensors and thermal actuators[91] (c) Illustration of a smart bandage [92].

However, these studies still indicate most wound healing sensors are in need of complex design and fabrication methods or lack flexibility and comfort in compensation for their functionality. These are areas which can be improved upon in the future. .
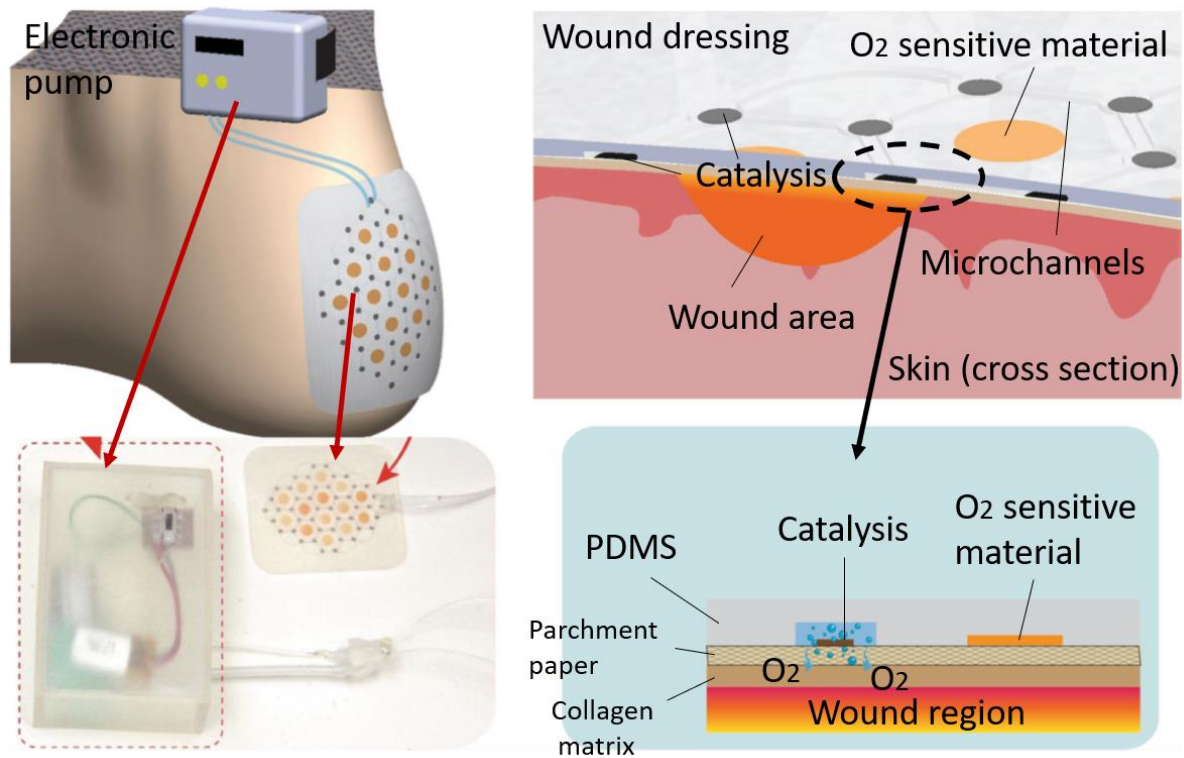
Figure 1.7 Illustration of the integrated oxygen sensing and delivery patch[93].

A new study by Ochoa et.al [93] illustrated in figure 1.7 proposed an integrated flexible oxygen sensing and delivery patch for chronic foot ulcers, that monitor via a layer-by-layer technique. Through the catalysis of hydrogen peroxide, oxygen can be generated in a gel substrate by 13% (5 ppm) in 1 h. This can assist oxygen delivery during the chronic wound healing process. Meanwhile, a phosphorescent oxygen-sensitive ink is applied to enable the optical sensing of oxygen delivery in a wound region. This novel platform takes advantage of flexible microsystems and enables mass production at low cost fabrication. However, this is only suitable for shallow and early-stage chronic wounds, and its ability to be reused requires further investigation.

(3) Wound pH sensors

For chronic wounds, while there are various important biomarkers, pH is a key indicative parameter which allows early detection of infections, since bacteria are often responsible for a change in pH. The pH value in chronic wounds is often higher than 7.4 because of the alkaline by-products produced in the process of bacterial colony proliferation[94],[95],[96], whilst healthy skin is usually pH 5.5-6.5 (slightly acidic)[97]. In order to promptly and effectively treat wound areas, pH is measured at different locations across the wound, however, chronic wounds are in need of multiple measurements throughout the wound with high spatial resolutions which is beyond the capacity of most commercial probes.

Recent pH sensors have a solid-state design replacing the glass probe with an electrode coated with pH sensitive film (metal oxide or conducting polymer). This technology is based on the principle that valence changes occur in the oxygen atoms of the metal oxide, which is caused by absorption of hydrogen ions from the test solution, generating a potential relative to the reference electrode[98]. This technology exhibits high sensitivity, increased stability and cost effectiveness[97]. However, it requires complicated manufacturing methods and expensive materials. Another electrochemical method proposed by Rahim Rahimi et.al[99] (see figure 1.8 (a)) achieved an inexpensive and flexible PANI array of pH and AgCl/Ag reference electrodes fabricated on a paper substrate. The PANI is doped with hydrogen ions to form PANI emeraldine salt, giving high electrical conductivity. The electrical potential of sensing electrode is increased by the resulting surface charge relative to the reference electrode. However, when the sensing electrode is immersed in the alkaline solutions, the captured hydrogen ions are neutralized, causing the decrease of electrical potential/charge on PANI surface. This has increased sensitivity as well as

decreased the manufacturing cost, however it still requires expensive laser assisted fabrication and the lifetime is not long enough due to the use of paper. Novel smart bandages embedded with flexible pH wound sensors are developed as showed in figure 1.8 (b) and (c). Figure 1.8 (b) illustrates the fabrication process of a multi-layered wound alkalinity monitoring system DETEC® pH device, testing discarded wound dressings without contact with the entire wound bed. This bandage can be used as an aid for home health care outside clinical facilities. However, the reliability of this technology requires further testing with greater numbers of patient samples. In addition, although it provides an early indication of whether the treatment is effective, the device cannot be reusable, and monitoring does not occur in real-time. Another study in figure 1.8 (c) proposed a flexible uric acid (UA), pH and temperature sensor by functionalizing a 3D porous laser-guide graphene (LGG) electrode on 2D multi-layered MXene nanosheets (PANI is doped in a pH sensor array), which has enhanced detection of various wound parameters at the same time. However, though it is a novel and promising technology, further investigations on *in vitro* and *in vivo* biocompatibility tests may be required to confirm biocompatibility before use in contact with wound areas.

In summary, recent advancements in wound pH sensors can be categorized as pH indicative sensors and electrochemical sensors, where the electrochemical sensors can provide real-time monitoring and more accurate sensitivity. In electrochemical sensors, PANI is often selected as a pH sensitive layer and biocompatible, oxygen-permeable PDMS is employed as flexible substrate.
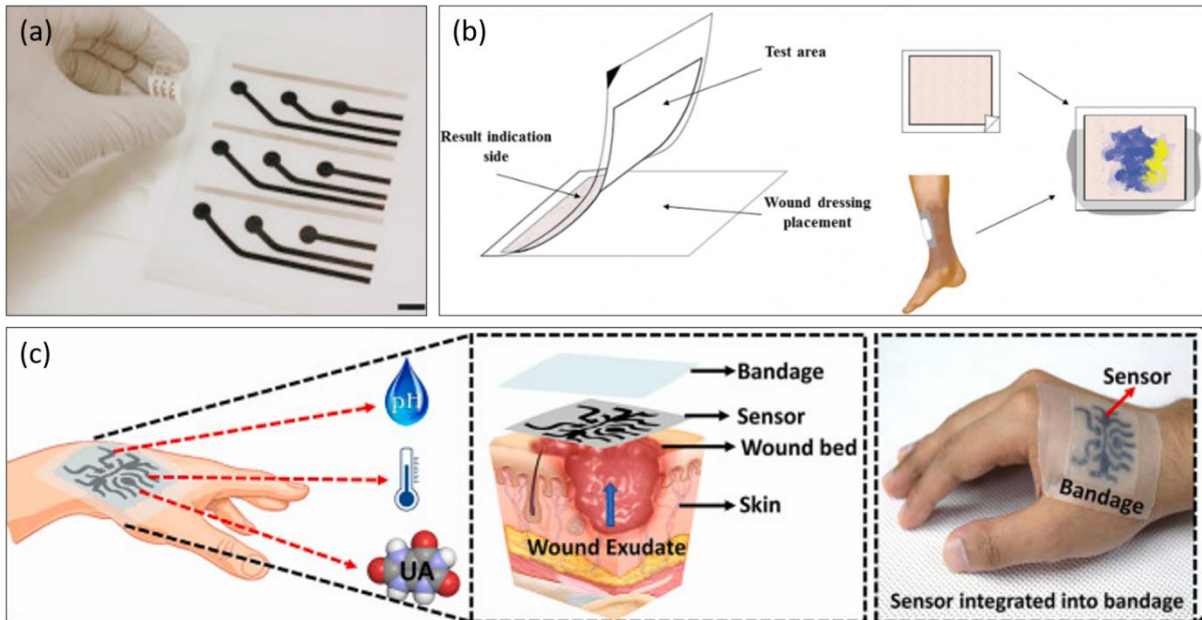
Figure 1.8 Flexible pH sensors: (a) fabricated on paper substrate[99], (b) fabricated via a DETEC® pH testing scheme where the dressing is removed from the wound and placed on the dressing holder on the device with a colour map indicating pH pattern for wound management[100].(c) LGG-MXene electrode using layer-by-layer fabrication methods and tested on a hand[101].

1.3   Bacterial cellulose (BC)

1.3.1   BC introduction

Bacterial cellulose (BC), also called microbial cellulose, is a polysaccharide, produced by aerobic bacteria in both synthetic and non-synthetic mediums through oxidative fermentation[102]. When compared to plant cellulose, BC has a unique structure solely consisting of glucose monomers, exhibiting great properties such as a unique nanostructure[103], high water holding capacity[104], high degree of polymerization[105], high mechanical strength[106], high crystallinity[107], biocompatibility and moisture retaining ability *via* an ultra-fine network structure of non-aggregated nanofibrils[108],[109],[110]. During the assembly of BC fibrils, the cellulose fibrils are

synthesized by cellulose synthase enzymes which locate in the outer membrane of bacterial cell walls. Cellulose fibrils are extruded from bacteria into medium and crystallized into microfibrils and ribbons *via* inter-chain hydrogen bonds. The obtained crystallinity results from the macro-structural assembly controlled by micro-assembly of extruded BC ribbons[111][112]. Previous studies have revealed that BC as well as its derivatives are promising materials in the biomedical, electronic and food industries[113]. The chemical structure of BC is shown in the figure 1.9. BC is a linear polymer made of glucose molecules.
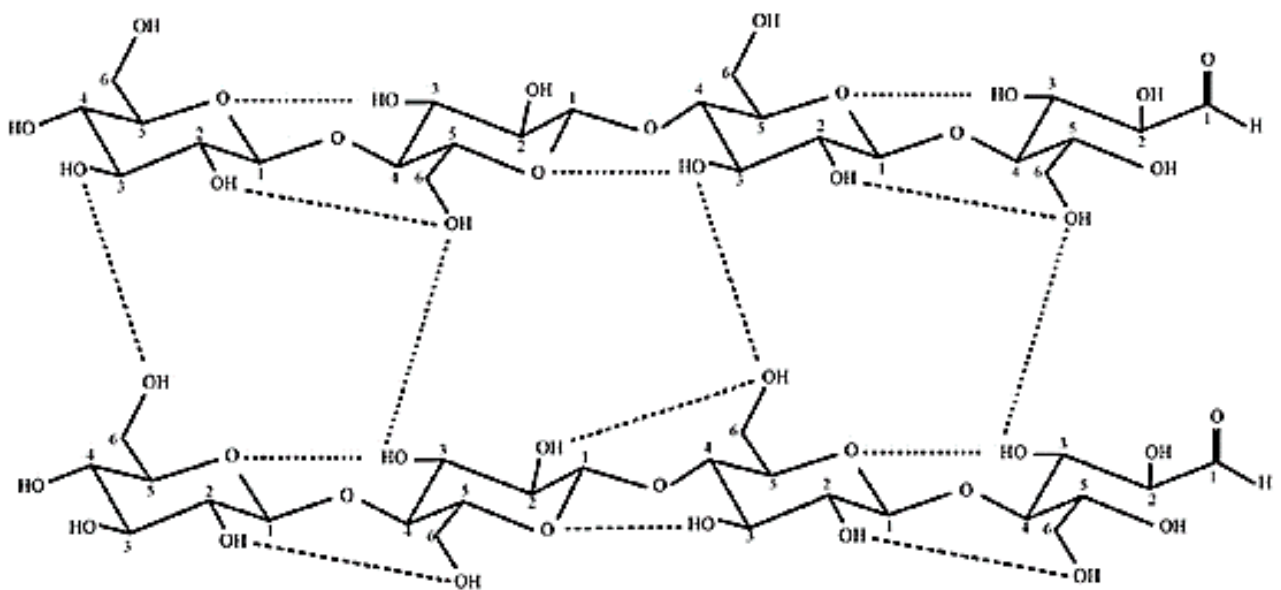
Figure 1.9 Chemical structure of BC. [114]

Research suggests BC has a highly porous network structure (as shown in Figure 1.10), made of well-arranged nanofibres, resulting in hydrogel sheets with high surface area and porosity, providing great possibility for incorporation with other substances, which expands its application scope[115]. The synthetic process involves the secretion of protofibrils of glucose chains through the bacterial wall, and aggregation to form nanofibril cellulose ribbons[116]. The properties of hydrophilicity, biodegradability, and chemical-modifying capacity are due to the structure of cellulose formed[117]. The term

"biodegradability" is often defined as degradation of materials from biological reaction. BC is biodegradable by the enzymes such as cellulase which can be found in nature, however, there is absence of this enzymes in human body. BC can be degradable in human body only by modification and functionalization to enhance the decomposition and absorption in a living system. BC can degrade through surface erosion or bulk erosion, due to the hydrolytically or enzymatically labile bonds[118][119]. BC based biomaterials maintain the structure and functionality at the initial stage in physiological environment, while the rapid mass loss can occur through hydrolytic reaction in the amorphous region and breakdown of glycosidic bonds into short fragments when it approaches the disappearance time[120]. When more chains are fragmented, they are metabolized and converted into oligomers resulting in decreased mechanical properties, losing the functionality. Followed by which, the degraded products are excreted or absorbed by the body[121].
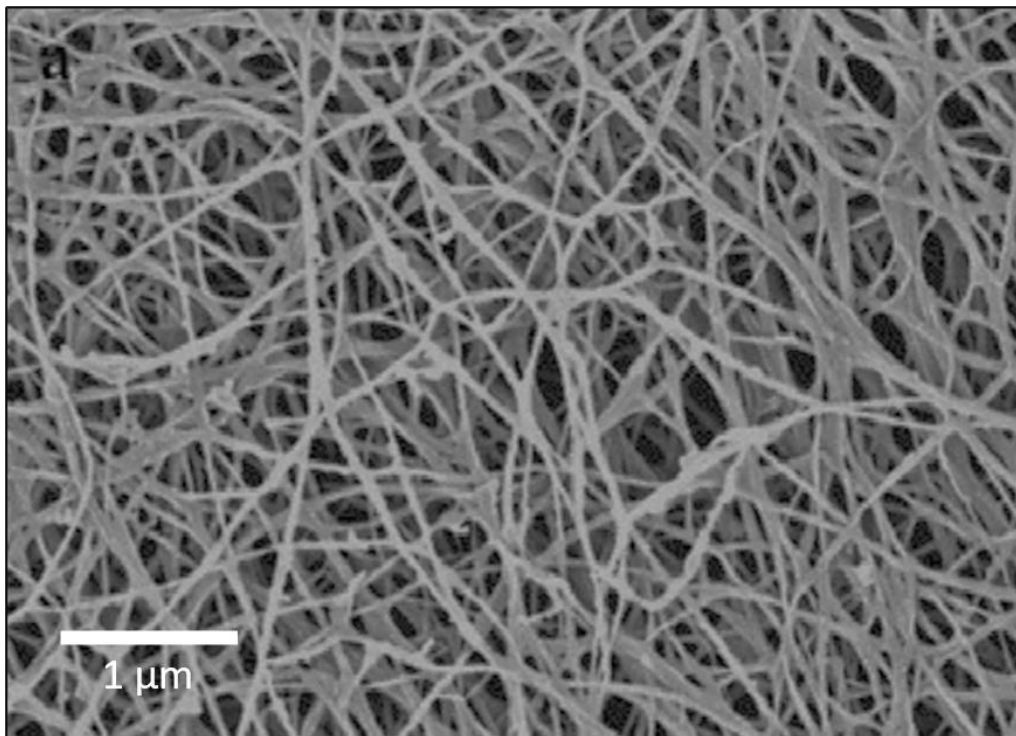
Figure 1.10 SEM image of bacterial cellulose fibres [122]

BC, a nanomaterial produced by ubiquitous species of fermentation bacteria, mainly by the bacterium *Gluconacebacter xylinus* (also named *acetobacter xylinus*), is a highly crystalline linear polymer of glucose[123]. However, other species of *Gluconacebacter*, such as *Agrobacterium tumefaciens*, *Rhizobiium* spp., and Gram positive *Sarcina ventriculli*, are also capable of biomaterial synthesis[124],[125]. Produced in a pure form without animal origins, BC has a unique nanostructure in which the cellulose fibrils and anhydro glucose units interact with each other forming a crystalline structure by internal and external hydrogen bonds, thus resulting in hydrating and water-insoluble nanofibres, with diameters of 20-100 nm[126],[127]. This feature proffers increased moisture and water-holding capacities, combined with excellent physical and mechanical properties. Therefore, BC has specialised biomedical applications such as artificial skins[128] and temporary skin substitutes for cuts, burns, and chronic wounds[129],[130].

Figure 1.11 from research by Hsieh et.al [131]shows a typical BC fabrication from static growth in a 250 ml conical flask and 50 ml medium, in terms of glucose concentration, pH level of culture medium and cultivation time (days). *G. xylinus* (ATCC 11142) in Buffered Schramm & Hestrin's Medium (BSH) medium was used in their study. It is notable that after rapid growth at first, on day 7 of cultivation, BC could yield 2.0 g/L. Meanwhile, the production rate was greatly reduced after 7 days. However, following investigation of glucose consumption, not all nutrients were completely consumed and BC yields its maximum at around pH 6.3.
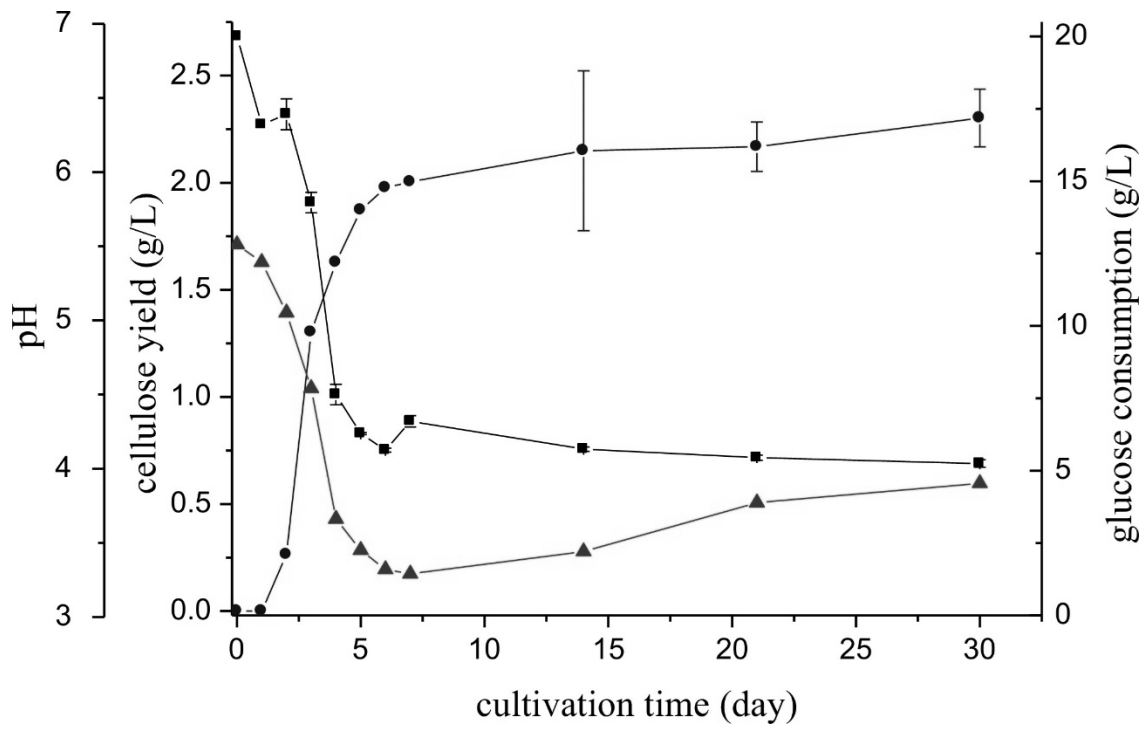
Figure 1.11 Typical yield of static culture of BC (●), the glucose concentration (■) and pH level of culture medium during the cultivation process (▲) (reproduced from publication by Hsieh et.al [131])
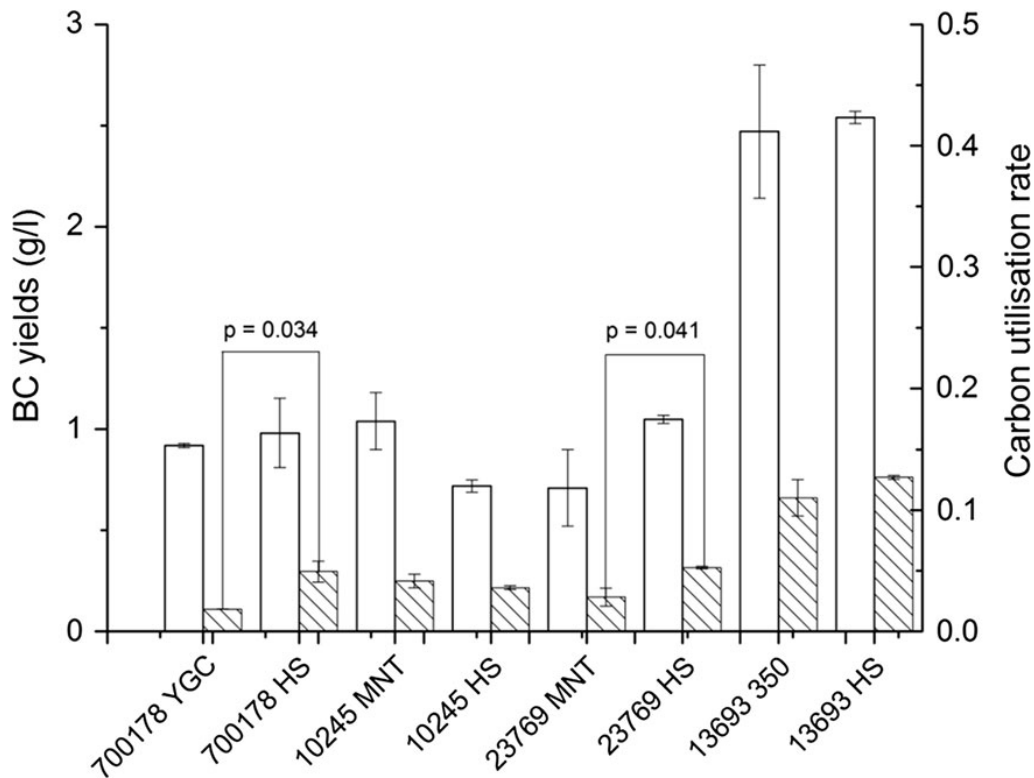
Figure 1.12 The BC yields (blank columns) and carbon utilization rate (pattern columns) of K. xylinus ATCC 700178, K. xylinus ATCC 10245, K. hansenii ATCC 23769 and K. xylinus NBRC 13693 in different culture conditions. The statistical significances ($p<0.05$) of BC yields and carbon utilization rate for the same strain in different culture medium were calculated by the one-way analysis of variance (ANOVA). Figure reproduced from a publication by Chen et.al [132].

As shown in Figure 1.12, another study by Chen et.al [132] investigated BC yields and carbon utilization of the four *Komagataeibacter* strains in their recommended medium compared with HS medium. The results indicated that the HS medium is acceptable for the four strains, and the mannitol and ethanol contained in MNT and 350 medium can limit the BC yields by reducing the carbon consumption.

1.3.2 BC properties

As introduced before, BC has a high degree of crystallinity (above 60%)[133], where most of its crystalline structure contains cellulose type I (70% contains cellulose type Iα compared with plant cellulose)[134]. The XRD fitting method is commonly used to determine crystallinity values, which is not related to BC samples with different drying methods (air dry or freeze-dried)[132].
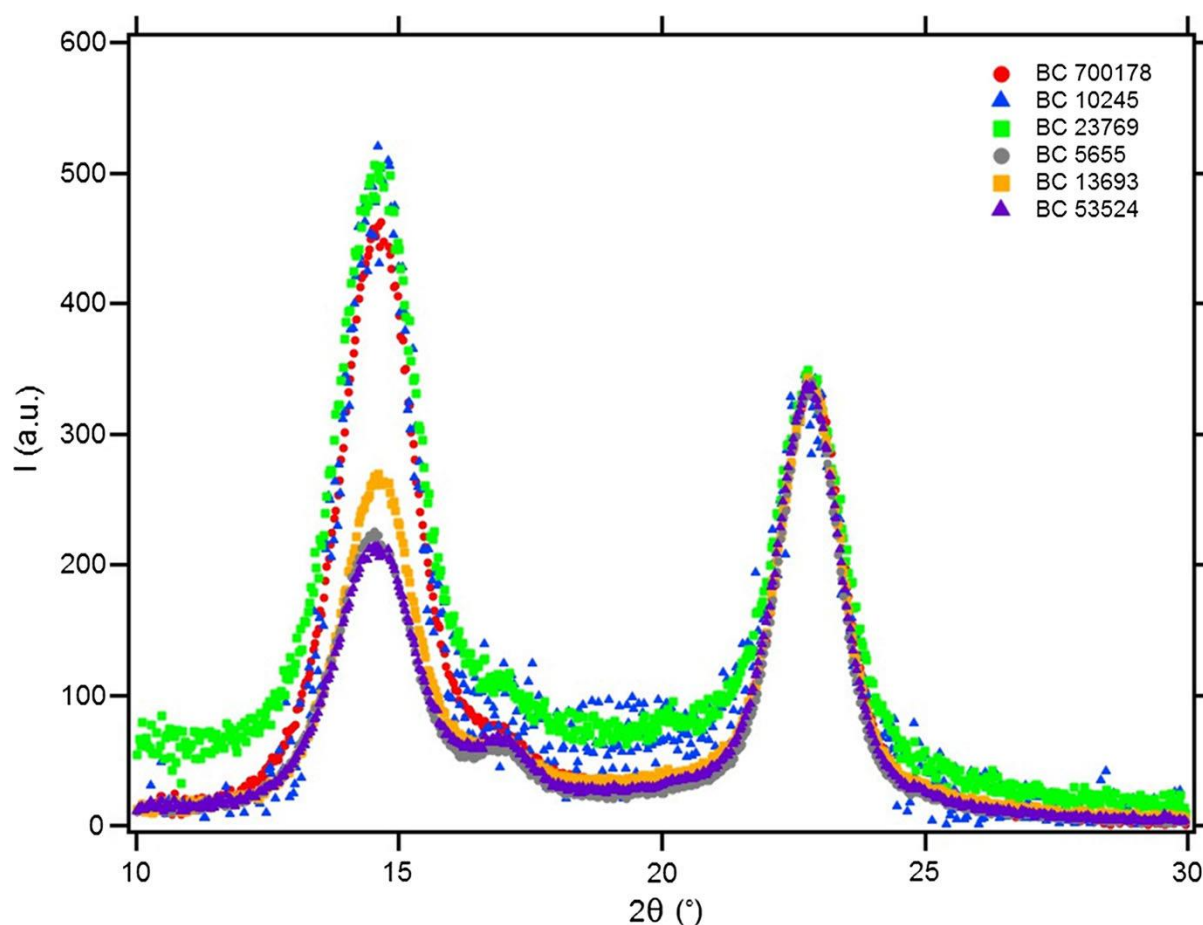
Figure 1.13 The XRD spectra of BC synthesised by *K. xylinus* ATCC 700178, *K. xylinus* ATCC 10245, *K. hansenii* ATCC 23769, *K. xylinus* KTH5655, *K. xylinus* NBRC 13693 and *K. xylinus* ATCC 53524. Figure reproduced from publication by Chen et.al[132].

Figure 1.13 shows the results of XRD characterizations of BC samples grown from six *Komagataeibacter*. The results indicate that six BC samples exhibit 70-90% crystallinity. The XRD patterns display three typical cellulose diffraction peaks which are located at 14.5°, 17.0° and 22.7°, presenting the [100], [010] and [110] cellulose type Iα crystalline planes[132].

Since BC and BC nanocomposites are widely used as tissue scaffolds for cell seeding, it was essential to test their compatibility with human cells. Studies have confirmed that BC and some BC nanocomposites are compatible with different cells, such as bone forming osteoblasts (OB)[135], human embryonic kidney cells (HEK)[136], corneal epithelial cells[137], human fibroblasts[138], and keratinocytes[138]. In most studies, cell adhesion cannot be achieved from native BC structures but can be achieved by incorporation with surface modification by plasma or other biomaterials, such as collagen[139]. As figure 1.14 indicates, after 24 h growth of keratinocytes and fibroblasts, the area of BC is fully covered due to cell proliferation and spreading. Both results indicate high biocompatibility of BC. However, as fibroblasts tends to detach from BC, keratinocytes are more compatible with BC. This phenomena can be explained by cohesion among keratinocytes, and adhesion of BC and keratinocytes affecting cell attachment and spreading. The junctional structures like desmosomes, are comprised of proteins such as E-Cadherin contributing to the intercellular adhesion of keratinocytes[140][141]. However, the contractile force in cells is stronger than adhesion force between BC and fibroblasts, resulting in the failure to reach confluency on BC film[138].
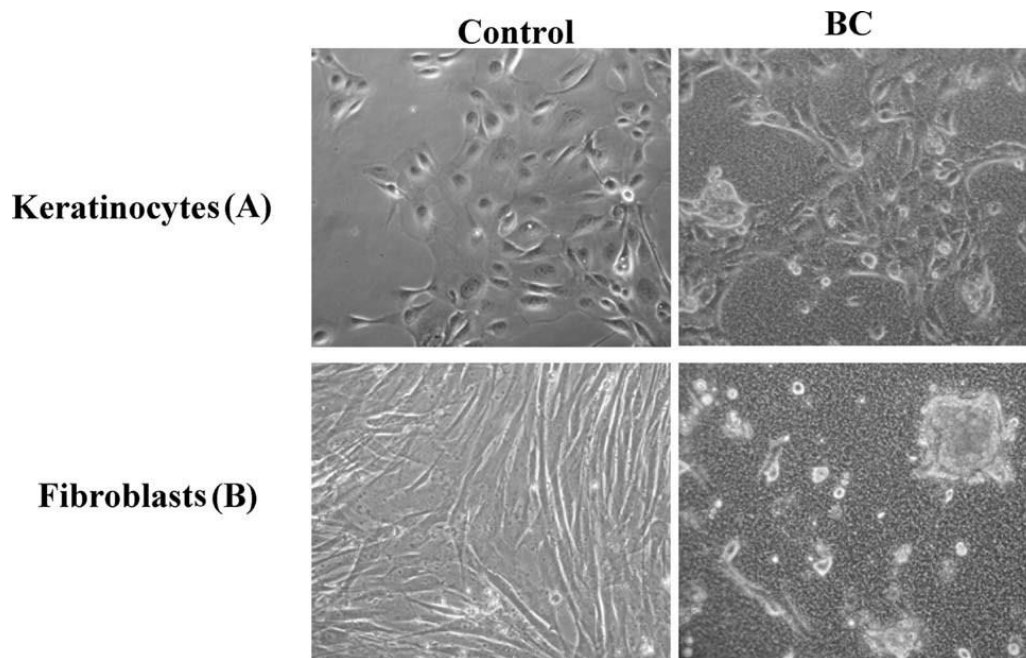
Figure 1.14 The microscopy of morphology and distribution of human keratinocytes (A) and fibroblasts (B) grown on BC for 24 h[138].

1.3.3 BC in biomedical applications

Although BC biocompatibility has been proven, promoting attachment of cells and proliferation *in vitro*, BC is not enough to be used in wound dressing, due to its hydrogel properties in which poor rehydration ability is exhibited once it is in the dry state[114]. The poor rehydration ability of BC is attributed to hornification, an irreversible structural changes caused by cocrystallization of BC fibres. When water evaporates, the fibres gather together and aggregate, forming hydrogen bonds between adjacent crystalline domains. However, the bonds will not break on resuspension in water without external energy, which results in the hornification[142][143]. Wound dressings are capable of accelerating the healing process and reducing the influence of debris by maintaining the moisture and temperature of the wound bed. In addition, they provide both permeability and protection of regenerated tissues[144],[145], and maintain suitable hydration[115]. Therefore, BC nanocomposites [146] are a suitable solution for

improvement of the rehydration ratio. Table 1.5 summarises typical reinforced

biomaterials for BC composites in biomedical applications.

Table 1.5 Typical reinforced biomaterials for BC composites in biomedical applications.

Reinforced Materials	Synthetic approaches	Improved properties	Applications	Disadvantages
Chitosan[147]	Immerse BC gel in Ch solution followed by freeze-drying	Biocompatibility, thermal stability, strength, antibacterial properties	Wound dressing and tissue engineering scaffolds	N/A
Gelatin[148]	Immerse BC gel in polysaccharide solution	Mechanical properties, low frictional coefficient	Artificial articular cartilage	Good properties only in wet state
Polyaniline (PANI)[149],[150]	In situ nano-assembly of BC nanofibres and PANI	Electronic conductivity, biocompatibility	Tissue engineering scaffolds, deep brain stimulation electrodes, biosensors	Conducting properties require improvement
Poly(ethylene glycol) (PEG)[151]	Immerse wet BC pellicle in PEG aqueous solution followed by freeze-drying process	Mechanical properties, biocompatibility	Wound dressing, tissue engineering scaffolds	Water retention is not greatly improved

Graphene oxide[152]	Vacuum-assisted self-assembly technique	Mechanical properties, electrical conductivity	Biosensor, tissue engineering	Conductivity needs to be improved
Collagen[153]	In situ addition	Improved concentration of elastase *in vitro*, antioxidant capacity	Tissue engineering scaffolds	Lack of antibacterial properties
Aloe Vera gel[104]	Static cultivation with BC	Mechanical strength, crystallinity, water absorption capacity and water vapour permeability, improved healing properties	Tissue engineering, wound healing	Infections need to be controlled
Silver nanoparticle[154]	In-situ addition	Antimicrobial capacity	Tissue engineering, wound healing	Mechanical properties need to be improved
Copper nanoparticle[155]	In-situ and ex-situ method	Antimicrobial capacity	Wound healing	Mechanical properties need improvement

Gold nanoparticle[156]	One-step bio-templated method in aqueous suspension	Highly sensitive detection of hydrogen peroxide	Enzyme immobilization and biosensor fabrication	Further applications to immobilize other enzymes
Montmorillonite (MMT)[157]	Impregnate BC sheets with MMT suspension	Mechanical and thermal properties, water adsorbed capacity	Wound dressings	The wound healing capabilities need to be further improved
Zinc-oxide[158]	Immerse BC films into suspension of ZnO nanoparticles	Antimicrobial capacity, healing properties	Burns wound dressing	/
Silk sericin[159]	Solution impregnation	Healing properties, cell viability, biocompatibility	Wound dressing and tissue engineering	Mechanical properties need to be improved

1.3.4 Antimicrobial BC composites

However, in addition to the improvement of the rehydration ratio, the most important aim is to improve the antimicrobial properties of BC/BNC. It has been proven that wound infection is a major problem in the healing process.[160] Various types of solutions have been employed to deal with this problem. One solution involves BC-chitosan composites which are proven to maintain moisture and offer enhanced mechanical and antibacterial properties[154]. Another solution is addition of silver nanoparticles, in which silver ions interact with thiol groups of enzyme and proteins involved in bacterial respiration and transport of nutrients, thus effectively preventing wound infection[161],[162]. Identically, the nanocomposites of cellulose/copper were also found to have antibacterial activities, with increasing copper content in nanoparticle forms instead of nanofibril forms[155]. In addition, nanocomposites such as BC/Pd, BC/Pt, BC/Au, and BC/FeO have been investigated for addition of conducting properties of BC which is required in cooperation of biosensors, display devices, electronics and security papers[163],[144],[156]. BNC may also be loaded with antiseptics such as povidone-iodine (PI) and polyhexanide (PHMB)[164], and the antibiotic tetracycline hydrochloride (TCH)[165] to form nano-structured bio-composites. The high ratio of nano-fibrils in BC provides a high porosity and surface area, which makes BC a suitable material for physical interaction with antimicrobial agents and other active compounds[166][167]. The interaction is physical or happens through definite hydrogen bonding between BC and reinforced materials, where nano-particles or liquid compounds can easily penetrate and be engrossed inside the porous BC nanofibrils matrix. As the original structure of BC plays the most important role in this *ex-situ*

synthesis method, BC obtained from static growth is often used for composite synthesis, which is widely employed in a number of BC composites including polymers, metals, metallic oxides, and liquid antimicrobials in various biomedical applications[166][168]. However, the major drawback of this *ex-situ* synthesis method is the limited size of impregnated materials, which can only apply to nano-sized particles, liquid components and hydrophilic materials. Although the impregnation of chemically synthesized nanoparticles or antiseptics is cheap and simple, the penetrating materials may not be homogeneously distributed inside the BC matrix. In addition, due to the physical absorption, some chemical ingredients can remain on BC matrix after completion of synthesis. Therefore, new BC composite synthesis routes need to be identified to solve the problem[167]. *In situ* BC composites synthesis utilizing a method where reinforcement materials are added during the growth process of BC and become part of BC fibril network, is often widely used in BC composites synthesis process[169][170]. However, this technique is limited to certain kinds of materials, and not applied to some important antimicrobial agents such as silver, metal oixide, nanoparticles and other materials due to their toxic effect on microorganism[167]. As summarized in the table 1.6 below, BC membranes are incorporated with non-silver or silver-based materials *via in situ* synthesis or *ex situ* synthesis, where the *ex situ* method is mostly used. The release mechanism of *ex situ* method is often studied using Korsemeyer-peppas equation[171]: $M_t/M_\infty = k*t^n$

Where M_t is the amount of drug released at time t, M is the amount if drug released as time approaches infinity, t is the releasing time, k is the kinetic constant, and n is the diffusion exponent.

The loading and release behaviour is mainly driven by diffusion of active antimicrobial agents through the highly porous and swollen BC network. The amount of absorbed active agent can be controlled by the concentration of loading solution. The increased density of BC network fibrils can slow down the diffusional speed and rate of release. The release kinetics can be described as the combination of diffusion and swelling controlled processes[172][164]. The mechanisms are the same when there are interactions between BC and active agents, as it did in the case of Huang et.al[173] investigating the non-covalent bonds between berberine and BC, and Trovatti et.al[174] reporting the intermolecular interactions of hydrogen bonds between cellulose and lidocaine. The storage of *in situ* synthesis of BC composites are the same as *ex situ* synthesis method, where resulted BC composites are either autoclaved and stored in aseptic conditions or freeze-dried (in some cases oven-dried) before further use[175][164][165][182].

Table 1.6 Antimicrobial BC composites proposed in recent years.

Categories	BC composite	Fabrication method	Test method	Antimicrobial properties
Non-silver based BC composite	BC/chitosan[175]	In situ synthesis on a rotating drum composed of fabrics	The absorption and shake flask method	Percentage of bacterial reduction was 88.37% against S. aureus, and 27.36, 69.26, 85.98% against E. coli
	BC/PI[164]	BC was loaded by PI solution	*In vitro* direct contact test and microplate laser nephelometry (MLN)	Inhibition of Staphylococcus aureus growth, lower than 7.5%

BC/PHMB[164]	BC was loaded by PHMB solution	*In vitro* direct contact test and microplate laser nephelometry (MLN)	Inhibition of Staphylococcus aureus growth at 7.5%
BC/TCH[165]	BC was loaded in TCH solution	The disk diffusion method and plate count method	Diameters of inhibition zone (DIZ) against E. coli, S. aureus and B. subtilis were 45.7 mm, 38.5 mm and 34 mm
BC/NH$_2$[176]	BC was immersed in 3-aminopropyltrimethoxysilane (10 mL) in acetone then washed and dried.	The standard Dynamic Shake Flask Method	3.1 and 3.5 log reduction of the initial inoculated *E. coli* and *S. aureus*
BC/Cu[154]	Cu/BC was prepared by in situ chemical-reduction method	The disk diffusion method	DIZ of Cu/BC against *E. coli* and *S. aureus* are 3.0 and 4.0 mm

	BC/ZnO[177]	BC monolayer and multilayer films were incorporated with 5wt% ZnO nanoparticles by ultrasound irritation method.	The disk diffusion method	ZOI against *E. coli* and *S. aureus* 5.6 and 11.8 mm
	BC/antibiotic fusidic acid (FA)[178]	BC films were cut into pieces and saturated with FA	The disk diffusion method	DIZ against *S. aureus* is 30 mm after 1h
	BC/bovine lactoferrin (BLF)[179]	BLF was surface adsorbed onto BC films	The disk diffusion method	1-log reduction in the *S. aureus*
Silver-based BC composite	BC/ sodium alginate(SA) [180]	Introduce silver sulfadiazine particles into BC/SA matrix	The disk diffusion method	DIZ against *E. coli* , *S. aureus* and *C. albicans* are 17, 20, and 15 mm
	BC/AgNP[181]	AgNPs were photo-chemically deposited on BC gel network	The disk diffusion method	The DIZ of the composite against *E. coli* 6.5 mm
	BC/laccase/AgNP[182]	laccase was immobilized onto BC	The shake flask method	Display about 92% (*S. aureus*) and 26% (*E. coli*) of bacterial inhibition

Table 1.6 above, concludes that instead of BC/Chitosan, other BC nanocomposites had greater antimicrobial activity against gram-positive bacterium. However, the application of silver containing compounds can be hazardous to human health, causing conditions such as Argyria or argyrosis[183].Non-silver based nanocomposites especially those loaded with antiseptics also showed greater antimicrobial properties than others. Therefore, BC loaded with antiseptics is an important trend for further antimicrobial improvement of BC composites in the future. There is still a large amount of scope for chemical modifications.

1.4   Introduction of general characterization techniques

The aim of this section is to give introductions and summarise the analytical methods used to characterize hydrogel materials in terms of physical, chemical and functional properties. This includes a brief background overview including methodology, and apparatus. The characterization methods involved are listed below:

- **Structural characterization:** material structure, surface morphology, surface area, porosity, pore volume and elemental composition were analysed by Field-Emission Scanning Electron Microscopy (FE-SEM), Energy-dispersive X-ray

Spectroscopy (EDX), Brunauer–Emmett–Teller (BET), and Atomic Force Microscopy (AFM).

- **Chemical composition characterization:** the functional groups of materialswere characterized by Fourier transform infrared spectroscopy (FTIR). The crystallinity and size of cellulose crystals were determined by X-ray diffraction (XRD).

- **Water-holding capacity (WHC) characterization:** the water holding capacity of materials were measured and calculated by related equations.

- **Mechanical property characterization:** The tensile strength of materials was characterized using an Intron Tensile Tester. An *in vivo* stitching test was also carried out to further investigate the mechanical behaviours.

- **Electrical conductivity and pH sensing characterization:** the electrical conductivity and open circuit potential were measured by PalmSens and Auto-lab potentiostats.

- **Antimicrobial characterization:** The antimicrobial properties of materials are characterized by disk diffusion test, against different pathogenic bacterial strains.

- ***In-vitro* biocompatibility characterization:** the biocompatibility of materials was characterized by a cell-attachment test involving human fibroblast cell lines.

Scanning electron microscopy (SEM)

SEM is a type of electron microscope which produces images of samples via scanning the surface with a focused beam of electrons interacting with atoms in the sample.

This produces signals that provide information about the samples' surface morphologies, topography and composition. In order to be observed, samples are coated with a conductive layer such as gold or carbon (normally 5-15 nm in thickness). Meanwhile, samples should be able to sustain high vacuum by losing water molecules or gasses. Samples were coated with gold of 20 nm thickness prior to SEM measurement. A ZEISS Ultra 55 field emission gun scanning electron microscope (FESEM) was used to take images of the inner nanostructures of the surface of BC and BC nanocomposites.

A FESEM is suitable for observing material structures as small as 1 nm on the surface. Magnification can be adjusted as required. It is suitable for characterizing particles such as the nuclei of cells, polymers, coatings and electro-spun nanofibers. The schematic of a typical FESEM working mechanism is illustrated in figure 1.15. Instead of light, the FESEM works with electrons with negative charges which are liberated by a field emission source and then accelerated in a high electrical field gradient. The primary electrons are focused and detected by electronic lenses within a high vacuum column, to produce a narrow scan beam bombarding the object. During this process, secondary electrons are emitted by each spot on the object and caught by a detector to produce an electronic signal. As a result, the signal is amplified and transformed to a digital image which can be saved on a computer.
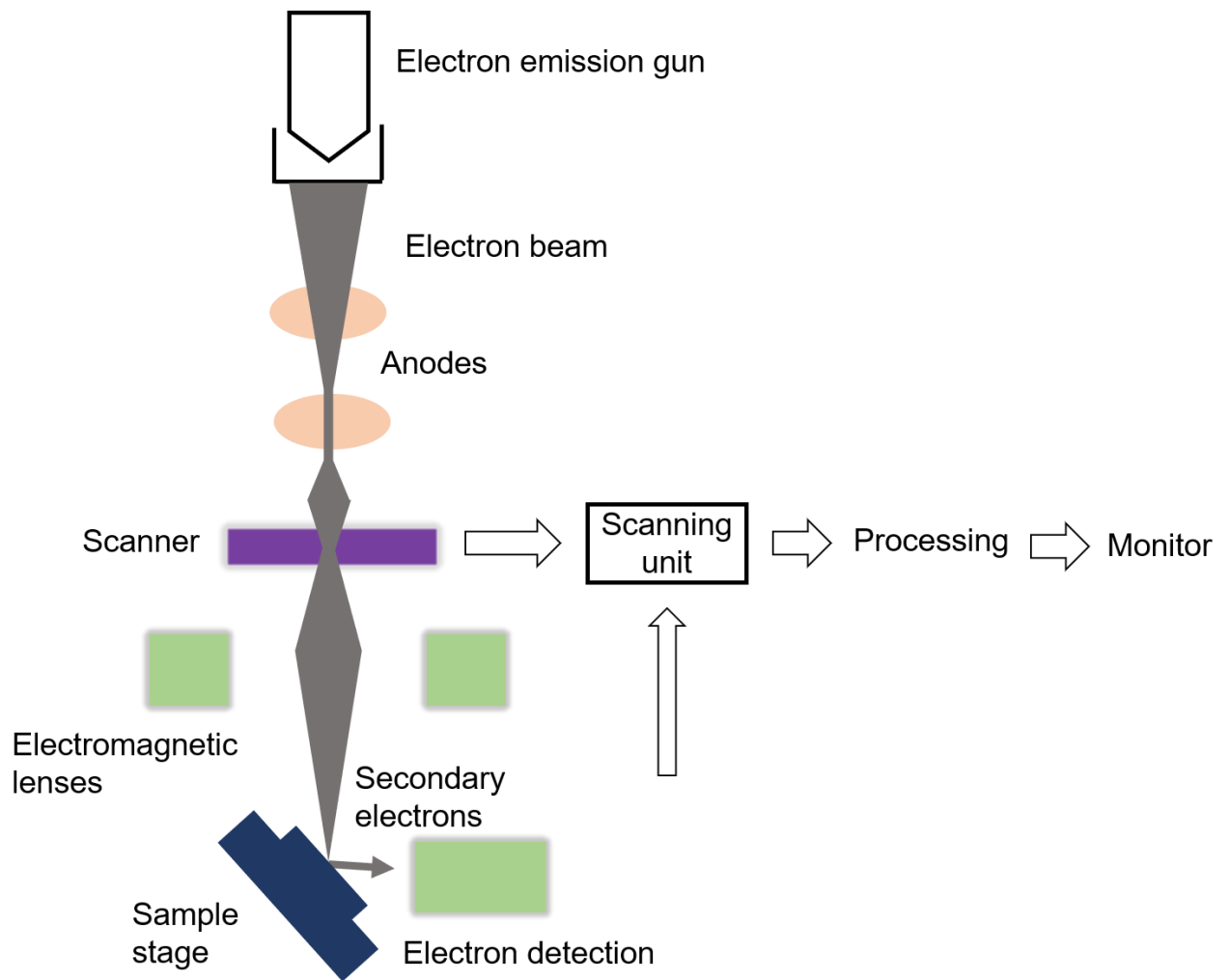
Figure 1.15 A schematic of FESEM modules (adapted from Semnani [184])

Atomic Force Microscopes (AFM)

AFM is a widely used technique enabling the imaging of most types of surface, including polymers, composites, ceramics, glass and biological samples. Different forces including adhesion strength, magnetic forces and mechanical properties can also be measured and localized by AFM. An AFM involves a sharp tip which is approximately 10 to 20 nm in diameter and attached to a Si or Si_3N_4 cantilever. When the tip moves in response to tip-surface interactions, the movement is measured by focusing a laser beam with a photodiode.

The contact and tapping modes are the two basic modes an AFM operates with. The AFM tip is continuously contact with the surface in a contact mode and this mode is only used for force curve measurements. In a tapping mode, which is commonly used for imaging, the cantilever is vibrated above the surface of sample and in intermittent contact with the surface. Different from SEM which provides two-dimensional projection of sample surface, the AFM can provide three-dimensional surface profile without any pre-treatments which could cause irreversible damage of the sample. In addition, the true atomic resolution in ultra-high vacuum in liquid environment can be provided by AFM, which makes it higher resolution compared with SEM. However, the image size of an AFM is in the order of micrometres and maximum scanning area around 150 by 150 micrometres, due to the depth of field in the order of millimetres[185].

Fourier transform infrared spectroscopy (FTIR) characterization

FTIR is a technique used to obtain an infrared spectrum of absorption or emission of a substance (powder or liquid).The data is converted into a spectrum *via* Fourier transform.
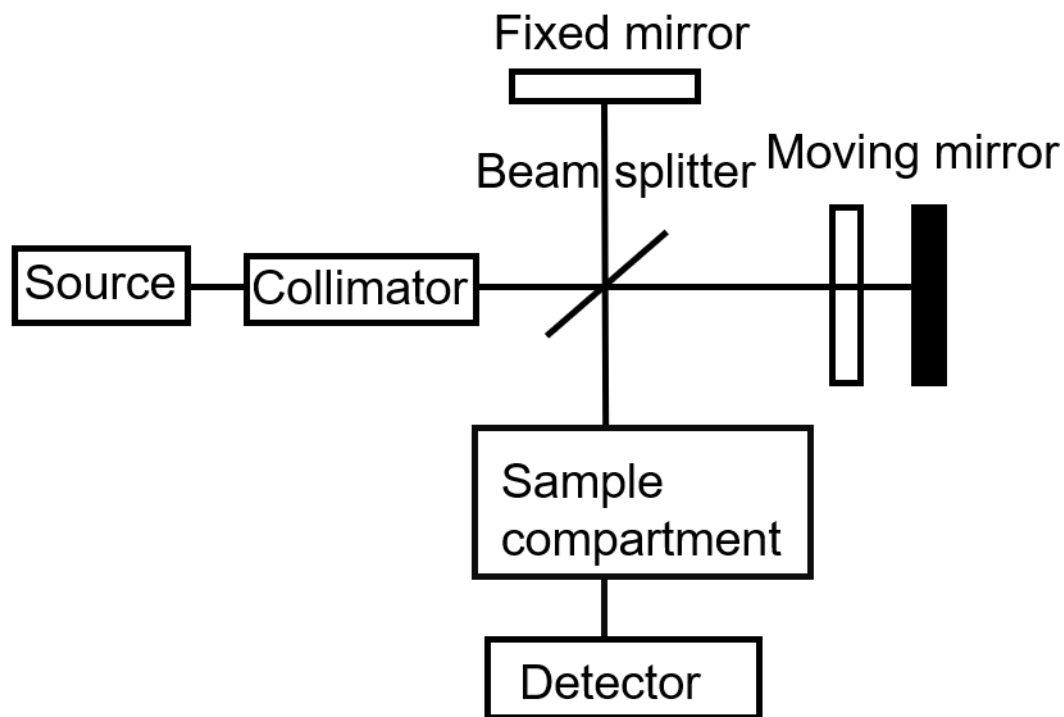
Figure 1.16 A brief illustration of FTIR spectrometer components (adapted from publication by Birkner [186])

As figure 1.16 indicates, a common FTIR spectrometer often contains an IR source, collimator, sample compartment, detector, beam splitter, fixed mirror, moving mirror, amplifier, A/D convertor and a computer. The sample is tested via radiation generated by the source which passes the sample via interferometer and then reaches the detector, followed by the amplifier and A/D convertor. This amplifies the signal and converts it to a digital signal. After that, the signal reaches the computer, where the Fourier transform is performed.

Fourier transform is a mathematical method to transform one function into a new function. The obtained interferogram is a plot of the intensity of signal versus optical path difference (OPD) and after the Fourier transform, a plot of intensity versus wavelength is generated, which forms the IR spectrum.

Tensile test

The mechanical properties of BC and BC nanocomposites are characterized by tensile testing of the materials tensile strength and elongation. Tensile tests are carried out according to the standard ASTM D638 with 1kN static load cell. Each sample is tested five times to achieve maximum accuracy.
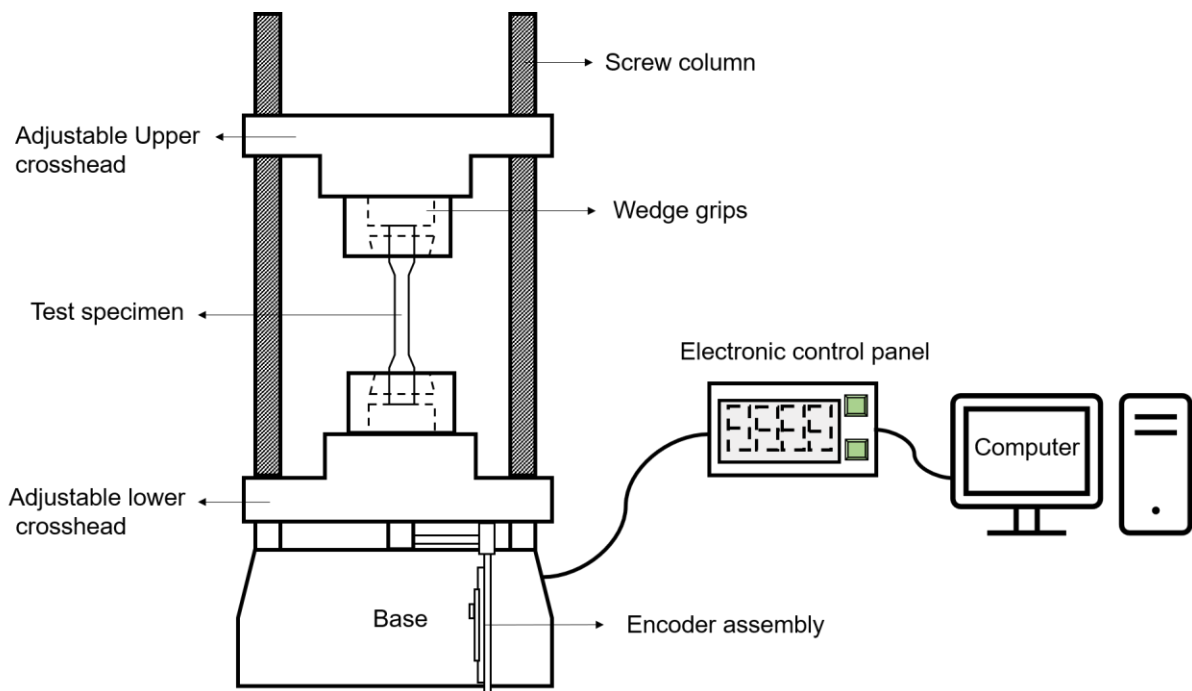
Figure 1.17 Schematic diagram of a tensile testing machine (adapted from Sabarinathan et.al [187])

Tensile testing provides information about the mechanical properties of materials in terms of the tensile strength (at yield and at break), Young's modulus, tensile strain, elongation and ductility, by measuring the force required to break a specimen by which it stretches or elongates to the breaking point. As figure 1.17 illustrates, the dog shaped specimen is fitted on the top and bottom by two cross pitch gripping jaws. During the test, loads are applied gradually with an increment of 0.1kN. The sample displacement is measured by a high-resolution encoder which transform signals to the computer. The tensile tests performed in this thesis are all in accordance to ASTM standard D638 and the hardware units of the machine initiated the related parameters of gauge length, width, thickness and loading rate.

In addition to tensile test, compression test also allow the assessment of materials mechanical behaviours. However, normally materials with high tensile strength tend to exhibit low compressive strength. Therefore, compression testing is applied on brittle materials and corrugated materials as they are often used in a load-bearing capacity and the materials integrity under compressive forces is essential[188].

Brunauer, Emmett and Teller (BET) surface area

The surface area and pore sizes of BC and BC nanocomposites are characterized by nitrogen gas (N_2) isothermal sorption technique at 77°K. The pressure changes in a known volume as a function of partial pressure of N_2, determining the amount of gas absorption on a surface to form mono or multi layers.

The specific surface area of a porous material is determined by physical adsorption of nitrogen gas on the surface by calculating the amount of absorbate gas resulting from Van der Waals forces between the adsorbate gas molecule and adsorbate porous

surface. The measurement is usually taken at the temperature of liquid nitrogen to allow the amount of adsorbate gas to be measured in a volumetric and continuous flow procedure.

The data results from the BET adsorption isotherm equation[189]:

$$\frac{1}{[V_a\left(\frac{P_0}{P}-1\right)]} = \frac{C-1}{V_mC} \times \frac{P}{P_0} + \frac{1}{V_mC}$$
(1.3.1)

Where P is the partial vapour pressure of adsorbate gas in equilibrium with the surface at 77.4 K (in liquid nitrogen), P_0 is saturated pressure of adsorbate gas, V_a is volume of gas adsorbed at standard temperature and pressure (STP), V_m is volume of gas adsorbed at STP to produce a monolayer on the sample surface, C is the dimensionless constant. For multi-point BET, in the P/P_0 range 0.025 to 0.30 can be used to successfully determine the surface area with a minimum of three data points (ideally five data points). When the relative pressure exceeds 0.5, the capillary condensation is onset whilst only a monolayer is formed at exceedingly low relative pressure. Therefore, the BET method is insufficient in obtaining data for the surface area if the graph is not linear with a positive slope. The monolayer capacity V_m and total surface area S, can be obtained using equations 1.3.2 and 1.3.3 below:

$$V_m = \frac{1}{s+i} = \frac{C-1}{C_8}$$
(1.3.2)

$$S = \frac{V_m L_{av} A_m}{M_v}$$
(1.3.3)

Where L_{av} is Avogadro's constant, A_m is the cross sectional area of the adsorbate, M_v is the molar volume. By setting the intercept to 0 as well as ignoring the value of C, single BET can also be applied over the more accurate multipoint BET in order to determine the appropriate relative pressure range.

Thermogravimetric analysis (TGA)
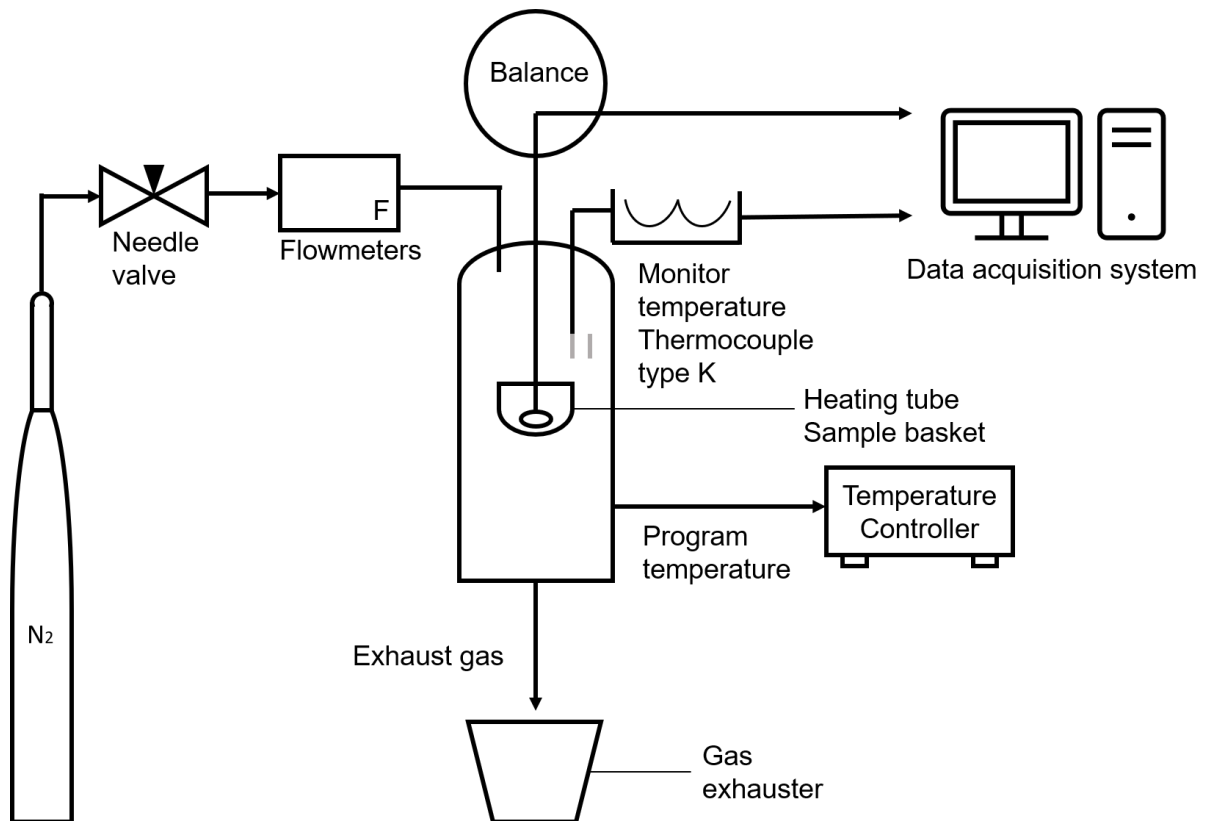
Figure 1.18 Schematic diagram of TGA (adapted from Unapumnuk et.al [190])

TGA is a thermal analyst used for monitoring the sample mass against time or temperature in a controlled furnace, where samples are analysed in a crescent or decreasing temperature at an isothermal temperature or a constant rate. As figure 1.18 illustrates, a TGA comprises the radiant heating chamber, microbalance, the furnace, gas feeding system, temperature controller, and a data acquisition system. Before and during the test, the mass of sample is measured on the highly sensitive microbalance when heated or cooled in the furnace controlled by a predetermined program[191]. A type K thermocouple placed in the middle of the heating system monitors the reaction temperature. Nitrogen gas is introduced via a nozzle at a controlled flow rate to purge gas in the heating system[190]. The plot of TGA curve

indicates specimen weight loss percentage against temperature which provides thermal decomposition behaviour with residue amount as a function of temperature.

In this thesis, TGA (10 mg test samples for BC/BC nanocomposites) (TGA Q1000, TA Instruments) were performed in an inert nitrogen atmosphere at a flow rate of 40 mL/min, heating rate of 10°C/min across a temperature range of 30 to 800°C.

Differential scanning calorimetry (DSC)
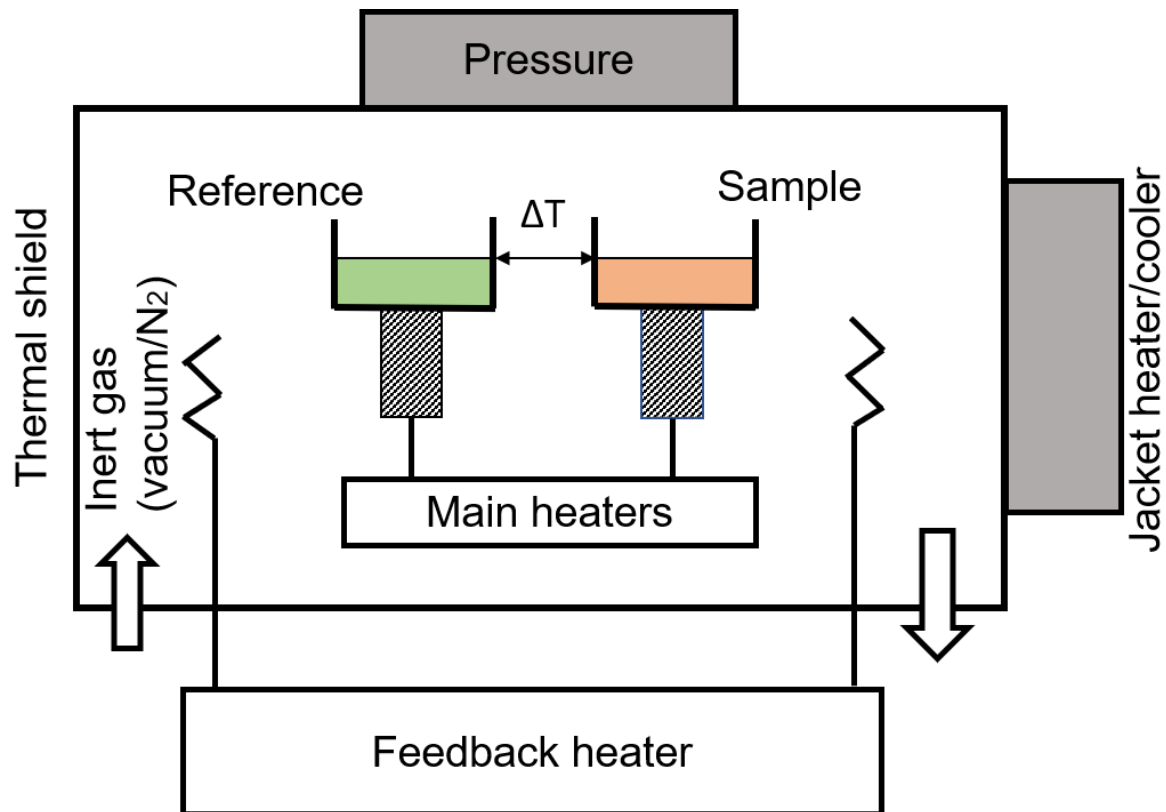
Figure 1.19 Schematic diagram of a heat-flux DSC (adapted from publication by Bibi et.al [192] and Rai et.al [193])

DSC is a widely used technique to analyse the thermal response of BC/BC nanocomposites by measuring changes in heat capacity due to exothermic or endothermic reactions. In thermal set polymer characterizations, DSC is used to identify the glass transition temperature thus determining the curing behaviour for monomers[194]. A heat-flux DSC is used in this work to characterize the thermal stability of BC/BC nanocomposites. Figure 1.19 shows the schematic diagram of a heat-flux DSC where two chambers (sample and reference) are heated at a controlled rate by the main heaters under nitrogen gas with constant pressure. As the thermal events occur, the temperature difference (ΔT) between two chambers is monitored and the feedback heaters keep the chambers in thermal balance. The power signal from

feedback heaters provides measurements of the heat capacity of the occurring thermal events. In this thesis, DSC was used together with TGA to measure the thermal behaviours of BC/BC nanocomposites.

X-ray powder diffraction (XRD)
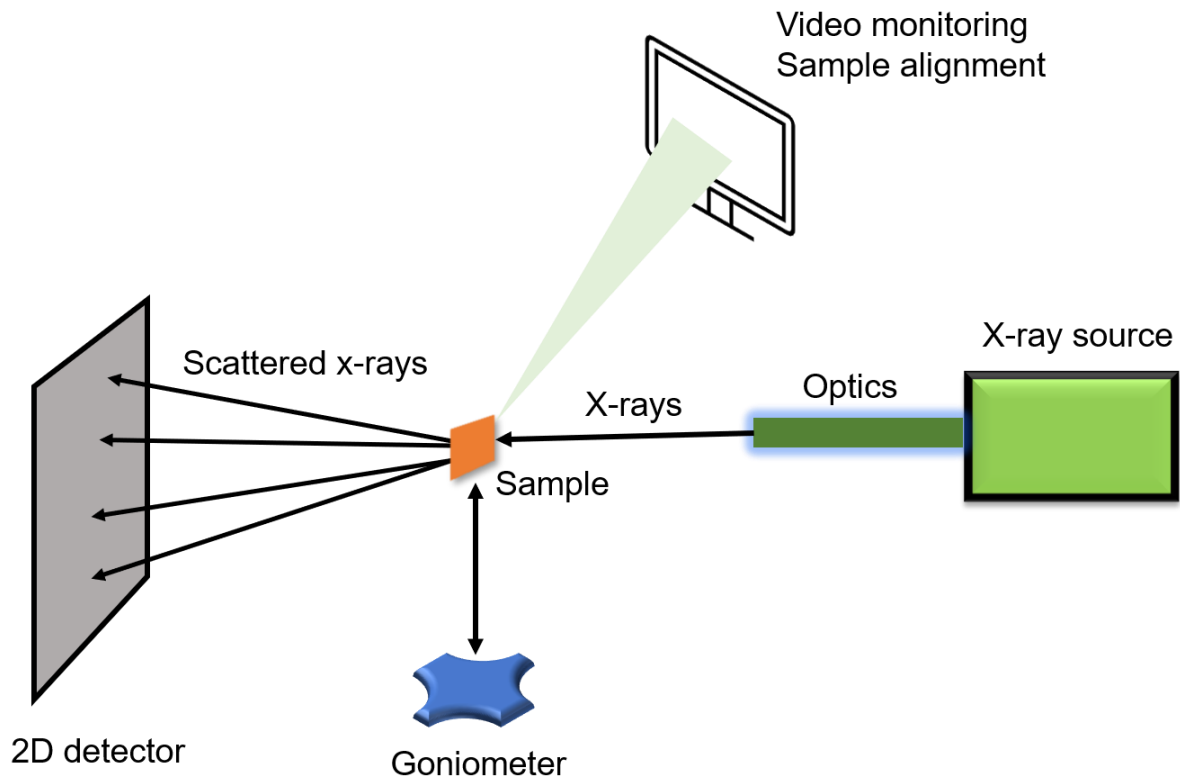
Figure 1.20 Schematic diagram of XRD (adapted from Gianfrancesco [195])

XRD is a highly versatile technique that has been used to provide chemical information for crystalline materials in terms of identification of a crystalline phase, structure, crystal orientation, average grain size and strain distribution. As figure 1.20 illustrates, XRD patterns are generated by a goniometer rotating at specific angles when the specimen is bombarded with X-rays. The distribution of atoms within the lattice in the specimen determines the peak intensities of the resultant diffraction pattern[195]. The crystal structure, degree of crystallinity and size of crystals of BC were investigated by XRD. Dried BC samples were ground into powder for testing by powder XRD. During characterization; the specimen is irradiated with an incident X-ray beam with a wavelength around 1.5 Å. When the specimen was impinged by an X-ray beam, a

crystal is reflected by the layers of atomic planes which diffract only a fraction of the incident X-ray amplitude[196].

The radiation source was Cu, which generated signals at 40kV and 30mA. The range of diffraction angle (2θ angle) was 3 to 40 degrees with a step size of 0.01. The crystallinity index (Crl) was calculated according to the published equation by Segal et.al[197]:

$$Crl = \frac{(I_{002} - I_{am})}{I_{002}} \qquad (1.3.4)$$

where I_{002} is the intensity at (002) peak and I_{am} is the minimum intensity between (101) and (002) peaks. Crystallite size (CrS) could be calculated by the Scherrer equation as following:

$$CrS = \frac{k\lambda}{\beta \cos\theta} \qquad (1.3.5)$$

where k is the shape factor (0.9), λ is the X-ray wavelength(1.54°A), β is the line broadening at half the maximum intensity (FWHM) in radians and θ is the Bragg's angle. The spacing of atomic planes which is also called lattice planes, relates to the Bragg's law which can be expressed as follows:

$$n\lambda = 2d \sin\theta \qquad (1.3.6)$$

In vitro biocompatible test

Biocompatibility of a biomaterial refers to the extent to which the material are not toxic or injurious in biological systems. It is important for biomaterials used in chronic wounds dressings to be submitted to a numerous pre-toxicity tests *in vitro* or *in vivo*. However, *in vitro* toxicity tests are preferable to *in vivo* test. The newly produced materials are examined outside the body in order to facilitate more reproducible clinical evaluations of a medicinal product to be replicated and estimated[198][199]. It is necessary for the biocompatibility of a biomaterial to be evaluated and characterized in the potential harmful effect before it is used on humans.

Traditional assays measured cytotoxicity by measuring the effects on cells during exposure to toxic substances at multiple concentrations and time. The colorimetric 3-(4,5-dimenthylthiazol-2-yl)-2,5-dipheyl tetrazolium bromide (MTT) assay is commonly used to investigate the detrimental intracellular effects on mitochondria and metabolic activities, utilizing the selective ability of viable cells to reduce tetrazolium bromide into organic-soluble purple formazan crystals. The cytotoxicity screening is used to investigate the extent of formazan crystal formation which depends on intact metabolic activity[200][201].

The cellular proliferation and cell viability assays are commonly used to monitor the response and health of cells when cultured with newly-produced material. Cell proliferation assays can be used to monitor the cells over time, the number of cell divisions, the metabolic activities or the DNA synthesis. The rate of proliferation and percentage of viable cells can be investigated using viability dyes such as trypan blue[200].

pH Sensitivity Test

A standard potentiometric electrochemical sensor is comprised of a working electrode (WE) and a reference electrode (RE)[202]. It analyses samples through direct measurement of electrochemical reactions. The fabricated pH sensor was connected in WE, and commercial AgCl/Ag is used as RE.

The principle of the measured pH is based on Nernst's law, where it is found that a potential difference occurs when a metal object is immersed into ionic solutions with the same metal[203]. The potential difference generated by the exchange of ions between metal and liquid, E, is given as:

$$E = E_0 + \left(\frac{RT}{nF}\right) \cdot In[M^+] \qquad (1.3.7)$$

Where R is the gas constant (=8.314JK^{-1}mol^{-1}), F is Faraday number (=96493 Cmol^{-1}), n is valency of the metal, [M$^+$] is the metal ion concentration, T is the absolute temperature in Kelvin, E$_0$ is the normal potential difference when the solution contains 1 mole [M$^+$] per litre. As hydrogen ions have similar properties to metal ions, this equation can be applied to the electrode which is immersed in a solution containing hydrogen ions. Therefore, this equation can also be expressed as:

$$E = E_0 + \left(\frac{RT}{nF}\right) \cdot In[H^+] \qquad (1.3.8)$$

The theoretical pH voltage sensitivity is 59 mV/pH with a Nernstian response of a 1:1 proton: electron process (T=298 K), which is known as the Nernst limit[203][204].
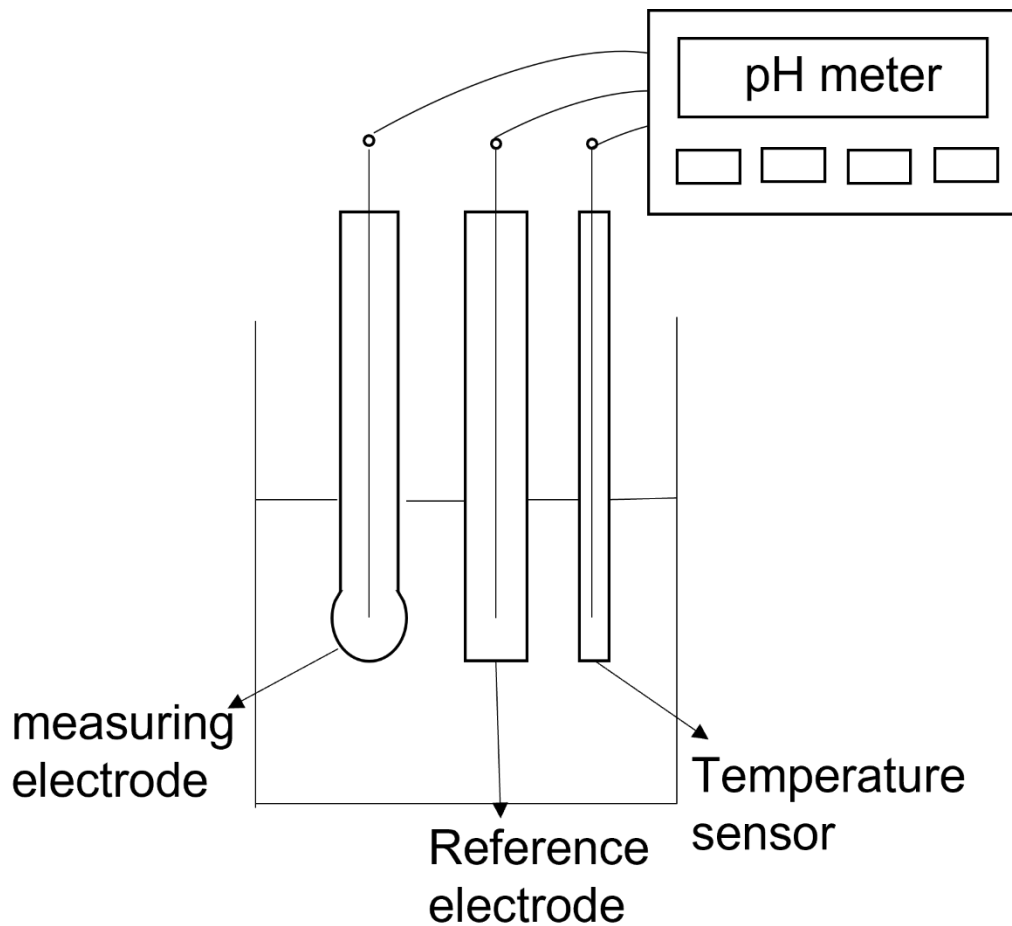
Figure 1.21 The pH measurement system

As figure 1.21 illustrated, a pH measurement system consists of a measuring electrode and a reference electrode. The voltage between the two electrodes is proportional to the pH of the test solution. The temperature determines the potential contrast, thus a temperature sensor is necessary to be put in pH measurement process. The heart of measuring electrode is a thin piece of pH sensitive glass where a potassium chloride buffered at pH 7 is sealed inside. The outer surface of pH sensitive glass contacts the solution being measured, and the inner surface of the glass contacts the filling solution while an electrical potential develops at glass-liquid interface. The pH of test solution is determined only by the measuring electrode potential. The reference electrode consists of the silver wire-silver chloride combination with the filling solution. A silver wire plated with silver chloride is used to contact the test solution. The potential of

reference electrode is determined on the chloride concentration in the filling solution, for the reason that the electrode potential is constant when the chloride concentration is fixed[205].

Ultraviolet-visible (UV-vis) spectrophotometer

UV-vis is a most commonly used technique applied to quantitative measurement of solutions to determine the concentrations of known solutes. When lights of known wavelength and intensity is passing through the measured sample, the final intensity is measured by a detector. The particular wavelength can be calculated by comparing the incident radiation (I0) and the transmitted radiation (I). The absorption is used to measure the concentrations of the known solutes by using the Beer-Lambert law:

$$A = log_{10}\left(\frac{I_0}{I}\right) = \varepsilon \times c \times L \tag{1.3.9}$$

Where A is absorbance, ε is the molar absorptivity (L/mol/cm), c is the concentration of the dissolved solute (mol/L), and L is the path length (cm)[206].

Chapter 2 Experimental Section

2   Experimental section

2.1 Preparation of BC samples

2.1.1 Bacterial strains for BC inoculation

Freeze-dried bacterial strains of *Gluconacetobacter xylinus* JCM 10150 were purchased from Sigma-Aldrich (UK) and provided by Professor Ipsita Roy, and *Komagataeibacter xylinus* DSM 2004, *Komagataeibacter xylinus* DSM 2325, *Komagataeibacter xylinus* DSM 16663 were purchased from Leibniz Institute DSMZ-German Collection of Microorganisms and Cell Cultures GmbH and provided by Professor John Ward. All reagents were purchased from Sigma-Aldrich (UK). Ultra-pure Milli-Q water with resistivity of 18 mΩcm^{-1} was used for medium preparation.

2.1.2 Culture medium for bacterial strains

Acetobacter medium was used in the cultivation of JCM 10150 with glucose (10wt./v.%) as the carbon source, yeast extract (1wt./v%) as the nitrogen source, CaCO$_3$ (3wt./v%) in 1L Milli-Q water. The pH of the medium was adjusted with HCl acid and NaOH solution at 5.5, and the growth temperature was 30°C using an incubator. For DSM 2325, DSM 2004, Gluconobacter oxydans medium was used to cultivate the strains of bacteria with glucose (10wt./v%), yeast extract (1wt./v%), CaCO3 (2wt./v%) in 1L distilled water, pH adjusted to 6.8 and a cultivation temperature of 30°C. Gluconacetobacter rhaeticus medium was used to cultivate DSM 16663, where the medium includes glucose (5%wt./v%), yeast extract (0.5wt./v%) in 1L Milli-Q water, with cultivation temperature at 30°C and pH adjusted to 6.5. Prior to cultivation, the culture medium was sterilized in an autoclave at 121°C for 15 min and freeze-dried bacterial strains were taken out and inoculated in a 1000 ml Erlenmeyer flask containing 300 ml of culture medium. A small amount of bacteria was inoculated in 50

ml flasks with 10 ml culture medium to maintain the viable bacterial population. Then the flasks were placed inside a 30°C incubator for 5-7 days, while the small flasks for bacterial population were only incubated for 3 days and put into a refrigerator for bacterial stock. After 5-7 days of static growth, BC pellicles produced from different culture conditions were collected and washed with distilled water, followed by heating in 1M NaOH solution at 75°C for 2 h to be purified and further washed with Milli-Q water until neutral pH was reached. Purified BC pellicles were observed in a light microscope to confirm there are no bacteria remained on the surface. Purified BC pellicles were stored in 4°C in deionized (DI) water for further use. Prior to characterization, BC pellicles were cut into 3*3 cm square and freeze-dried with liquid nitrogen overnight. The size and thickness of each sample was measured by a calliper.

2.1.3 Antimicrobial BC nanocomposites

Pure BC has no antimicrobial properties, as discussed in the introduction section of this thesis. Therefore, in order to study the BC based nanocomposites for antimicrobial wound dressing purposes and evaluate different antimicrobial activity, BC films produced by *K. xylinus* DSM 16663 were incorporated with different antimicrobial agents/materials. In this part, the incorporated antimicrobial agents/materials were divided into organic and inorganic groups. For organic BC nanocomposites, BC/Methylglyoxal (BC/MGO) and BC/polydopamine/eggshell membrane (BC/PDA/ESM) were synthesised and were main composites studied in this chapter while BC/lysozyme was synthesized to make comparison with main nanocomposites, while in inorganic nanocomposite materials, BC/silver nano-particles (BC/AgNP) were synthesised to make comparison with main nanocomposites. In this chapter, bio-

inspired BC/MGO and BC/PDA/ESM nanocomposites were proposed for the first time. The thickness and size of all samples were measured by a calliper.

(1) BC/AgNP
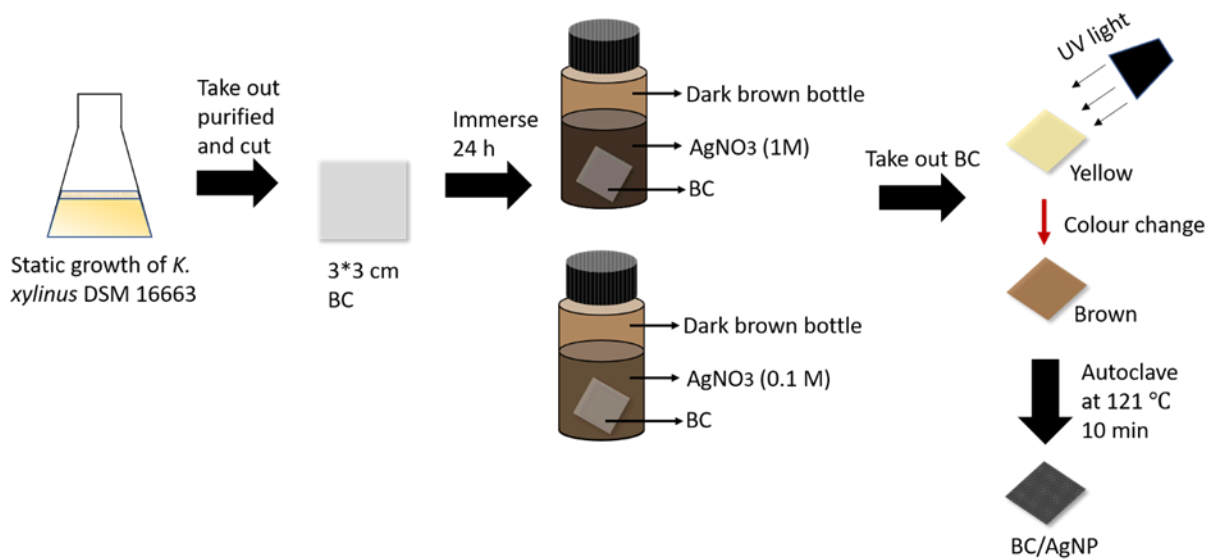
Figure 2.1 Fabrication process of BC/AgNP (1M and 0.1M).

Figure 2.1 illustrates the fabrication process of BC/AgNP (1M and 0.1M) nanocomposite. This method was based on a publication by Li et.al [207]. BC was prepared by static growth from *A. xylinus* DSM 16663 and taken out after 7 days of cultivation. After purification, the BC pellicle was cut into the 3*3 cm square shape and stored at 4°C for further usage. The BC samples were immersed in 10 mL of silver nitrate ($AgNO_3$) solutions (with concentration of 0.1 M and 1 M in DI water) for 24 hours.

The BC samples were turned from yellow to brown in colour which indicates the AgNP formation. A UV lamp can also be used to increase the speed of the colour change. After impregnation, the positive charged Ag ions were bonded to negative charged BC fibers and become AgNP after the exposure of UV light[208]. Then the BC samples were autoclaved at 121°C for 10 min at 0.103 MPa. During the autoclave treatment, the silver ions were reduced by cellulose end aldehyde and alcohol groups. All samples were washed with DI water to remove the excess chemicals and stored in 4°C. Before the disk diffusion test, the samples were punched by a biopsy punch into 6 mm round shaped samples. For other characterizations, samples were freeze-dried using a -50°C vacuum based freeze-dryer. During the autoclave process, the silver ions can be reduced by cellulose aldehyde and alcohol groups. The resulting BC/AgNP samples were dark and dry.

(2) BC/lysozyme
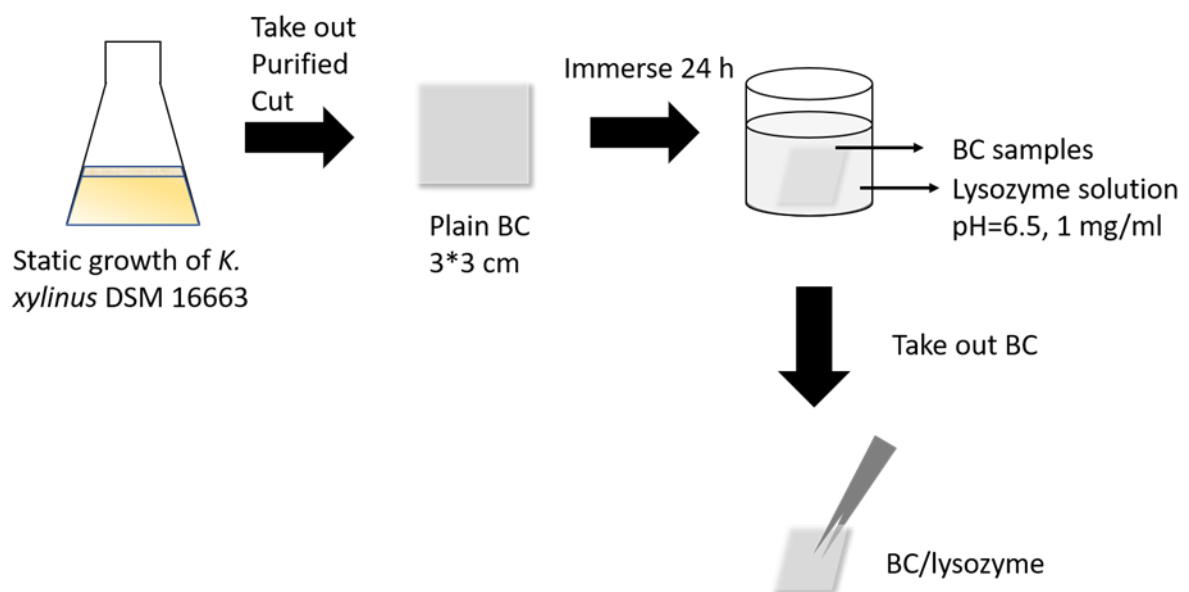
Figure 2.2 Fabrication process of BC/lysozyme nanocomposite.

Figure 2.2 shows a schematic of the BC/PDA/ESM fabrication process. Pellicles were taken from the same culture medium and cut into the 3*3 square shape as described above. Lysozyme enzyme and phosphate buffer (pH = 6.24, 0.1M) were obtained from Sigma-Aldrich (UK). The method was based on work by Bayazidi et.al [209].1 mg/ml concentration of enzyme was prepared using 0.1 M phosphate buffer solution. BC samples were immersed in a prepared lysozyme solution and stored at 4°C for 24 hours. After punching into 6 mm round shaped samples, the BC samples were stored in DI water at 4°C until further usage. The resulting BC/lysozyme sample exhibited the same colour as the plain BC sample, which was semi-transparent.

(3) BC/PDA/ESM
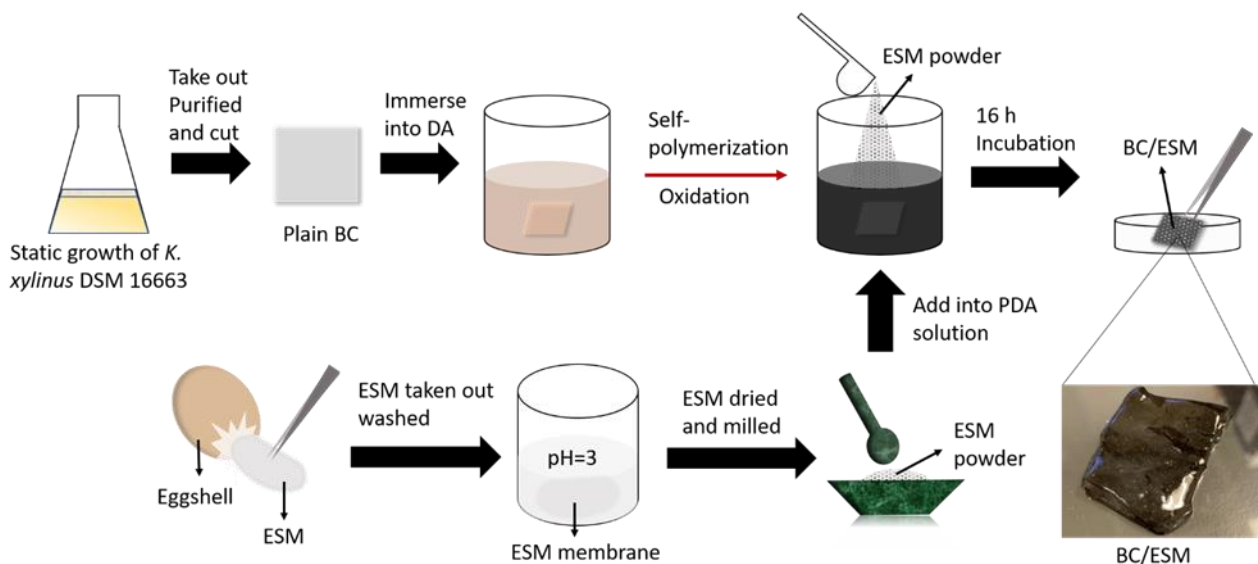
Figure 2.3 A schematic of the fabrication process of BC/PDA/ESM nanocomposite.

Figure 2.3 illustrates the fabrication process of BC/lysozyme nanocomposite. Hen eggs were purchased from Tesco (UK). Dopamine hydrochloride was obtained from Sigma-Aldrich (UK). The method was based upon published work by Liu et.al [210]. Fresh eggshells were cleaned with Milli-Q water (18.2 mΩ-cm) and ethanol. Then the

inner ESM were carefully removed from the eggshells using forceps. The obtained ESM were washed with deionized (DI) water 3 times, cut into small pieces (10 × 10 mm), and then immersed into DI water or an aqueous solution with a pH value of 3 for 72 hours to dissolve residual calcium carbonate compounds and collagen. The samples were then ground into powder. BC pellicles were cleaned with DI water, and went through heating and immersion in DA solution at room temperature for 16 h. The DA treated BC were incubated with an aqueous EM powder solution at 1mg/ml concentration for another 18 h in darkness at room temperature. Finally, the composite pellicles were washed with DI water and dried at room temperature. The resulting BC/PDA/ESM formed a dark, gel-like membrane with white powder on the surface.

(4) BC/MGO
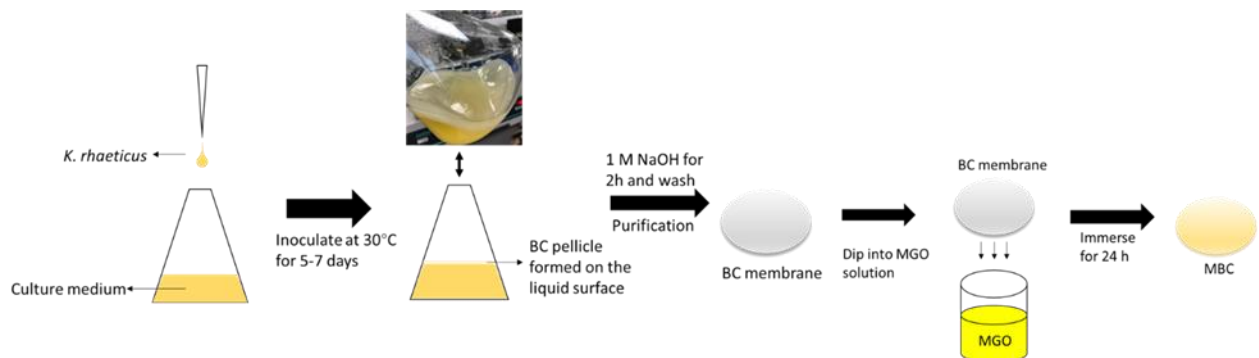
Figure 2.4 Fabrication process of a BC/MGO nanocomposite.

Figure 2.4 illustrates the fabrication process of a BC/MGO nanocomposite. The BC samples were taken from the same culture conditions of *K. xylinus* DSM 16663 as described before. The purified BC pellicles were cut into 3*3 cm squares before dip-coating in 20 ml 4% (v/v) MGO solution in DI water, 0.4% (v/v) MGO solution and 0.04% (v/v) MGO solution for 48 hours. The samples were named BC/MGO (4%), BC/MGO (0.4%), and BC/MGO (0.04%). The prepared samples were stored in 4°C and

remained in a wet state until further use in tensile testing. For the disk diffusion test, the wet samples were punched into 6 mm round-shape discs. The samples were freeze-dried in a -50ºC vacuum based freeze dryer for SEM, FTIR, and AFM characterization. The freeze-dried samples were more yellow and had a stiffer surface than plain freeze-dried BC, whilst the shrinkage remained the same.

2.2 Preparation of a BC based flexible sensor

2.2.1 Conductive BC aerogels

The purified BC pellicles grown from *G. xylinus* JCM10150 bacteria strain were cut into 3*3 cm and frozen in liquid nitrogen (-196ºC) before being freeze-dried in a bulk tray at -48ºC with a pressure of 0.04 mbar overnight. The freeze-fried BC aerogels were pyrolyzed in a tube furnace with flowing argon under 600-800ºC to generate black, ultralight pyrolyzed BC (p-BC) aerogels. Another method was also used in the freeze-drying process, where plain BC pellicles were immersed in tert-butanol solution and stirred. The tert-butanol solution was replaced three times, every two hours to exchange the water in the BC pellicles. The treated BC pellicles were stored in a freezer (-15ºC) for 24 hours before being placed in a freeze-dryer. Commercial melamine foam was pyrolyzed in the same way for comparison.

2.2.2 p-BC/PDMS/PANI nanocomposite for pH sensing

Polyaniline ink was prepared in accordance with a publication by Rahimi et.al[99]. The polyaniline emeraldine base in 25 ml dimethyl sulfoxide solution was prepared to ensure a uniform coating and was stirred in HCl solution in a vacuum chamber for 5 hours. Prior to coating, Polydimethylsiloxane (PDMS) was diluted with 50%

cyclohexane at weight ratio 1:1 and the resulting p-BC/PDMS/PANI nanocomposite was fabricated by infiltrating p-BC with a mixture of PANI ink and PDMS prepolymer which is a viscous mixture of base/curing agent (10:1). Finally, the p-BC coated with PDMS/PANI composite was degassed in a vacuum oven for 30 min and cured at room temperature for at least 24 hours. Carbon paper and pyrolyzed melamine foam which were used as comparison groups were also used in the same coating procedures.

2.3 Characterization

2.3.1 Structural characterization

1) SEM and EDX

A ZEISS Ultra 55 Field Emission Gun Scanning electron microscope (FESEM) (Germany) was used to take images of the surface morphology of samples. Prior to SEM characterization, freeze-dried samples were cut into small pieces (approximately 1*1 cm) were coated with gold of 20 nm thickness *via* a sputter. For conductive samples; p-BC and p-BC/PDMS/PANI nanocomposite, SEM characterization was taken without gold coating. Energy-dispersive X-ray spectroscopy (EDX) (ZEISS, Germany) analysis was taken during the SEM imaging with a sample distance of 8.5 mm.

2) AFM

Freeze-dried samples with dimensions of 3*3 cm were characterized using an AFM (Bruker Dimension Icon with ScanAsyst, USA) with tapping mode to give more details on the surface morphology and surface roughness.

3) XRD

The crystalline structure of freeze-dried samples with dimensions of 3*3 cm were characterized using a powder XRD (Bruker D8 Discover Diffractometer). The radiation source was Cu at 40kV and 30mA. The diffraction angle range (2θ angle) was 3 to 40 degrees with 0.01 step size.

4) BET

The surface area, pore size and pore volumes of samples were investigated using a BET analyser (NovaTouch, Germany). Prior to characterization, the samples were cut into a tiny piece with dimensions around 0.5*0.5 cm. freeze-dried using nitrogen at 77k in a gas sorption system, followed by degassing at 200 °C under reduced pressure before each measurement. In the analysis process, degassed BC sample was added dead volume with Helium and then vacuumed again. After experiencing adsorption isotherm in nitrogen gas, BC sample went through desorption process where nitrogen gas was evacuated for desorption isotherm. Novatech 5.0 software was used to collect the adsorption and desorption rate and then analyse all the parameters.
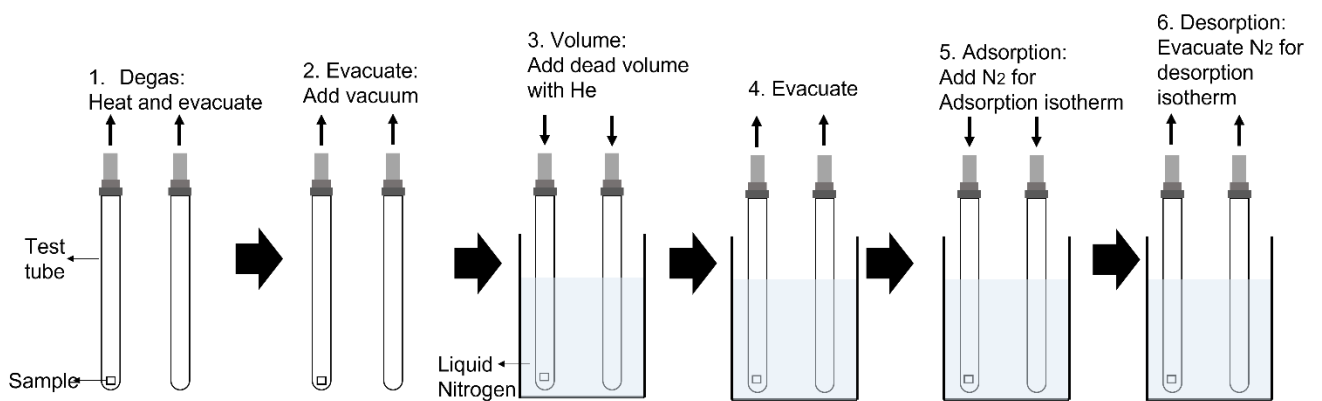
Figure 2.5 The measuring process of BET (adapted from the publication[211])

2.3.2 Chemical composition characterization

1) FTIR analysis

The chemical composition of freeze-dried samples was grounded into powder. analysed by a FTIR spectrometer (Perkin Elmer, USA) at wavelengths ranging from 400-4000 cm^{-1} at a resolution of 2 cm^{-1}. Samples were cut into tiny chips and scanned for 5 min for investigation of the spectrum of transmittance versus wavelength.

2.3.3 Thermal analysis

1) TGA analysis

The thermal stability and thermal degradation of samples were carried out by TGA analysis (Perkin-Elmer 2000, USA) under a continuous nitrogen flow of 70 mL min^{-1}. Prior to testing, samples were chopped into tiny chips and 10 mg of sample was placed into the system for testing across a temperature range from 30°C to 800°C at a heating rate of 10°C per minute.

2) DSC analysis

The thermal behaviour of samples was characterized by DSC analysis (Perkin-Elmer, USA), which monitors the difference of the power output between a sample and a reference pan. The measurements were carried out in a nitrogen flow of 70 mL min^{-1}, across temperatures from 30°C to 500°C at a heating rate of 10°C/min. Prior to testing, samples were grounded into powder and 10 mg of samples were weighed and sealed in an aluminium pan. The thermal cycle of samples being tested was analysed.

2.3.4 Mechanical tests

1) Tensile tester

The tensile strength of wet samples was tested by an Instron tensile tester (Instron 3400, UK) equipped with a 10kN load cell. Prior to testing, samples were cut into a dumbbell shape with a gauge length of 10 mm according to ASTM D882 standard. The thickness and width of each sample is measured by a vernier calliper. The tissue paper is used to absorb extra moisture for each sample to be firmly clamped on the machine. The test for each sample was carried out at least five times with a cross-head speed of 1 mm/min.

2.3.5 Samples wettability

1) Estimation of water absorption capacity (WAC)

The moisture sorption behaviour of samples (3*3 cm in dimension) was investigated by immersing BC samples in DI water at room temperature and measuring the weight after removal of excess water on the surface. The samples were dried in an oven at 50^oC overnight before testing. The moisture sorption was assessed by weight change, and the final moisture content of a sample was:

$$WAC(\%) = (\frac{W_1 - W_0}{W_0}) \times 100 \qquad (2.1)$$

Where W_1 is the samples mass (g) in wet BC and M_0 is dry weight (g) of BC.

The test was performed in triplicate.

2) Release profile in water

In order to investigate MGO release in water, BC/MGO (4%) sample (3*3 cm) which loads the most MGO solution among three samples was placed into 30 ml DI water and the aliquots (4 ml) of the supernatants were collected after 0, 0.5,1,2,3,4,5,24,30,

and 48 h. The sampling volume was not replaced after each collection and the concentrations of MGO in supernatants were measured by a Lambda 850+ UV/Vis spectrophotometer (PerkinElmer, USA). For sample saturation test, BC/MGO (4%), BC/MGO (0.4%) and BC/MGO (0.04%) (3*3 cm) were taken out after 24 and 48 h of static impregnation and the absorbed liquid was squeezed out and measured by spectrophotometry for MGO concentrations. The tests were performed in triplicate.

2.3.6 Antimicrobial test

1) Disk diffusion test

The antimicrobial activity of BC nanocomposites and control groups were tested by a disk diffusion test against four common pathogenic bacteria in chronic wounds as discussed in chapter 1 section 1.2.1; *Micrococcus luteus* (*M. luteus*) NCIMB 1327, *Pseudomonas aeruginosa* (*P. aeruginosa*) DSM 8626, *Staphylococcus aureus* (*S. aureus*) DSM 111729, and *Escherichia coli* (*E. coli*) DH5α. The test was performed by a standard Kirby–Bauer Disk Diffusion Susceptibility Test Protocol. Prior to testing, samples were punched into 6 mm round-shaped discs by a biopsy puncher. Around $1*10^5$ CFU per plate test bacteria were cultured and prepared from Luria-Bertani (LB) broth overnight and spread onto LB agar plates during the test. The samples were tested against positive control samples which were dipped with Kanamycin (50 mg mL^{-1}) and Ampicillin (50 mg mL^{-1}), and control samples of plain BC. The specimen was placed into a bacteria-spread LB agar plate and marked. After 24 hours cultivation at 37°C in an incubator, the plates were taken out and the diameter of inhibition zones was measured using a ruler. The tests were performed in triplicate.

2.3.7 Electrical conductivity and pH sensing tests

1) Electrical conductivity test

The electrical conductivity of p-BC and p-BC/PDMS nano-composites with dimension of 1*1*cm and thickness of 0.1 cm was measured by a PalmSens4 potentiostat (Palmsens BV, Netherlands) at room temperature in air. The sample size was measured by a standard calliper. In the test, the current and output voltage of each sample was measured, and the electrical conductivity was calculated. This test was performed in triplicate.

2) pH sensing test

The pH sensing test was carried out to investigate the pH sensitivity of samples (with dimension of 1*1 cm, and thickness of 0.1 cm). This was measured by an Autolab potentiostat (Metrohm, UK) at room temperature in air via open-circuit potential measurement with different pH solutions (from 4-10) (Sigma-Aldrich, UK), which is the pH level range associated with chronic wounds. A commercial Ag/AgCl reference electrode (Metrohm, UK) was used for measurement, and a platinum electrode (Metrohm, UK) was used as the counter. As figure 2.5 illustrated, the pH sensor was clamped by an electrical connector and connected with a working electrode, immersed partially in test solution. *In vitro* pH sensitivity testing was performed in simulated wound fluid; composed of diluted phosphate buffer solution (PBS) and Male AB human serum from the USA (Sigma-Aldrich, UK) in a 1:1 ratio. The test was performed in triplicate.
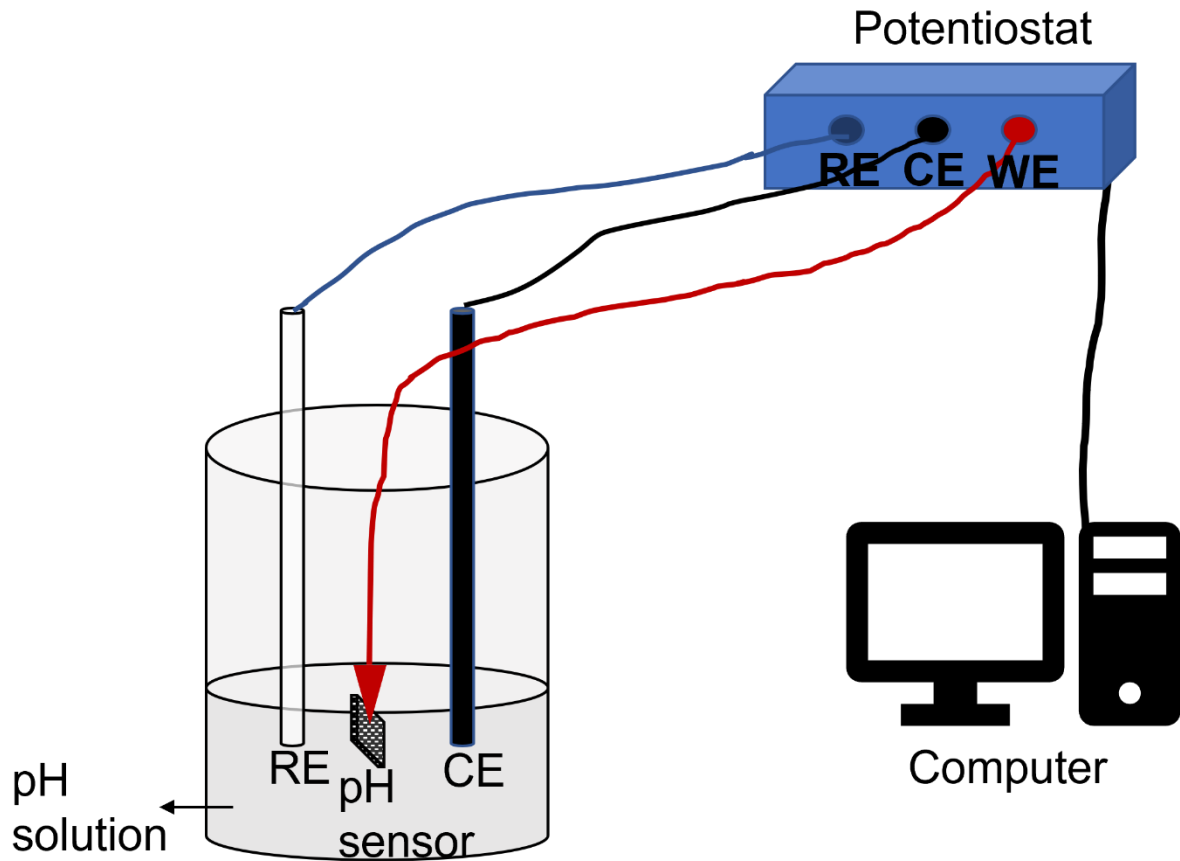
Figure 2.6 Illustration of setting of the pH sensitivity test

2.3.8 *In vitro* biocompatibility test

1) Culture of human dermal fibroblasts (HDF)

The procedures followed are standard operating procedure ISO (the International Organization for Standardization) 10993-5:2009. Previous HDF cell (Sigma Aldrich, UK) cultures were checked by a microscope to confirm there was no bacterial or fungal contamination, and the spent medium was removed. The cell monolayer was washed with phosphate buffer saline (PBS) (pH 7.4, 0.01M, Sigma Aldrich, UK) twice before the trypsin (Trypsin-EDTA 1× including phenol red: 10.62 mg/L, NaHCO3: 350 mg/L, Sigma Aldrich, UK) was pipetted onto the washed cell monolayer. The Corning® cell-

culture flask (Sigma Aldrich, UK) was returned to the incubator and left for 10 min, followed by examination of the cells *via* a microscope to ensure the cells were detached and floating. The attached cells were released by gently tapping the flasks. The cells were re-suspended in a small volume of fresh medium (EmbryoMax M2 medium 1x, Sigma Aldrich, UK), inactivating the trypsin and centrifuged at 2000 rpm before cell counting (Corning® cell counter, Sigma Aldrich, UK). The number of cells were inoculated in fresh medium flasks (Corning® cell-culture flask, Sigma Aldrich, UK). The BC samples were punched into disk shapes with 6 mm in diameters to be fit into a 96-well plate. A Corning® 96-well plate (Sigma Aldrich, UK) was used to seed BC samples with HDF cell cultured, with 25,000 cells/mL(20 µl), 10,000 cells/mL(10 µl) and 5,000 cells/mL(5 µl) on BC samples of different thickness (0.8 mm and 3 mm), respectively. The 96-well plate was then placed into a 37°C incubator for 48 hours.

2) Phase-contrast light microscopy characterization of cells growth on BC

A phase-contrast light microscope (Agar Scientific Ltd, UK) was used to characterize the HDF growth on BC.

2.3.9 *Ex vivo* stitching test

In order to further investigate whether wet BC nanocomposite (with dimension of 3*3 cm and thickness of 0.1 cm) was a suitable skin substitute for larger and deeper chronic wounds, an *Ex vivo* stitching test was carried out by collaborators on the skin of the belly of a three-year old dead pig to assess whether BC/PDA/ESM nanocomposite is suitable for being sewed onto skin thus allowing the further potential application of temporary skin substitute. This test is to simulate temporary skin substitute being sewed onto the skin. The suture size used in this experiment was USP (United States Pharmacopeia) 3-0. As with the surgical stitching process, a surgical thread was carried by a needle and used to sew BC samples on the surface of skin. After stitching on four sides, a hooked tweezer was used to grip and stretch the stitched BC sample via multi-directional force to test the mechanical behaviour. After 10s testing both compression and stretching, repeated multiple times, the BC sample was photographed and compared with the original sample.

Chapter 3 BC Production

3 BC production

3.1 Introduction

3.1.1 Aims and objectives

The aims of the work in this chapter were to present the bio-synthesis of BC grown from different *Acetobacter* bacteria strains and investigation of the important parameters which can affect the materials properties, to optimize the production of BC materials.

The objectives of the work in this chapter were:

1) Fabrication of BC pellicles by static growth from *Gluconacetobacter xylinus* JCM10150, *Komagataeibacter xylinus* DSM 2004*, Komagataeibacter xylinus* DSM2325, and *Komagataeibacter xylinus* DSM16663, and comparison of different BC properties

2) Characterization of BC morphology of the nano-porous network structure, chemical composition, BET surface area, surface wettability, thermal stability and estimation of the water absorption capacity.

The present chapter describes different BC materials cultured from different bacteria strains and their comparisons. In this chapter, BC samples produced from four different bacteria strains and comparisons in terms of different materials properties are proposed for the first time.

3.1.2 Introduction

BC is a nanofibrillar polysaccharide which can be produced by diverse bacteria in both static and shaking culture conditions. As different carbon sources exist in different bacterial culture mediums, the product efficiency may differ. In theory, carbons which induce bacterial metabolism in glucose can be used for BC production[212][213][214]. BC can be produced as an extracellular proactive layer of the bacteria including *Acetobacter*, *Azotobacter*, *Agrobacterium*, *Achromobacter*, *Aerobacter*, *Sarcina*, *Salmonella*, *Rhizobium*, and *Escherichia*[215]. The most well-known bacterial species for BC production is the group of *acetobacter* bacteria; *Komagataeibacter xylinus (K. xylinus)*. This types of bacteria is classified as α-*proteobacteria*[216]. However, *K. xylinus* is not the only species that produces BC, other species in acetobacter such as *Komagataeibacter hansenii (K. hansenii)*, *Komagataeibacter medellinensis*, *Komagataeibacter nataicola*, *Komagataeibacter oboediens*, and *komagataeibacter rhaeticus (K. rhaeticus)*, have been proven as strong BC producers[217][218][219][220]. Studies show that *Acetobacter* sp.A9 strain isolated from apples can produce maximum 2.2g/L BC [221], and *k. hansenii* P2A in shaking conditions can produce 3.25 g/L BC[222], and *k. rhaeticus* strain P 1463 extracted from Kombucha can yield 4.4 g/L BC under static conditions[223]. The carbon sources used in the culture medium can affect the BC water-holding capacity, porosity, crystallinity index and mechanical properties[214]. It has been shown that whilst BC production can be improved via addition of ethanol and acetic acid to culture medium, this can decrease the crystallinity index, which reflects an inferior mechanical strength[224]. It has been reported that improved BC production can also be achieved by addition of vitamin C into the culture medium[225]. In addition, keeping the pH of the growth medium at an

optimal level by adding buffers can contribute to an increased yield of BC[219]. In the literature, *G. xylinus* and *K. xylinus* are the most common bacterial strains used for BC production. Though both static and agitated culture are commonly used in BC production, the static growth is a traditional method where cellulose is formed in the form of a gelatinous pellicle at the interface between air and liquid[226].

In this chapter, BC samples produced from four Acetobacter bacteria strains *Gluconacetobacter xylinus* (*G. xylinus*) JCM10150, *Komagataeibacter xylinus* (*K. xylinus*) DSM 2004, *K. xylinus* DSM2325, *K. xylinus* DSM16663 were characterized and compared in terms of surface morphology, chemical structure, crystallinity, thermal behaviour and an *in vitro* cell biocompatibility test.

3.2 Results and Discussions

3.2.1 BC fabrication
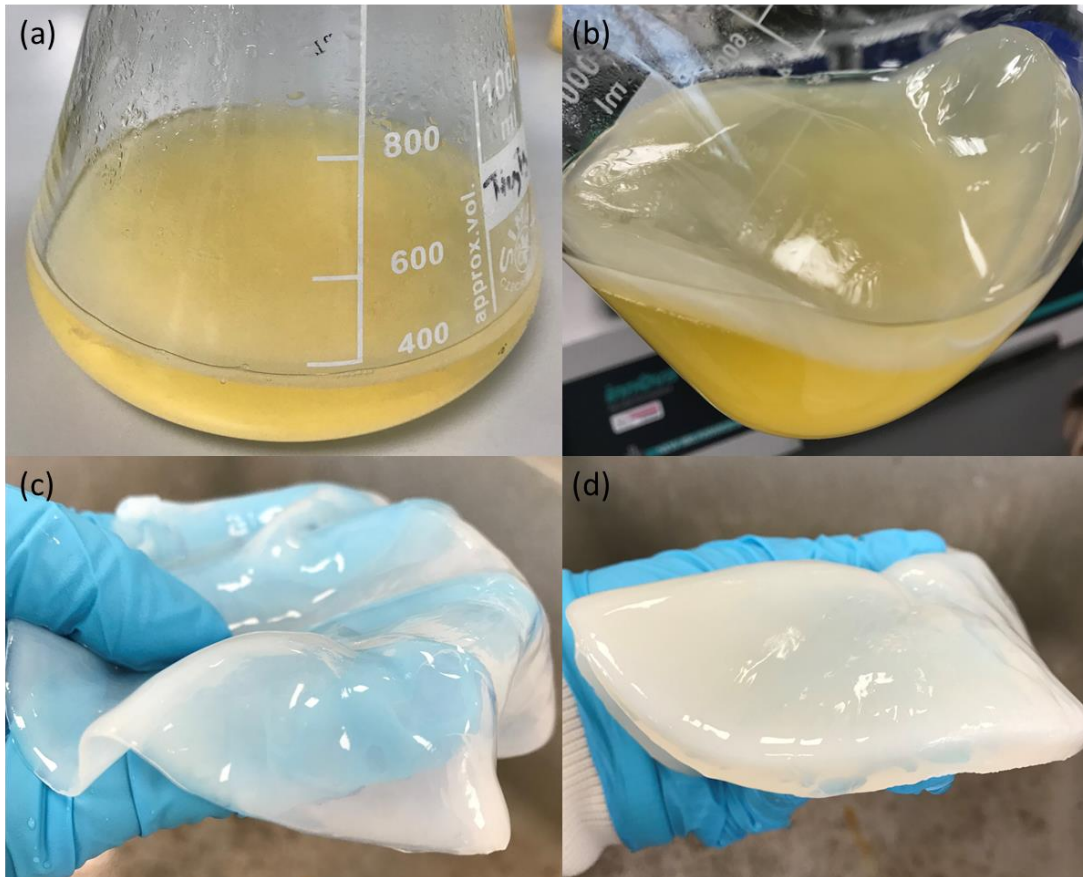
Figure 3.1 Cultured BC in acetobacter medium from *G. xylinus* 10150 (a) after 3 days, (b) after 5 days; BC pellicles after purification (c) taken out after 3 days of growth, (d) taken out after 5 days of growth.

Figure 3.1 shows the BC grown from *G. xylinus* 10150 over different time-periods. As indicated in the figure, a thin layer of BC can be grown after three days static cultivation, and after five days growth, a much thicker BC pellicle was obtained. The thickness of BC pellicles were additionally measured, where three-day incubated BC had a thickness of 0.15-0.25 mm while the thickness of five-day incubated BC could reach

an ultimate length of up to 0.75-0.8 mm. It was obvious that BC grown on the surface layer of the medium turned out yellow and semi-transparent, whilst after removal and purification, the BC pellicles became pale and more transparent. Figure 3.1 (d) illustrates that *G. xylinus* 10150 could grow BC pellicles with great thickness and high density, with good potential for mass production.
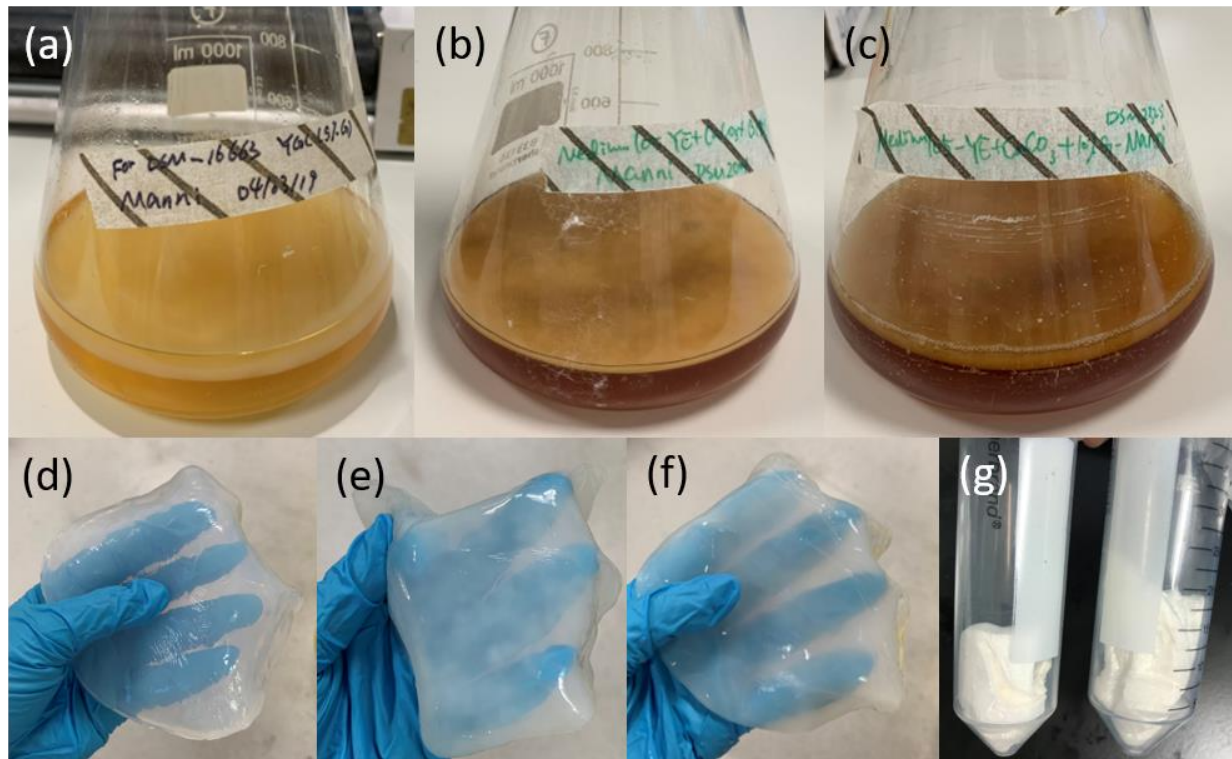
Figure 3.2 Cultured BC in (a) gluconacetobacter rhaeticus medium from K. xylinus DSM 16663 for 5 days, (b) gluconobacter oxydans medium from *K. xylinus* 2004 for 7 days, (c) gluconobacter oxydans medium from *K. xylinus* 2325 for 7 days; BC pellicles after purification (d) taken out after 5 days of cultivation from *K. xylinus* DSM 16663, (e) taken out after 7 days of cultivation from *K. xylinus* DSM 2004, (f) taken out after 7 days of cultivation from *K. xylinus* DSM 2325; (g) freeze-dried BC samples from *K. xylinus* DSM 16663.

BC pellicles grown from three other bacterial strains; *K. xylinus* DSM 16663, *K. xylinus* DSM 2325 and *K. xylinus* DSM 2004 are shown in Figure 3.2. In comparison with *G. xylinus* JCM 10150, these three strains required a longer culture time to achieve their

ultimate yield, where *K. xylinus* DSM 2325 and 2004 required a longer culture time than *K. xylinus* DSM 16663. In addition, the daker medium colour of *K. xylinus* DSM 2325 and 2004 indicated the reaction of glucose and calcium carbonate in the culture medium during the high temperature sterilization process. Meanwhile, Figure 3.2 (d), (e) and (f) shows that a thicker, denser, clearer and more transparent BC pellicle was formed in the *K. xylinus* DSM 16663 culture. Handling the BC pellicles showed that BC grown from *K. xylinus* DSM 16663 was stiffer and more solid than BC grown from the other two strains, while it was much the same compared with BC grown from *G. xylinus* JCM10150. Figure 3.2 (g) showed the freeze-dried BC samples of *K. xylinus* DSM 16663, which indicated that it retained most of the thickness as wet status, forming ultra-light and foam-like aerogels. The measurement of BC production and water holding capacity by four different bacterial strains is shown in Table 3.1 Compared with *K. xylinus* DSM 2004 and 2325, *G. xylinus* JCM 10150 and *K. xylinus* DSM 16663 yielded a larger quantity of BC (1.69 and 1.72 g/L) with a higher water retention capacity (99.4 and 99.3%). The detailed analysis of BC structures and properties were described in the characterization section.

Table 3.1 BC production from different bacterial strains and calculated water holding capacity.

Bacterial strain	BC yield (g/L)	WHC (%)
G. xylinus JCM 10150	1.69 ± 0.02	99.4 ± 0.01
K. xylinus DSM 16663	1.72 ± 0.05	99.3 ± 0.01
K. xylinus DSM 2004	1.18 ± 0.1	98.6 ± 0.02
K. xylinus DSM 2325	1.19 ± 0.1	98.6± 0.01

3.2.2 BC characterization

1) Surface morphology and chemical composition

The surface morphology of BC pellicles was characterized by SEM and a BET analyser and FTIR and XRD were used for chemical structure characterisation. Figure 3.3 showed the SEM images of BC samples grown from different strains of bacteria. Figure 3.3 (a)-(d) reveals the three-dimensional (3D) inter-connected nanostructure of cellulose nanofibers with width dimensions around 50-500 nm. Surface morphology of the four BC samples exhibited dense and porous nanostructures, where BC grown from *G. xylinus* JCM 10150 had the finest structure compared with other *K. xylinus* samples. The morphology observed was in good agreement with existing literature[227][228][229]. It is notable that BC produced from *K. xylinus* strains were much more affected by the freeze-drying method, where some of the fibrils were broken. Therefore, in order to keep the optimal shape, for experiments conducted in the next two chapters, BC samples were pre-treated with tert-butanol alcohol to allow the exchange of water before freezing. In addition, instead of being frozen *via* liquid nitrogen which can exert a large impact on the samples, sample were frozen at -15°C overnight before being placed into a freeze-dryer. In order to verify the relationship between sample thickness and density of nano-fibrils, BC produced from K. xylinus DSM 16663 with different thickness (0.8 mm grown for 5 days and 3 mm for above 10 days) were characterized in SEM as well, as shown in figure 3.4. It was evident that the thick BC sample exhibited much denser porous structure of cellulose nano-fibres than the thin BC sample.
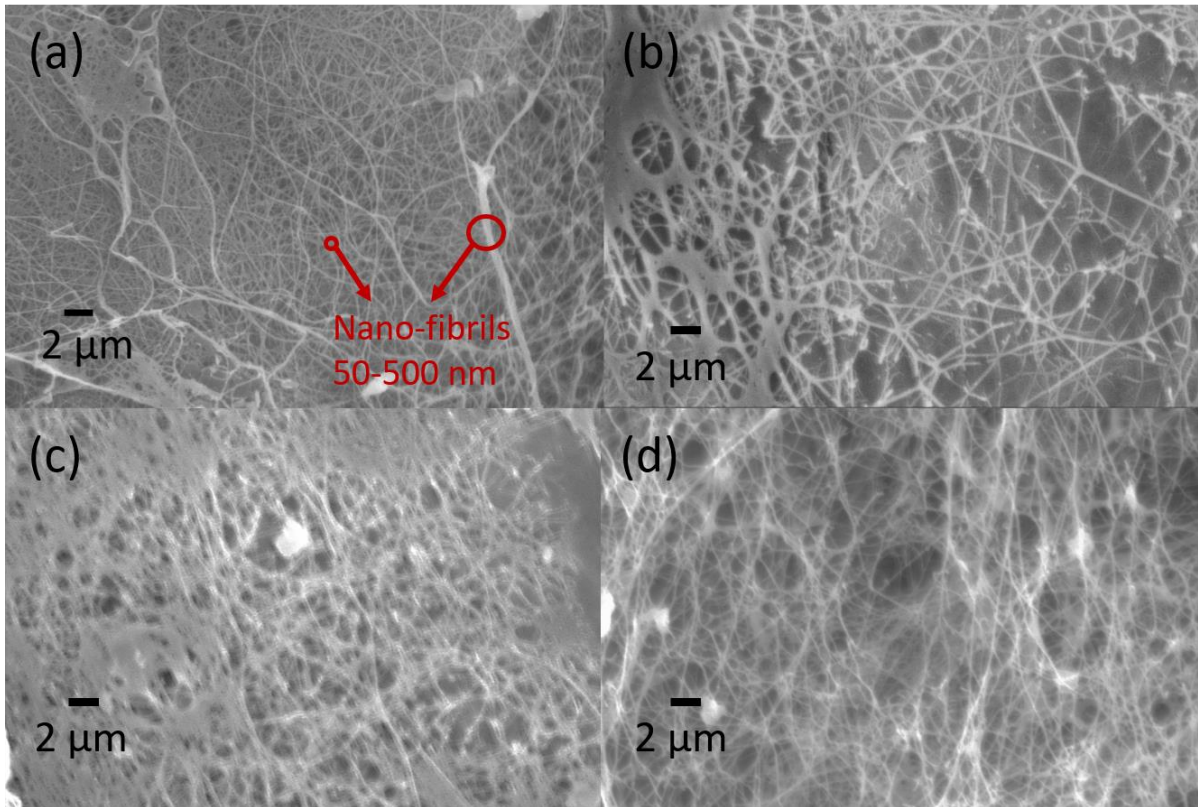
Figure 3.3 SEM images of BC (a) grown from G. xylinus JCM10150, (b) K. xylinus DSM 16663, (c) K. xylinus DSM 2325, (d) K. xylinus DSM 2004; (e) FTIR analysis of BC chemical structures (BC1: BC grown from G. xylinus JCM 10150, BC2: BC grown from K. xylinus DSM 16663, BC3: BC grown from K. xylinus DSM 2325, BC 4: BC grown from K. xylinus DSM 2004).
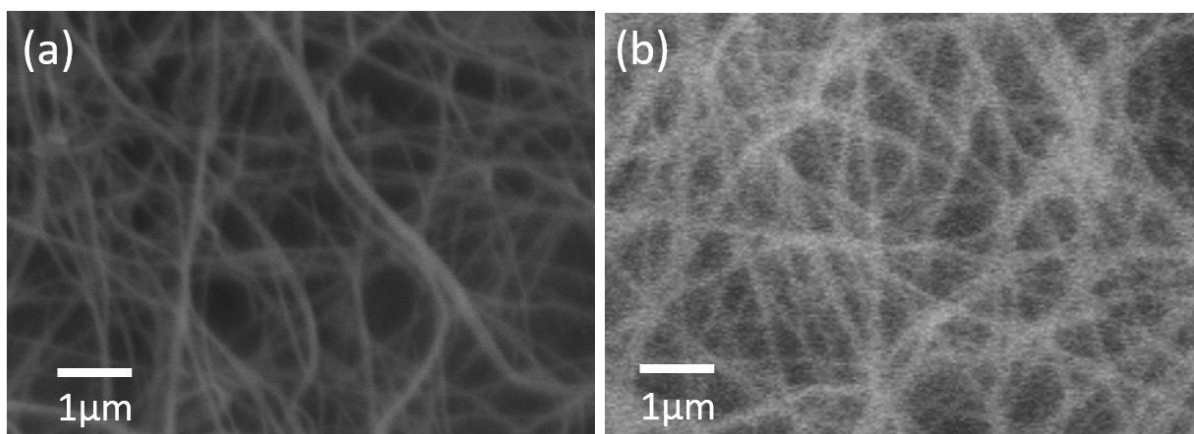
Figure 3.4 SEM images of BC grown from K. xylinus DSM 16663: (a) with thickness of 0.8 mm and (b) with thickness of 3 mm.

Table 3.2 Comparison of BET analysis of BC grown from different strains of bacteria.

	Surface area (m²/g)	Pore width (nm)	Pore volume (cm³/g)
BC-JCM10150	166.6 ± 0.2	2.27 ± 0.1	0.20 ± 0.1
BC-DSM16663	155.8 ± 0.1	2.77 ± 0.3	0.26 ± 0.1
BC-DSM 2325	116.7 ± 0.1	2.65 ± 0.2	0.24 ± 0.2
BC-DSM 2004	108.6 ± 0.1	2.11 ± 0.1	0.18 ± 0.1

BET analysis shown in Table 3.2 revealed that all four types of BC have high surface areas (above 100 m^2/g) and exhibit small pore widths and volumes, which corresponds to the highly porous nanostructure previously observed in SEM. The results were calculated by Novatech 5.0 software by applying multi-point BET method and DFT (density functional theory) method. This explains the high water-holding capacity. However, BC-JCM10150 and BC-DSM 16663 which were cultivated in 5% glucose medium have a much larger surface area compared with the other two samples, indicating they have denser structures. This corresponds to other results reported in the literature. Krystynowicz et.al [230] discussed the influence of glucose concentration on BC growth, where a reduced glucose content resulted in higher BC yields and denser structures.

2) XRD and FTIR analysis

Based on SEM characterizations, all four BC show the typical characteristics of known BC such as nanofibrils and inter-connected nanonetwork structures. In order to further verify the properties of BC and draw comparisons, FTIR and XRD analysis were performed. Figure 3.5 shows FTIR and XRD spectroscopy, indicating the chemical

bonds and crystallinity of BC produced by different bacterial strains. The XRD patterns of four BC are shown in Figure 3.5 (a). The figure indicates three typical diffraction peaks at 14.5, 17.4, and 23.9°, which correlate with (101), (10$\bar{1}$)and (002) polymorphism cellulose type I[231][232][233]. Owing to the sharpness of diffraction peaks observed, it can be concluded that the four BC are semi-crystalline[234]. The larger peaks at 14.5° than in 17.4° indicate all these cellulose samples contain mostly Iα[235].The degree of crystallinity (CrI) and crystallite sizes (CrS) of four BC materials determined by Segal's equation[197] were calculated and are exhibited in Table 3.3. It is obvious that BC grown from *K. xylinus* DSM 2325 had the highest CrI value which was 69.38%, followed by BC grown from *G. xylinus* JCM10150 with a CrI value of 64.93%, and BC grown from *K. xylinus* DSM 16663 with a CrI value of 60.66%. However, the degree of crystallinity in BC produced from *K. xylinus* DSM 2004 drops to 59.77%. From crystallite sizes measured by XRD, BC produced from *K. xylinus* DSM 2325 and DSM 2004 exhibit larger crystallite sizes in [002] compared with the other two BC. Research by Watanabe et.al [236] suggests that the reduction of degree of crystallinity and crystallite sizes can be attributed to the different culture conditions. From BET and SEM results, BC samples cultivated from *G. xylinus* JCM 10150 and *K. xylinus* DSM 16663 containing less glucose concentration in culture medium have much denser nano-network structures and higher porosity, compared with the other two BC samples. According to the findings by Zeng et.al [237] and Shibazaki et.al [238], BC with a larger accumulation of nanofibrils could alter the crystal structure due to the dense network structure restricting the motion of cells, resulting in a lower degree of crystallinity. From FTIR spectra (Figure 3.5 (b)), it is obvious that the peaks at 3300 cm^{-1} correspond to stretching vibration of intra and inter O-H bonds in cellulose I[233][239][240][234], which is in agreement with the XRD pattern. The peaks at 2900 cm^{-1}

indicate C-H stretching of CH_2 and CH_3, while peaks at 1650 cm^{-1} relate to H–O–H bending of absorbed water, and peaks located at 1425, 1370, 1330 and 1275 cm^{-1} correspond to the in-plane bending of the former C-H bond[241] and cellulose II[234][242]. The peaks around 1160 cm^{-1} are assigned to C-O-C antisymmetric bridge stretching of 1, 4-β-D-glucoside[234][243][244]. It can be induced from XRD and FTIR analysis that four BC specimen retain the features of cellulose I and high crystallinity which is in correspondence of typical BC crystalline structures [231][232][233]. This indicates excellent mechanical properties in the four BC specimen.
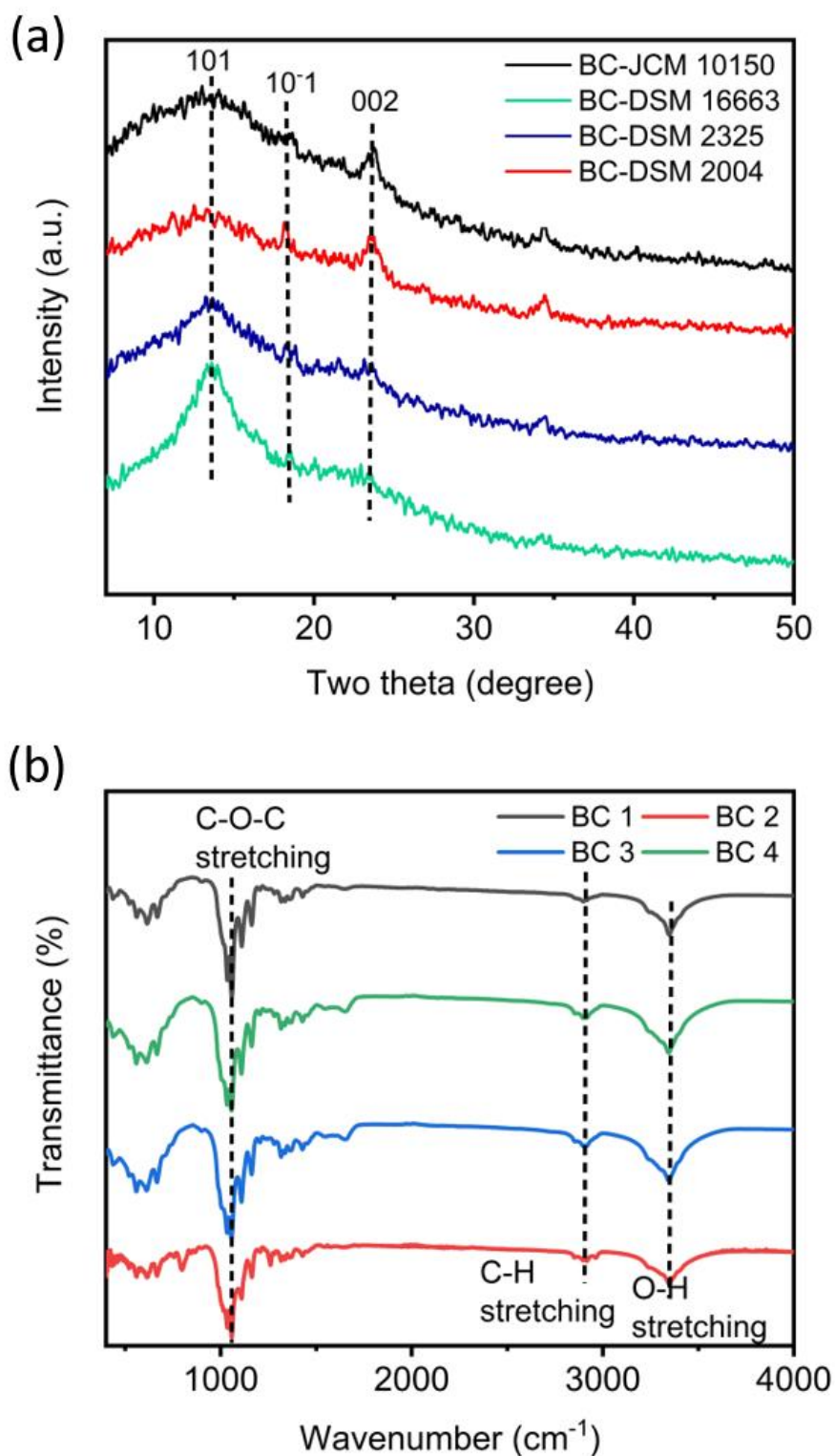
Figure 3.5(a) XRD characterization of BC produced by different strains of bacteria. (b) FTIR spectra of BC produced by different bacterial strains (BC1 is G. xylinus JCM 10150, BC2 is K. xylinus DSM 16663, BC3 is K. xylinus DSM 2325, BC4 is K. xylinus DSM 2004).

Table 3.3 The Crystallinity of BC grown from different bacterial strains and the crystal size of lattice [101], [10$\bar{1}$], and [002] in each sample.

Sample	CrI (%)	CrS (nm)		
		[101] (nm)	[10$\bar{1}$](nm)	[002] (nm)
BC-JCM 10150	64.93	1.02	2.28	1.96
BC-DSM 16663	60.66	2.12	0.57	2.41
BC-DSM 2325	69.38	1.76	0.53	6.03
BC-DSM 2004	59.77	1.35	0.87	7.13

3) Thermal degradation

The thermal degradation of BC specimens was tested by DSC and TGA under inert nitrogen atmosphere and presented in Figure 3.6. Figure 3.6 (a) shows the weight loss curves of four BC specimens (BC-JCM10150, BC-DSM16663, BC-DSM2325 and BC-DSM2004). In TGA curves, four BC samples experienced dehydration at around 100°C, depolymerization and pyrolytic decomposition at around 230 to 400°C. The first minor degradations result from water desorption from the cellulose polysaccharide structure. All BC samples show the degradation temperature at around 300 to 350°C, resulting from the change in weight loss due to organic decomposition. The amount of weight loss and temperature degradation differ owing to the various fermentation methods and culture medium[245]. DSC curves of four BC samples are showed in Figure 3.6 (b). It is indicated that the endothermic event occurs between 50 to 180°C for all samples due to the dehydration of surface water, the interaction between non-

substituted hydroxyl groups and water. This indicates a transformation related to the melting of the crystalline phase of cellulose[246][247].Subsequently, all BC samples showed great thermal stability after water removal. The exothermic maximum occurred between temperatures of 350 to 375°C, indicating the decomposition of BC samples. The observed DSC curves correlate with the TGA curves, both of which reveal the excellent thermal stability of BC samples.
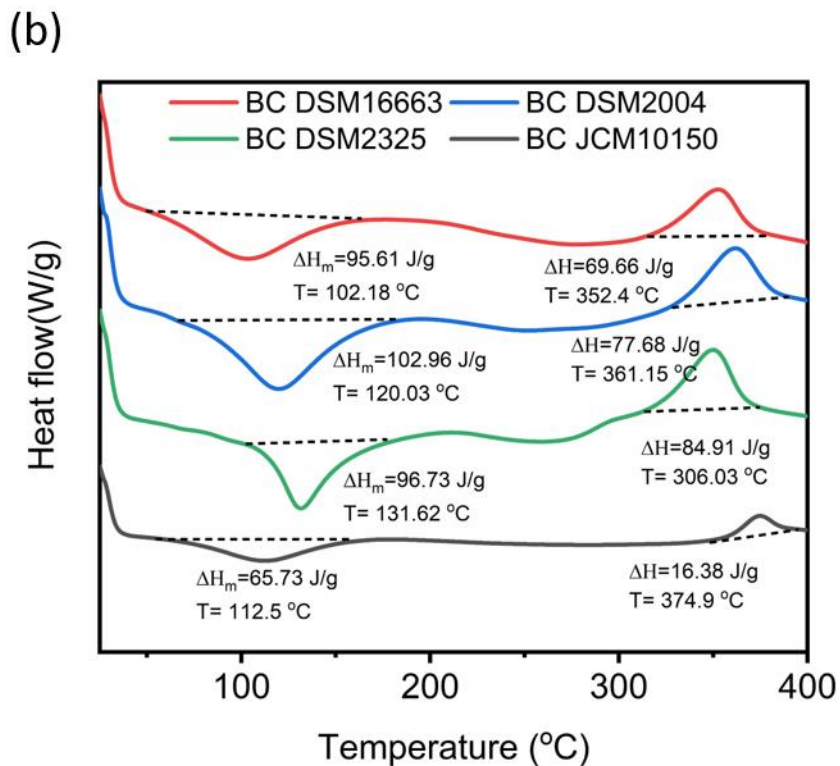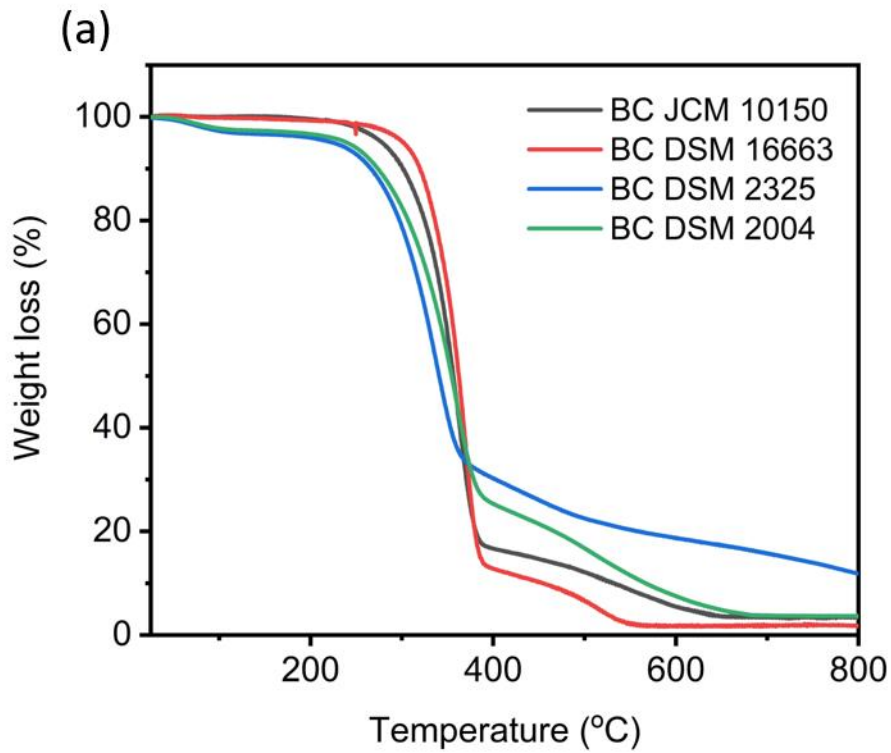
Figure 3.6 (a) TGA curves of BC grown from four strains of bacteria; (b) DSC analysis of BC samples grown from four bacterial strains (ΔH_m is the melting enthalpy of BC samples and ΔH indicates the decomposition enthalpy of BC).

In vitro biocompatibility test

Characterization in terms of the previously described materials properties indicate that BC is an excellent candidate as a substrate for wound dressings. However, high biocompatibility is also an important factor for wound dressing materials. In order to further investigate the survival of cells in BC substrate with different nano-fibres densities, , an *in vitro* cell study was performed on BC samples produced from *K. xylinus* DSM 16663 with two different thicknesses (0.8 mm and 3.0 mm).
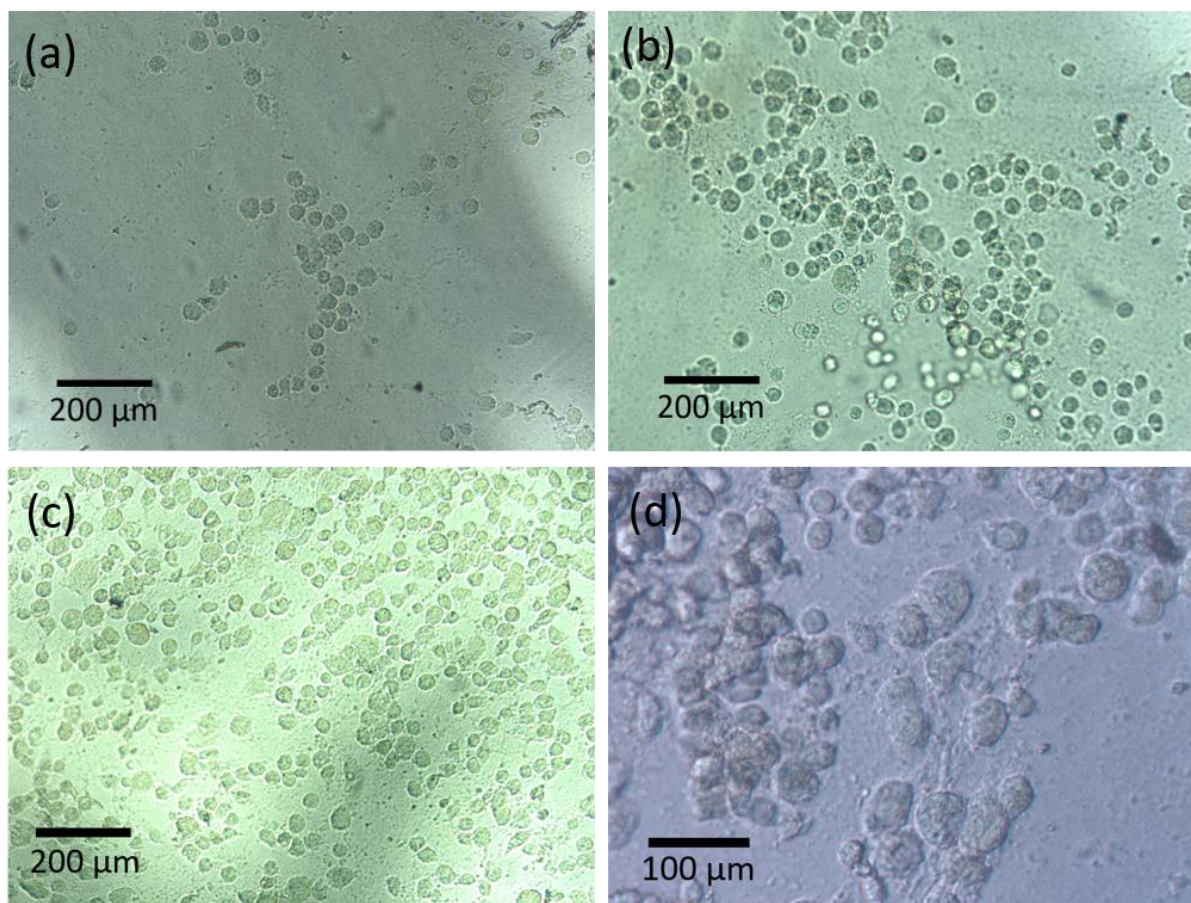
Figure 3.7 Morphology and distribution of HDF cells seeded on thin BC (BC-DSM 16663 with thickness of 0.8 mm) with density of (a) 5,000 cells/ml under 10×objective, (b) 10,000 cells/ml under 10×objective, (c) 25,000 cells/ml under 10×objective, (d) 25,000 cells/ml under 20× objective for 48 hours observed using a phase contrast microscope.

Phase contrast microscopy in Figure 3.7 showed that living HDF cells seeded on thin BC samples were comparable to HDF in culture medium after 48 hours incubation. However, for HDF cells seeded on BC samples, the HDF cells were more prone to being round-shaped, forming clumps of different sizes compared with normal fibroblasts shapes . This suggests cells can not adapted to the BC surface. The cells can grow but not fully spread and proliferated on BC samples. Large clumps were formed by proliferative fibroblasts which is more obvious in Figure 3.7 (b). According to Sanchavanakit et.al [138], this phenomenon occurs because the adhesive forces between BC and fibroblasts is much weaker than the fibroblasts among themselves, leaving groups of cells to roll up and grow less confluently on the BC surface. The surface of plain BC does not promote cell adhesion and fails to promote the specific absorption of proteins and subsequent cellular adhesion[248]. As a result, the adhesion to the BC surface is inadequate.
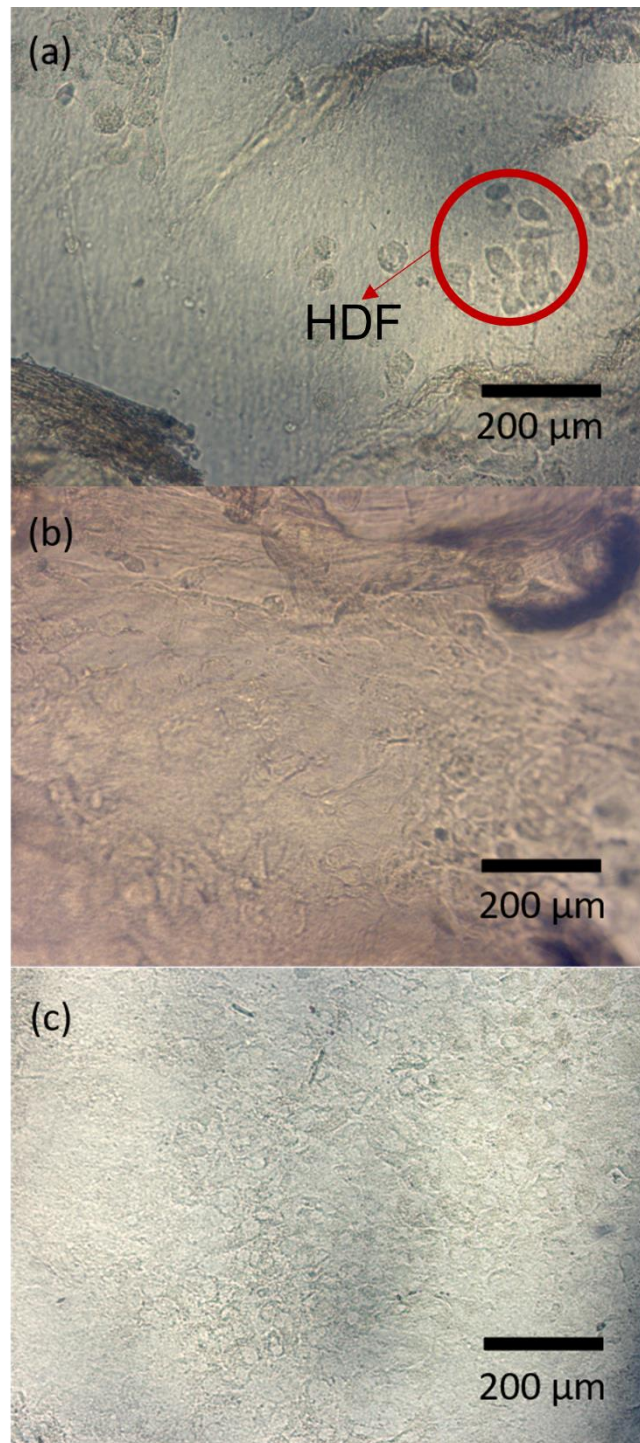
Figure 3.8 Morphology and distribution of HDF cells seeded on thick BC samples (grown from K. xylinus DSM16663 with thickness of 3 mm) for 48 hours with cell density of (a) 25,000 cells/ml, (b) 10,000 cells/ml, (c) 5,000 cells/ml, observed under a phase contrast microscope with 10× objective.

The phase contrast microscopy in Figure 3.8 that HDF grow on thick BC samples for 48 hours with different cell densities. It is obvious that only Figure 3.8 (a) exhibits a few cells grown on a thick BC sample. Compared with results from thin BC in Figure 3.8, it is more difficult for HDF cells to grow and attach to thick BC samples. As the subcellular proteins in HDF conduct forces to the ECM through integrin assemblies and form contractile stress fibres in conjunction with myosin, the contractile force of HDF plays an important part in HDF attachment[249][250]. For thick BC with higher water content and denser nano-network surface structures, resulting in less protein adsorption in HDF growth, thus the contractile force between cells and BC are considerably weaker.

3.3 Summary

In this chapter, the material properties of BC produced from four different strains of *G. xylinus* and *K. xylinus* were fabricated and characterized. *G. xylinus* JCM 10150, *K. xylinus* DSM 16663, *K. xylinus* DSM 2325, and *K. xylinus* DSM 2004 were cultivated in different concentrations of yeast, glucose and carbon media with the pH adjusted to the optimum levels for static growth under 30°C. BC produced from bacterial strains were taken out and their materials properties characterised in terms of surface morphology, chemical composition, porosity, water-holding capacity, crystallinity and thermal stability. The SEM and BET results show that BC samples grown from *G. xylinus* JCM 10150 and *K. xylinus* 16663 had the highest yielding and dense nano-network structures with the highest surface area due to the lower glucose content in the culture medium. In addition, this corresponds to a high water-holding capacity. From FTIR and XRD analysis, four BC samples had a high degree of crystallinity, around or above 60% and contained mostly cellulose type I. Whilst BC produced from

K. xylinus DSM 2004 and *K. xylinus* DSM 2325 have higher degrees of crystallinity than other two, this can be attributed to the different types of medium used in bacterial inoculation, where 10% glucose was used in the medium while others only contained 5% glucose. Lower glucose concentrations in BC culture media results in a reduction in degree of crystallinity due to restrictions in cell motion imposed by the dense network structure. Characterization *via* DSC and TGA curves on heat capacity and weight loss revealed the excellent thermal stability of all BC samples. *In vitro* biocompatible cell studies of HDF seeded on BC with different thicknesses demonstrates BC's potential biocompatibility, especially for BC with lower thicknesses. From all the characterizations, although further *in vitro* and *in vivo* biocompatibility need to be conducted, the fabricated four BC specimen with three-dimensional nano-network structure exhibits a high water-holding capacity, high crystallinity, great thermal properties, , making it an excellent potential material for wound dressings. In particular, it can be found from this chapter that the BC pellicles grown from *G. xylinus* JCM10150 and *K. xylinus* DSM 16663 requiring low glucose concentrations and less incubation time, were among the best in terms of the materials properties discussed above. Therefore they were chosen for BC matrices in pH sensor and antimicrobial BC composites discussed in the following two chapters.

Chapter 4 Pyrolyzed BC Aerogels for pH sensing

Published work by author[251], copyright by Elvesier.com

4 Conducting BC aerogels for pH sensing substrates

4.1 Introduction

4.1.1 Aims and objectives

Chapter 3 describes the four different BC grown by different strains of bacteria, where BC grown from G. xylinus JCM10150 exhibited considerably dense nano-network structure Therefore, by utilizing three dimensional (3D) nano structure of cellulose nanofibrils, a conductive flexible pH sensor based on pyrolyzed BC aerogels is proposed and discussed in order to investigate the potential applications of BC-derived nanocomposites for flexible pH wound sensors.

Smart wound dressings often contain dressing materials with wound sensors. The aim of this work was to fabricate the pyrolyzed BC (p-BC) aerogel as a conductive substrate for application as a flexible wound pH sensor using a dip-coating technique. Current flexible pH sensors in wound monitoring are fabricated by coating a conducting flexible substrate with a proton-selective polymer (such as polyaniline (PANI)). However, carbon aerogels are often used as a composite by incorporating them with resin or elastic polymers in for flexible pH sensing applications due to its poor mechanical properties. Same as freeze-dried BC samples, pyrolyzed BC aerogels retained the 3D inter-connected nano-network structure but in carbon nanofibers not cellulose. The 3D inter-connected nano-network structure of carbon nanofibers can induce the electrons to move quickly, conferring high electrical conductivity. In order to increase the mechanical strength, flexibility and biocompatibility of pyrolyzed carbon aerogels, polydimethylsiloxane (PDMS) is incorporated with p-BC acting as the sensor substrate.

Nanocomposites based on pyrolyzed BC are of great significance for study and optimisation for potential applications such as flexible sensors. Section 2.2 described the methodology used for pyrolysis of BC samples and fabrication of BC/PDMS/PANI nanocomposites as a flexible pH sensor. The objectives of this chapter were to fabricate pyrolyzed BC aerogels, compare the electrical properties *via* different pyrolysis temperatures, and investigate the pH sensitivity in commercial pH buffer solution and *in vitro* human serum solution. Complete fabrication and further pH sensor optimisation are introduced in the future work section.

4.1.2 Introduction to carbon aerogels and pyrolyzed BC

With the development of carbon materials, elastic carbon aerogels are a new trend in sensor fabrication. Carbon materials are generally classified into three main categories: graphic carbon (GC), soft carbon (SC) and hard carbon (HC) by the different hybrid orbitals of the carbon atom; sp, sp^2 and sp^3 [252][253]. 2D hexagonal crystalline carbon materials such as carbon nanotubes, graphite and graphene oxide belong to the GC category[254]. Carbon materials pyrolyzed from organic compounds are in the SC and HC categories where in this work, p-BC belongs to the SC category.

As introduced in chapter 1, chronic wounds often contain certain bacteria and their biofilms which delay the healing process and lead to serious infections, spreading to the bones or even systemic septicaemia which significantly threaten the patients' health[2]. In order to mitigate this risk, smart dressings, which refer to the use of biochemical cues to generate a readable output for diagnostic or theragnostic value by incorporating the biosensors into or near dressings[3], are capable of monitoring the wound healing process for early detection. pH is a key indicative parameter in chronic

wounds monitoring, as the changes in pH are often related to bacterial infections. The pH value in chronic wounds is often higher than 7.4, due to the alkaline by-products produced in the process of bacterial colony proliferation[94],[95],[96], whilst healthy skin is slightly acidic, with pH 5.5-6.5[97]. In order to promptly and effectively treat wound areas, pH is measured at different locations over the wound area, however, chronic wounds require multiple measurements throughout the wound area with high spatial resolution which is beyond the capacity of most commercial probes. Recent pH sensors have a solid-state design that replaces the glass probe with an electrode coated with a pH sensitive film (metal oxide or conducting polymer). This technology is based on the principle that valence changes occur in the oxygen atoms of the metal oxide, which is caused by absorption of hydrogen ions from the test solution, generating a potential relative to the reference electrode[98]. This technology exhibits high sensitivity, increased stability and cost effectiveness[97] but requires complicated manufacturing methods and expensive materials.

In recent years, a new strategy has been proposed for coating proton-selective polymers with conducting carbon deposited on a flexible substrate (such as paper[99],[255], polyethylene terephthalate[256] and cotton thread[257]). Owing to the employment of pH sensitive nanomaterials (PANI), these have increased sensitivity and decreased manufacturing cost[99],[255],[257]. However, most of this research fails to demonstrate a reversible, free-standing 3D platform for diagnostics and wearable devices in chronic wounds. It still requires green, scalable and versatile methods to lower the cost of the manufacturing process.

PANI is a widely used conductive and proton-selective polymer in pH sensor fabrication, owing to its wide conductivity range (doping dependent) and unique chemical structure of the material[258]. PANI has three base forms: per nigraniline base

(PNB) which is fully oxidized, emeraldine base (EB) which is half oxidized and leucoemeraldine (LEB) which is fully reduced[259]. After protonation with acids, EB can be transferred to highly conductive emeraldine salt (ES) by adding protons to the back bone of PANI[260]. Figure 4.1 reveals the reactions that cause reversible change of EB to ES, where the protonation process takes place on the imine nitrogen sites, and the polarons and bipolarons were formed during the doping process and function as the charge carriers in the system. However, when ES is placed in an alkaline solution, the deprotonation occurs and the conductivity decreases accordingly. This reversible process is attributed to the existence of amine and imine groups in the PANI polymer structure, which makes it the most suitable pH sensitive materials to be used in pH sensors[261][262].
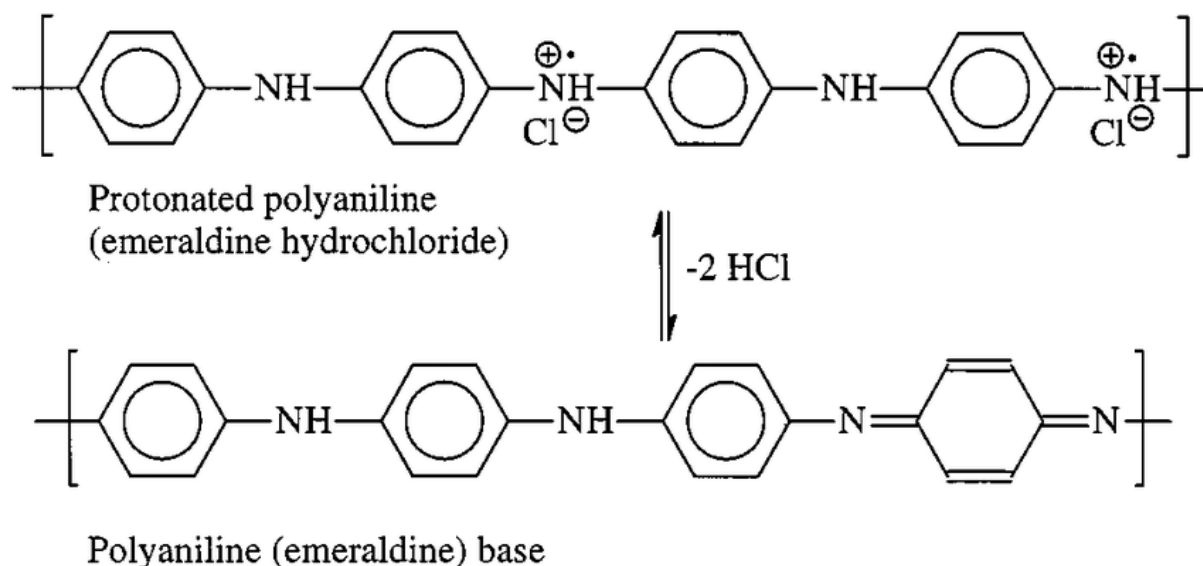
Figure 4.1 The protonation and deprotonation process of PANI[263].

Currently, taking advantage of the unique 3D nano-network structure of BC introduced in chapter 1, pyrolyzed BC (p-BC) has been used as a precursor material for carbon nano-fibres for stretchable conducting applications[264], super-capacitors[265],[266], and

lithium ion battery anodes[267],[268]. The major advantages of using p-BC lie in its easy fabrication, low-industrial cost and mechanically robust 3D carbon nano-network structures.

In this chapter, a true 3D p-BC CNF aerogel as a precursor pH sensor and novel p-BC/PDMS/PANI nanocomposite was proposed, which has potential to be used in chronic wounds with high spatial resolution. Wound monitoring is proposed which exhibited both high conductivity and pH sensitivity.

4.2   Results and discussion
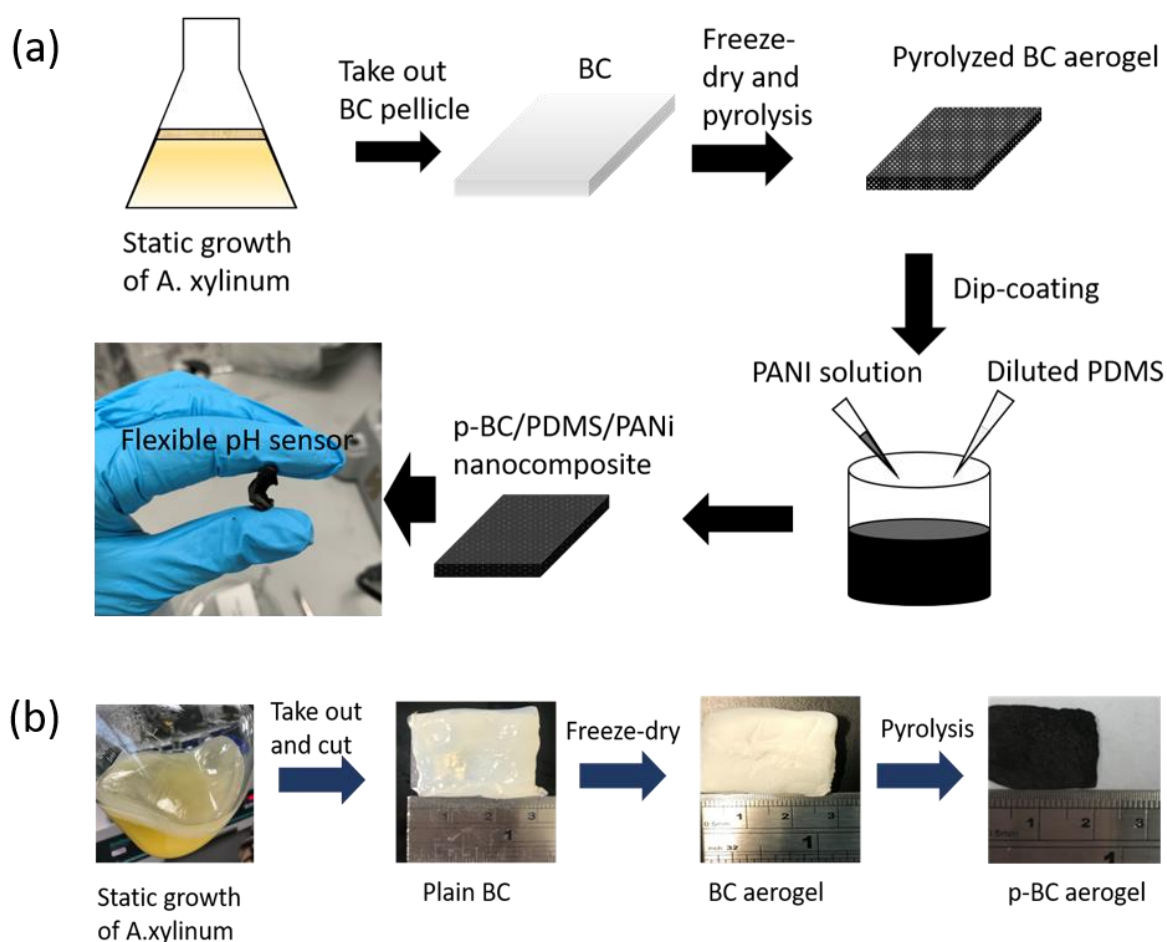
Figure 4.2 Photographs of (a) the fabrication process of p-BC/PDMS/PANI pH sensor; (b) BC grown from A. xylinum, freeze-dried BC aerogel and pyrolyzed BC aerogel samples.

Figure 4.2 shows the fabrication process of the p-BC/PDMS/PANI pH sensor and BC samples when taken out from cultivation, following freeze-drying and pyrolysis. As Figure 4.2 (a) indicates, the BC pellicle was removed after it was fully grown in YGC medium from *G. xylinus* JCM 10150 in a static condition for 5 days, followed by freeze-drying and pyrolysis. Then the p-BC aerogel was dip coated in a pre-diluted PDMS and PANI solution. Figure 4.2 (b) shows that BC samples experience at least 30% shrinkage in size after freeze-drying and 50% after pyrolysis. Post freeze-drying, the semi-transparent gel-like BC pellicle becomes a white foam-like aerogel. The foam-like aerogel turns into a light and black carbon aerogel after pyrolysis under high temperatures. The resulting flexible p-BC/PDMS/PANI nanocomposite has a similar appearance to p-BC but better material strength which allows compression by the fingers without breakage.
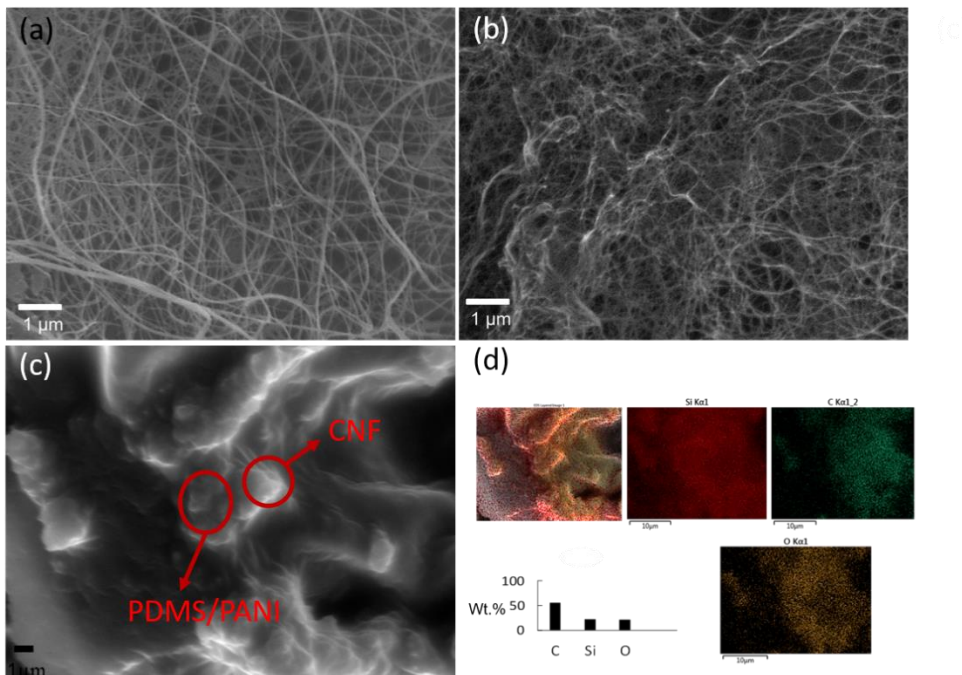
Figure 4.3 SEM images of (a) plain BC, (b) pyrolyzed BC aerogel, and (c) PDMS/PANI coated p-BC aerogel; (d) EDX analysis of p-BC/PDMS/PANI nanocomposite showing the types and amount of elements exist.

The SEM images in Figure 4.3 (a-c), show that BC has a 3D nano-network structure with interconnected nanofibers as in the previous chapter, p-BC has retained its 3D nano-network and transformed into a 3D carbon nano-fibre network structure, which can induce electrons to move faster[264]. In addition, this also guarantees p-BC the high surface area for PANI/PDMS to be coated. Using pre-diluted PDMS during dip-coating was helpful for maintaining thickness of resulted p-BC/PDMS/PANI nanocomposite, as non-diluted PDMS may result in extra PDMS residues in p-BC precursor. The EDX analysis in Figure 4.2 (d) confirms that in SEM, Si, C and O are the main three elements which show the incorporation of PANI and PDMS on p-BC aerogel.
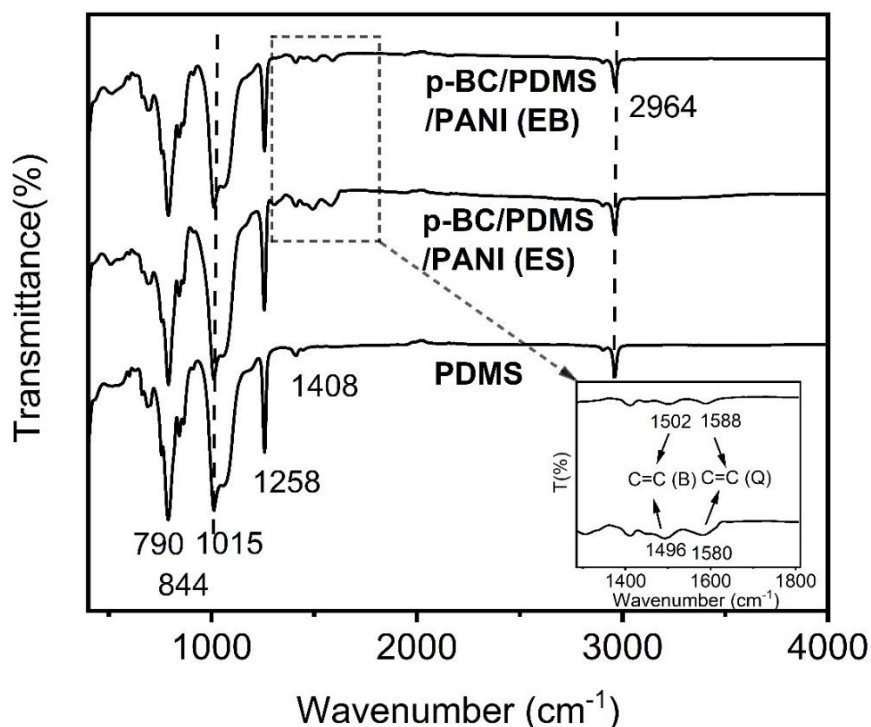
Figure 4.4 FTIR characterization of p-BC/PDMS/PANI before doping (p-BC/PDMS/PANI-EB) and after doping (p-BC/PDMS/PANI-ES).

In order to verify the chemical structure of the p-BC/PDMS/PANI sample, the FTIR spectra of p-BC/PDMS incorporated with PANI in emeraldine salt (ES) compared with p-BC/PDMS doped with PANI in emeraldine base (EB), and PDMS are shown in Figure 4.4. The peaks which shifted slightly from 1588 to 1580 cm^{-1} and 1502 to 1496 cm^{-1}, were assigned to the C=C stretching of the quinoid ring and benzenoid ring respectively, indicating PANI-EB [269] transformation into PANI-ES[270]. In addition, the peak intensity at 1496 cm^{-1} is stronger than 1502 cm^{-1}, further confirmation of the presence of PANI in ES[271]. The bands at 1408 and 1258 cm^{-1} indicate asymmetric and symmetrical deformations of the C-H in $Si(CH_3)_2$, and the peak at 1015 cm^{-1} could be assigned to Si-O, confirming PDMS infiltration[272][273]. The peaks at 844 and 790 cm^{-1} suggest the deformation of C-H and Si-C bond stretching in PDMS[274]. Therefore, all of the above confirm the incorporation of PDMS/PANI on p-BC aerogels.

Table 4.1 BET measurement of freeze-dried BC and p-BC aerogel in terms of specific surface area, mean pore diameter and pore volume.

Sample	Specific surface area (m^2/g)	Pore diameter (nm)	Pore volume (cm^3/g)
Freeze-dried BC	155.820 ± 0.1	1.380 ± 0.2	0.260 ± 0.1
p-BC aerogel	166.640 ± 0.1	2.270 ± 0.1	0.200 ± 0.2

Table 4.1 exhibits the results of BET analysis performed on the freeze-dried BC and p-BC aerogel. Technical data is reported based on the specific surface area, pore diameter, and pore volume, respectively. It is notable that both types of BC aerogels have ultra large surface areas, nano-scale pore sizes and relatively small pore volumes, which are beneficial for potential applications as conducting substrates for

pH sensing and likely provide a great surface area for PANI to be coated for higher pH sensitivity. In p-BC aerogel, the highly porous structure of carbon nanofibers can induce electrons to move quickly[264], which is beneficial as a conducting substrate for pH sensor and the high surface area can increase the amount of pH sensitive PANI being fixed and coated. By allowing more functional sensing area, there is more protonation occurs in the sensing process which is beneficial for increasing pH sensitivity.
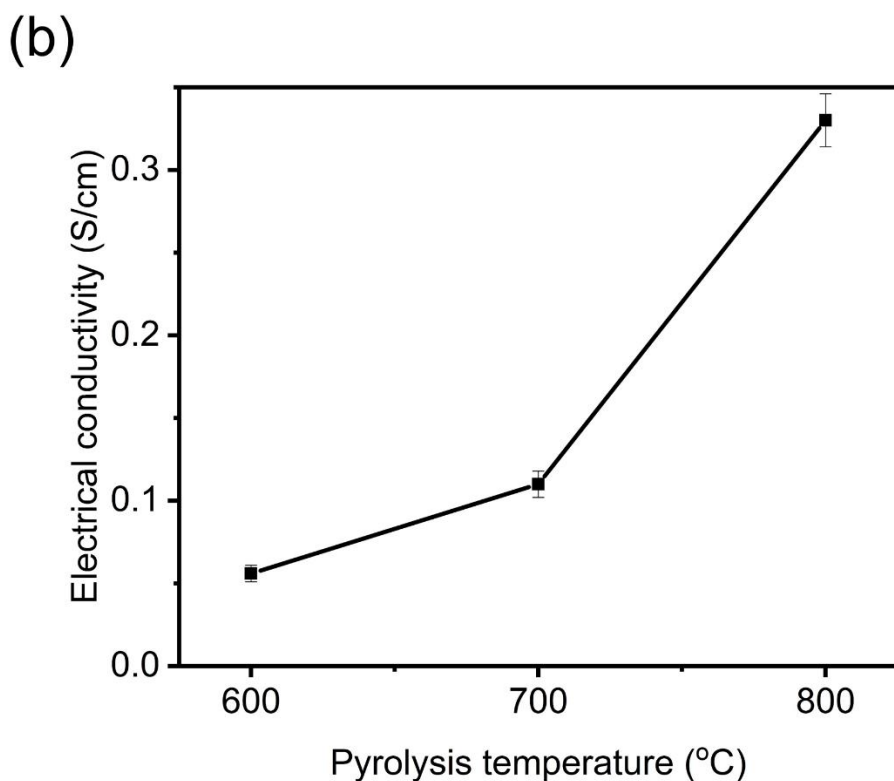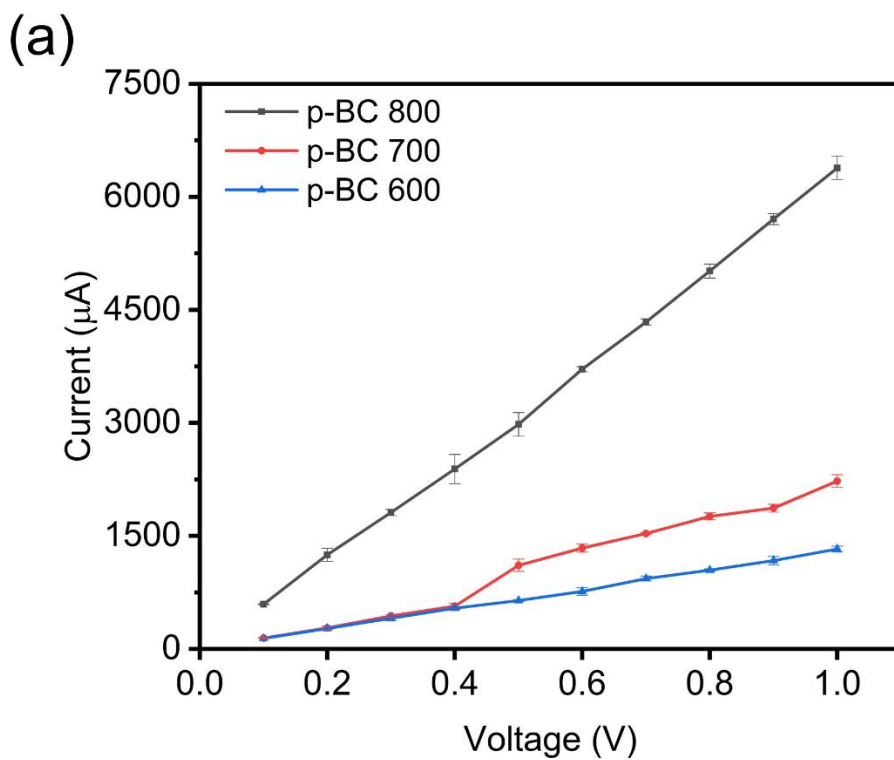
Figure 4.5 Electrical characterization of p-BC/PDMS/PANI nanocomposite: (a) the electrical conductivity test of BC aerogel pyrolyzed under 600°C, 700°C and 800°C, (b) the calculated electrical conductivity of p-BC pyrolyzed under 600°C, 700°C, and 800°C.

The conductivity test in Figures 4.5 (a) and (b) show the p-BC had increased conductivity with increasing pyrolysis temperature, and both p-BC/PDMS and p-BC had similar conductivity even when pyrolyzed at temperatures under 800°C. Additionally, p-BC with higher pyrolysis temperatures revealed higher output currents thus higher conductivity, whilst p-BC/PDMS still has great conductivity even when infiltrated with a certain amount of PDMS polymer. The reason for this phenomena is that higher pyrolysis temperature results in the higher graphitization of BC[264]. However, although infiltration of PDMS decreased the conductivity of the nanocomposite, it showed little effect on the pH sensing activity.
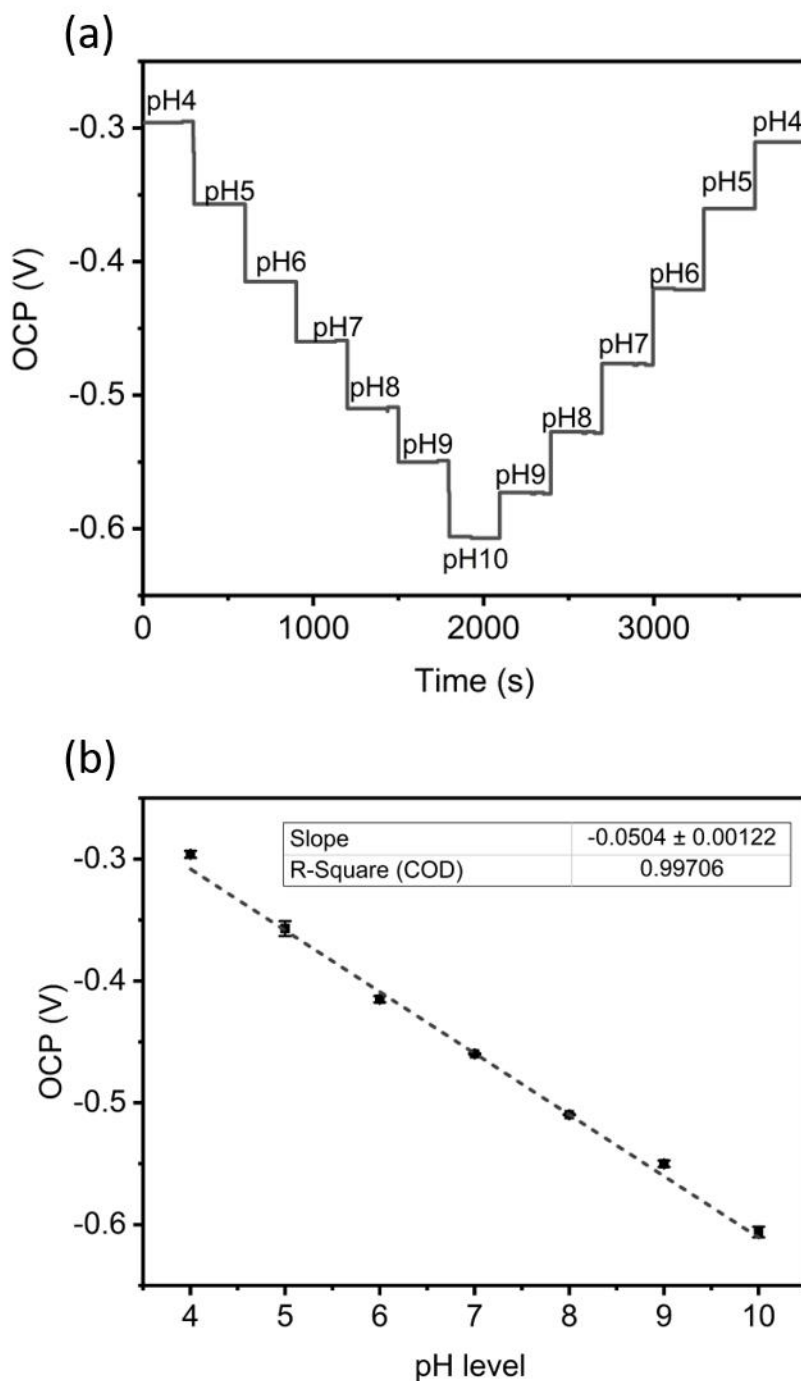
Figure 4.6 (a) The open-circuit potential measurement for p-BC/PDMS/PANI nanocomposite pH sensor in response to pH levels ranging from 4 to 10 in commercial pH buffer solutions; (b) The measured sensor response to various pH levels between 4 and 10. The data showed a linear response (r^2=0.997) with an average sensitivity of -50.4 mV/pH.

Figures 4.6 (a) and (b) show the sensor response for increasing and decreasing pH levels where there are great changes in output potential. It indicates that the proposed p-BC/PDMS/PANI composite has experienced steady pH sensitivity lasting for 5 minutes and the open-circuit potential has decreased with increased pH level (decreased H$^+$). The linear reduction has indicated a pH sensitivity of -50.4 mV/pH with coefficient of determination R^2 as 0.997, which is near-Nernst limit. The response time of the sensor is less than 20s. It also indicates that acidic solutions enabled more protonation in PANI. The results of the pH sensitivity test agree with existing literatures[58],[65],[275]. However, none of those pH sensors are three-dimensional which limits their use in deep wound beds, and our proposed p-BC/PDMS/PANI is easy fabricated , bio-derived and low-cost nanocomposite, which has great potential for smart wound monitoring materials for chronic wound beds.
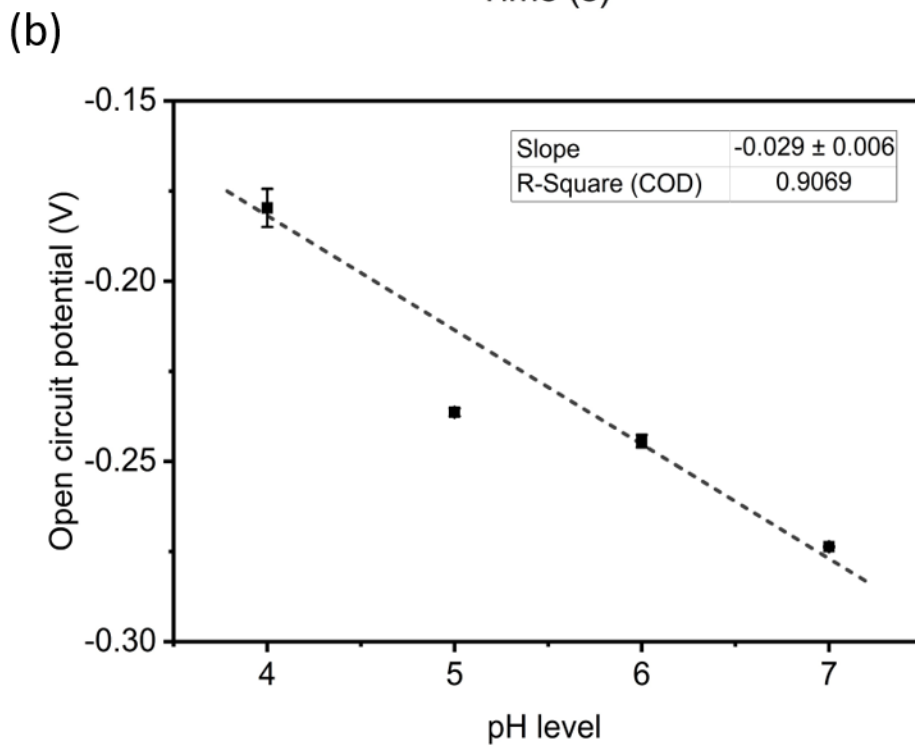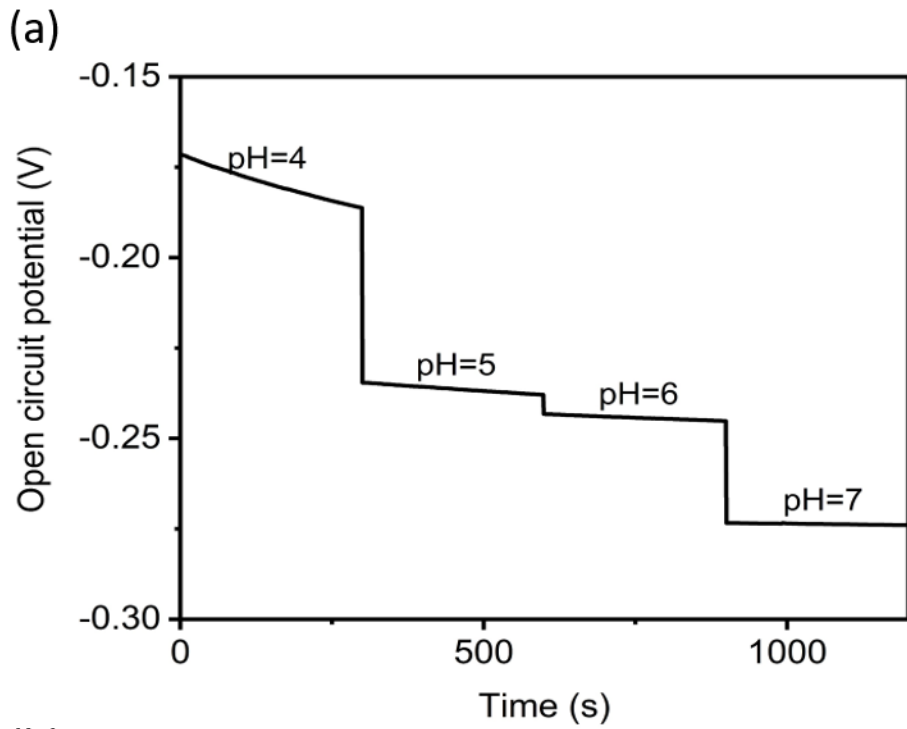
Figure 4.7 *In vitro* pH sensitivity test for open-circuit potential by placing fabricated samples into different pH solutions against (a) time, (b) pH level.

In order to simulate wound exudate to the maximum extent, *in vitro* pH sensing tests were additionally performed for our sensor by incorporating human serum into PBS buffer solutions (with different pH levels), which had a reportedly similar chemical environment to wound healing tissues[276] after debridement. Compared with figure 4.6, figure 4.7 (a) indicated the sensor tested in commercial pH buffer solutions responded similarly, where both indicate steady pH sensitivities for 5 minutes and response time less than 20s for pH level from 4 to 7. The potentiometric response as a function of pH level in Figure 4.7 (b) showed an average linear relationship between 4 to 7, with a sensitivity of -28.2 mV/pH and r^2 equal to 0.987. However, different from the sensor tested in commercial buffer solutions in figure 4.6, the sensor tested in human serum showed pH performance only in acidic solutions as the acidic solution allows the best observation of proton change. In addition, the *in vitro* test was not applied to pH levels above 7 due to the inconspicuous changes in OCP values in comparison with the acidic environment. The results indicate protonation can be affected by the high serum protein load that is able to bind to a lot of protons and this becomes more apparent under alkaline conditions. Therefore, as the reduced pH sensitivity in human serum, this pH sensor needs further optimization on sensing ability by allowing larger functional surface area of incorporated PANI to carry out more protonation to reduce the effect of human serum, in order to be used in real clinical applications. In this case, further experiments can be done in sensor optimization by various methods such as increasing the mechanical strength by employing folded carbon nanotubes to avoid the decrease of surface area instead of infiltration of PDMS, or using electrochemical deposition methods to dope PANI onto carbon aerogels to improve the fixation of PANI.

4.3 Summary

In this chapter, a nature-derived, cost-effective, and flexible 3D pH sensor was developed for use in chronic wound monitoring. The fabrication process developed is simple and green without chemical contamination. The sensor performance was tested in both commercial pH buffer solutions and *in vitro* wound simulated fluid, which showed a linear potential and sensitivity of -50.4 mV/pH and 28.2 mV/pH, with stable response at different pH levels. Further experiments on optimizations of sensing substrate can be performed in future to minimize the effect of proteins in human serum on protonation. The p-BC/PDMS/PANI nanocomposite showed great potential for integration with low-cost wound dressings in pH monitoring.

Chapter 5 Antimicrobial BC nanocomposites

Published work by author[277] included, copyright of Wiley.com

5 Antimicrobial BC nanocomposites

5.1 Introduction

5.1.1 Aims and objectives

The aim of the work reported in this chapter was to produce antimicrobial BC nanocomposites using dip-coating or surface polymerization methods. BC has no antimicrobial properties and thus only by incorporation with antimicrobial materials/agents can it be used in chronic or infected wound dressing applications. Herein, the concept of antimicrobial BC nanocomposites are introduced based on the recent development of BC based wound dressings. In this chapter, the inorganic BC nanocomposites like BC/AgNP and organic BC nanocomposites such as BC/lysozyme fabricated by ex situ synthesis, BC/polydopamine/eggshell membrane (BC/PDA/ESM) fabricated by surface polymerization of PDA, BC/methylglyoxal (BC/MGO) fabricated by ex situ synthesis, are introduced, and their antimicrobial activities investigated. This chapter is composed of four parts: a literature review, experimental methods, results and discussion and conclusions. Since most has been reviewed in chapter one, section 1.2.2, the literature review above includes a brief review of organic BC nanocomposites, especially nature-based materials.

5.1.2 Organic antimicrobial BC nanocomposite properties

As discussed in chapter 1, due to the limited antimicrobial spectrum of organic antimicrobial BC composites, and possible side effects caused by antibiotics and AgNP, there is a need to develop natural materials and greener methods for antimicrobial BC composite fabrication. The BC used in this chapter was produced from *K. xylinus* DSM 16663.

Eggshell membrane (ESM) has nowadays become a promising nature-derived material for chronic wound healing. Recent studies showed an ESM-positive effect in a rat skin wound model by decreasing the wound closure time via binding MMP-9 which is key to delayed wound closure[278]. Due to its similarity to the native extracellular matrix, ESM which is composed of collagen type I, V and X, is highly biocompatible and widely used in biomedical applications, such as bio templates, sorbents, biosensing and burn treatments[279]. It has been found that ESM has been used to promote wound closure and accelerate the early stage healing process[278]. It has also been prepared as a wound dressing *via* incorporation with polyurethane[280]. However, natural ESM is neither soluble nor fusible, meaning that reformation of natural ESM into various shapes and sizes is difficult. ESM kick-starts the healing process by virtue of distinct properties. Its properties help reduce tissue damage in a chronic inflammation scenario. Moreover, it binds matrix metalloproteases (MMPs) to reduce their presence in the wound. MMPs are a key risk factor in delayed wound healing. Highly significant, ESM promotes formation of new connective tissue and microscopic blood vessels[278].

Marine mussels have naturally tight adherence to solid surfaces in the sea *via* secretion of proteins containing 3,4-dihydroxyphenyl-L-alaine (DOPA) and lysine[281]. Inspired by the mussel adhesiveness, it was found that dopamine (DA) could undergo oxidative self-polymerization under alkaline conditions to form polydopamine (PD) for biomolecular and cellular attachment. This chemical reduction was conducted by the catechol group in PD. Therefore, DA is able to create a polymerized layer on various materials surfaces via self-polymerization[282][283], which is used to fabricate BC/PDA/ESM nanocomposite in this chapter.

Honey, especially Manuka honey has been studied for therapeutic management of chronic wounds in both *in vitro* and *in vivo* research[284],[285],[286]. Different from plain honey, Manuka honey contains a unique component, methylglyoxal (MGO), which can act as an antimicrobial agent during wound healing[287],[288],[289],[290]. The antimicrobial properties of MGO in multiple forms; solution[291], hydrogel[292], polymer, polymer fibres[293] and non-woven fabric[290] have been investigated. It has been found that MGO at a concentration of 0.0054 mg/cm^{-2} was sufficient to reach 100% colony forming pathogenic bacteria reduction. Rabie et.al[294] found that MGO can damage the structural integrity and function of bacterial DNA and proteins by disrupting glutathione (GSH) homeostasis, thus altering the membrane permeability leading to cellular lysis.

Therefore, inspired by the naturally antimicrobial Manuka honey, it is of great interest to study the degree to which MGO coated BC offers antimicrobial protection against broad-spectrum bacteria compared with other antimicrobial BC composites. In this report, we prepared BC/MGO composites by dip-coating MGO solutions onto BC membrane to produce BC/MGO (4%), BC/MGO (0.4%), BC/MGO (0.04%) samples with different MGO concentrations (v/v in H$_2$O) (see section 2.1.3 for detailed descriptions and illustration of the fabrication process), and tested against a broad spectrum in a range of bacteria including Gram-positive; *Micrococcus luteus (M. luteus)*, *Staphylococcus aureus (S. aureus)* and Gram-negative *Pseudomonas aeruginosa (P. aeruginosa)* and *Escherichia coli (E. coli)*.

Table 5.1 compares the antimicrobial activities of typical BC incorporated organic and inorganic antimicrobial agents. It is evident that BC incorporated with inorganic antimicrobial agents such as AgNP and CuO exhibited greater antimicrobial activity than organic agent incorporated BC nanocomposites.

Table 5.1 Summary of antimicrobial properties of typical BC incorporated organic and inorganic antimicrobial agents.

Incorporated Materials	Synthesis methods	Characterization methods	Antimicrobial property	Applications
Antimicrobial peptide ε-poly-L-Lysine [295]	Carbodiimide chemistry	Agar diffusion method	Significant reduction in growth of *S. epidermidis*	Wound infection prevention dressings
Copper oxide [296]	Hydrothermal deposition	Disk diffusion method	Significant antimicrobial response on *S.aureus*, *S.enterica*	Wound dressings
Silver nanoparticle [297]	AgNPs reduction from AgNO3	Disk diffusion method & broth diffusion method	Exhibits 99.9% antimicrobial activity for 72 h against a mixed culture of broth bacteria and fungi	Food packaging, wound dressing, hospital bed lining, surgical apparel
Lysozyme [209]	Physical absorption method	Agar diffusion method	Good antimicrobial activity against a broad range of microorganisms	Active packaging

5.2   Materials and methods

Materials are described in chapter 2 section 2.1.3.

The characterization methods are described in chapter 2 section 2.3.

5.3 Results and discussion

(1) BC/AgNP (BC/lysozyme for comparison in disk diffusion test)

SEM and EDX analysis
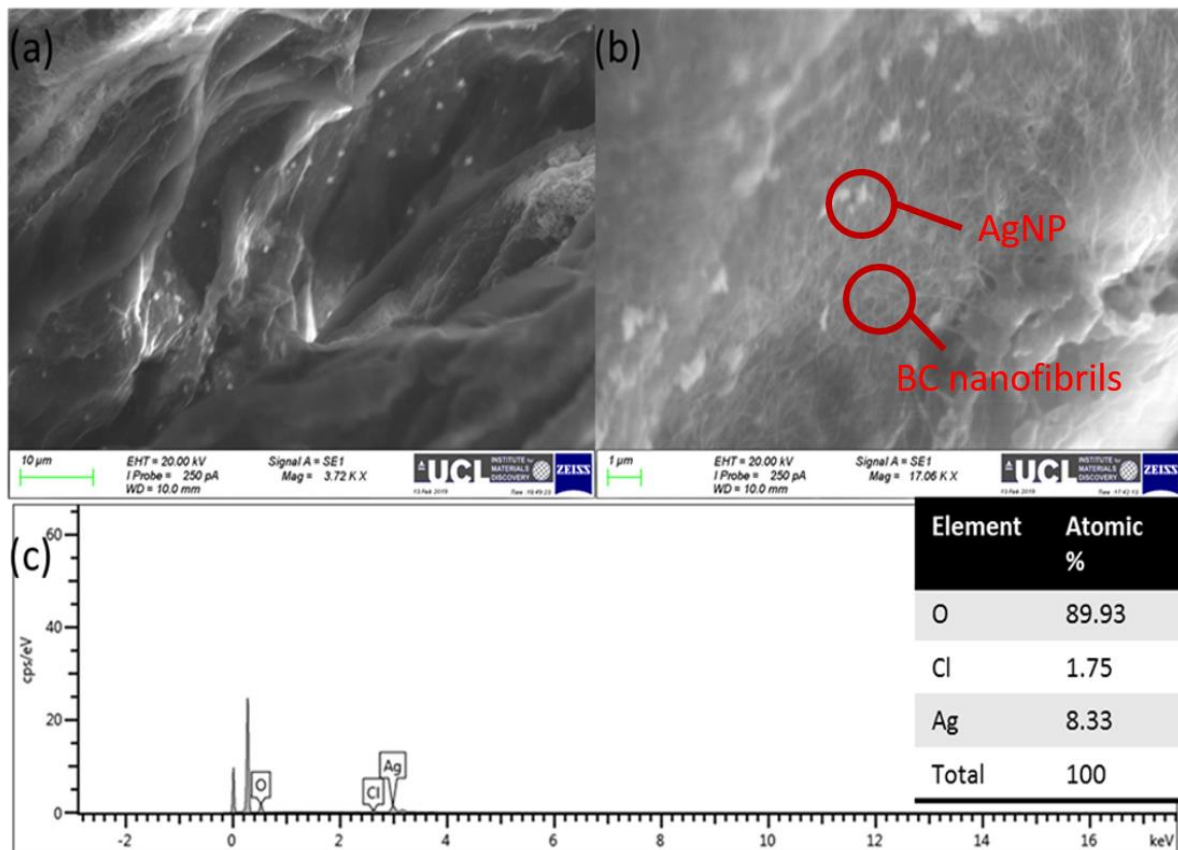
Figure 5.1 SEM image of BC/AgNP (a) low magnification, (b) high magnification; (c) the EDX analysis of elements in BC/AgNP.

The SEM and EDX results in Figure 5.1 show the surface morphology and elements in BC/AgNP. It is evident from Figure (a) and (b) that the nano-scale particles (with diameter of 100-500 nm) are embedded into the BC nano-network surface. Figure 5.1 (c) confirms that the nano-sized particles are silver whilst the large percentage of oxygen corresponds to the BC fibres.

Antimicrobial test
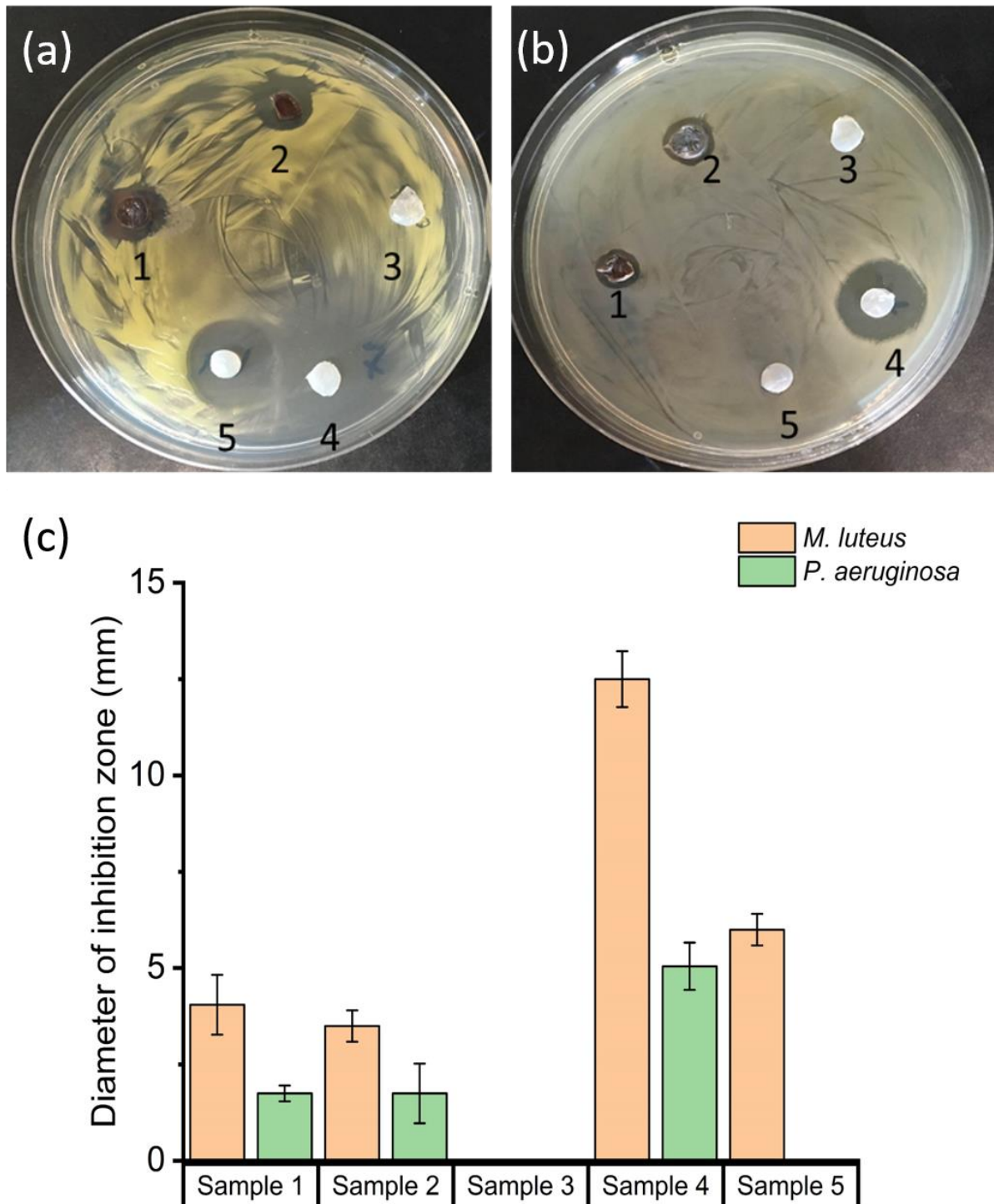
Figure 5.2 Disk diffusion test of BC/AgNP against (a) M. luteus, (b) P. aeruginosa; (c) the measured diameter of inhibition zone (DIZ) of five samples (sample 1: BC/AgNP (1M), sample 2: BC/AgNP (0.1M), sample 3: plain BC, sample 4: BC with Kanamycin (50 mg/ml), sample 5: BC/lysozyme.

Figure 5.2 indicates that the BC/AgNP has great antimicrobial activity against both Gram-positive *M. luteus*, and Gram-negative *P. aeruginosa*. In addition, the BC incorporated with a higher concentration of AgNP (1M) exhibits almost the same antimicrobial activity compared with BC/AgNP (0.1M). However, compared with positive control groups (BC/kanamycin), the antimicrobial activities of BC/AgNP nanocomposites are less pronounced. The BC/lysozyme has great antimicrobial activity against Gram-positive *M. luteus* but no antimicrobial activity against Gram-negative *P. aeruginosa*. Compared with BC/AgNP, BC/lysozyme has a larger DIZ value indicating greater antimicrobial activity against M. luteus. These results correlate well with existing publications[298][299].

(2) BC/PDA/ESM

SEM characterization

The BC/PDA/ESM (can also be in the form of BC/ ESM) was characterized *via* SEM in terms of surface morphology and structure. Figures 5.3 (a) and (b) show photographs of plain BC and BC/ESM nanocomposite. BC/PDA/ESM was darker in colour with less transparency, indicating full oxidation of DA during PDA self-polymerization. Figures 5.3 (c) and (d) show SEM images of plain BC compared with BC/PDA/ESM. From SEM images, while some EM particles aggregate on the surface, the BC/PDA/ESM still retains the typical nano-network structure. The EM particles were larger than BC nanofibrils, with diameters of approximately 500-800 nm.
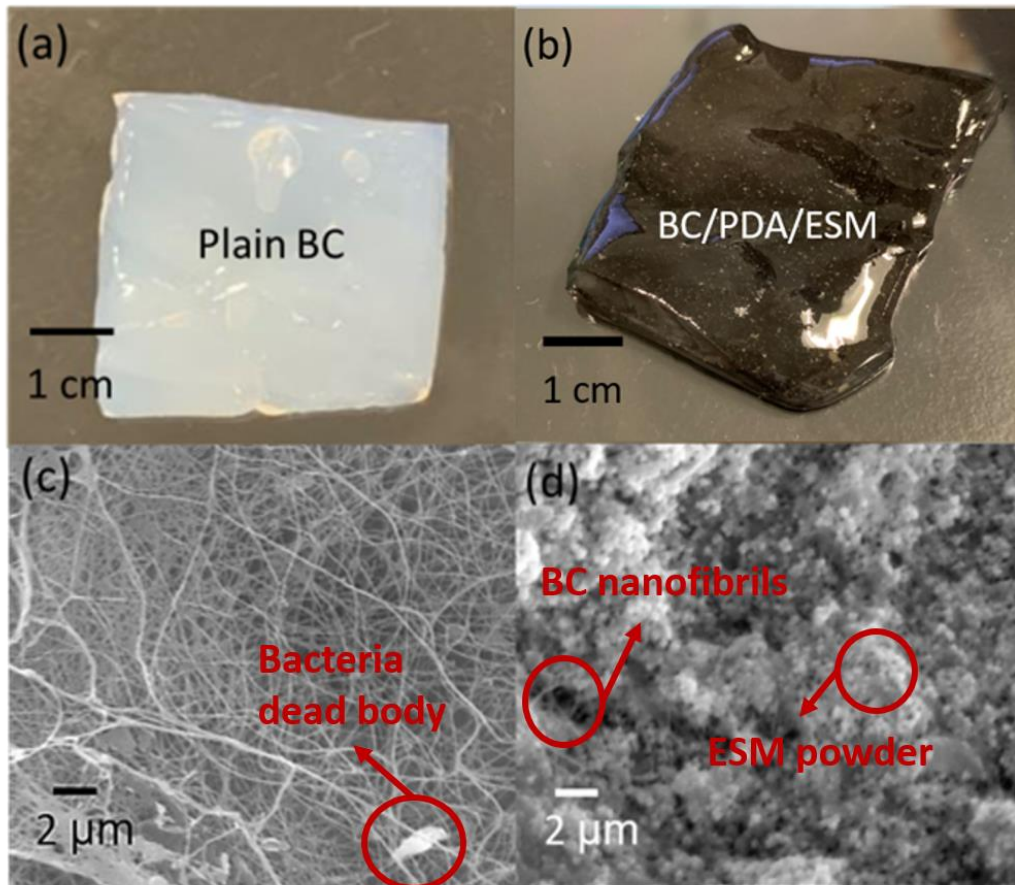
Figure 5.3 Photograph of (a) BC, (b) BC/PDA/ESM; SEM characterization of (c) BC, (d) BC/ESM.

FTIR analysis
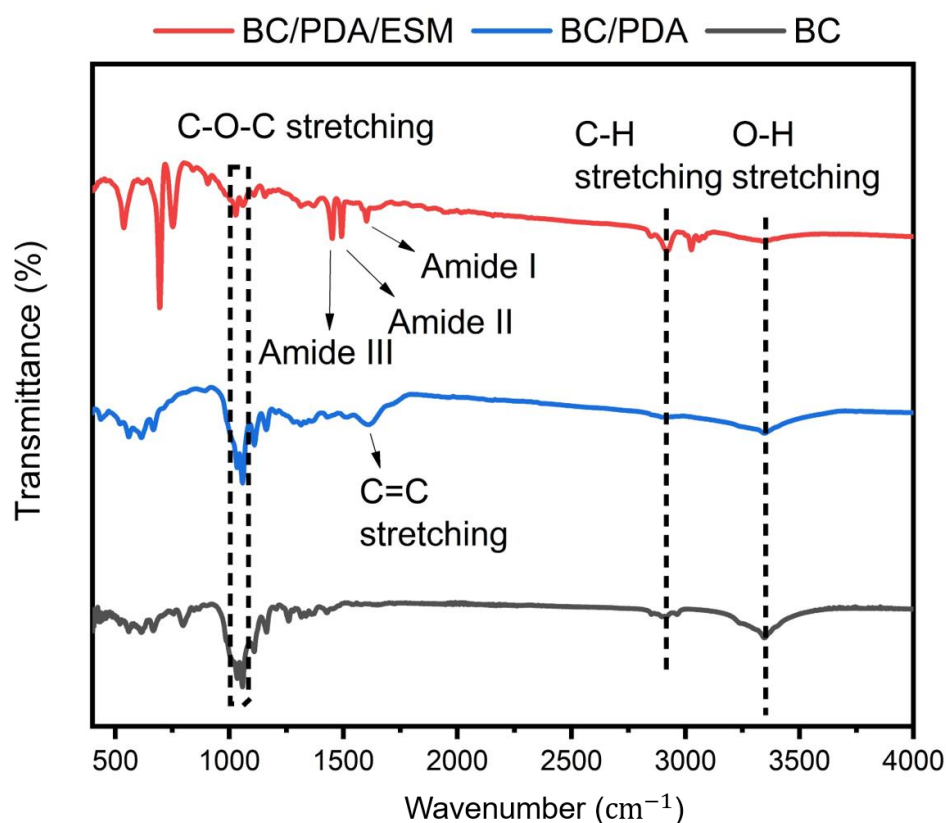
Figure 5.4 FTIR characterization of BC/PDA/ESM, BC/PDA and BC samples.

Figure 5.4 and Table 5.2 show the FTIR spectrum and chemical bond assignments of BC/PDA/ESM, BC/PDA and BC samples. As discussed in chapter 3, the peaks at 3344 cm^{-1} and 2800 cm^{-1} were correlated with O-H and C-H stretching and the peak at 1100 cm^{-1} corresponds to C-O-C stretching, which indicate the cellulose structure of BC[178][181]. In BC/PDA, the peak at 1700 cm^{-1} can be assigned to C=C stretching, indicating the incorporation of PDA[300][301]. The peaks at 1600, 1492 and 1198 cm^{-1} correspond to the amide I (C=O stretching), amide II (CN stretching/NH bending), and amide III (CN stretching/NH bending) of glycoprotein in ESM[279][210]. Meanwhile, the

156

broad peak around 3344 cm^{-1} in BC/PDA/ESM spectrum also indicates the phenolic hydroxyl stretching of catechol groups[279][210].

Table 5.2 Summary of main absorption bands and chemical bond assignment for FTIR spectra of BC, BC/PDA, and BC/ESM samples.

Peak wavenumber (cm^{-1})	Chemical bonds	Materials
3344	O-H stretching	BC[241][244]
2800	C-H stretching	
1605	C=C stretching	PDA[300][301]
1600	Amide I (C=O stretching)	ESM[279][210]
1492	Amide II (CN stretching/NH bending)	
1198	Amide III (CN stretching/NH bending)	

Tensile test
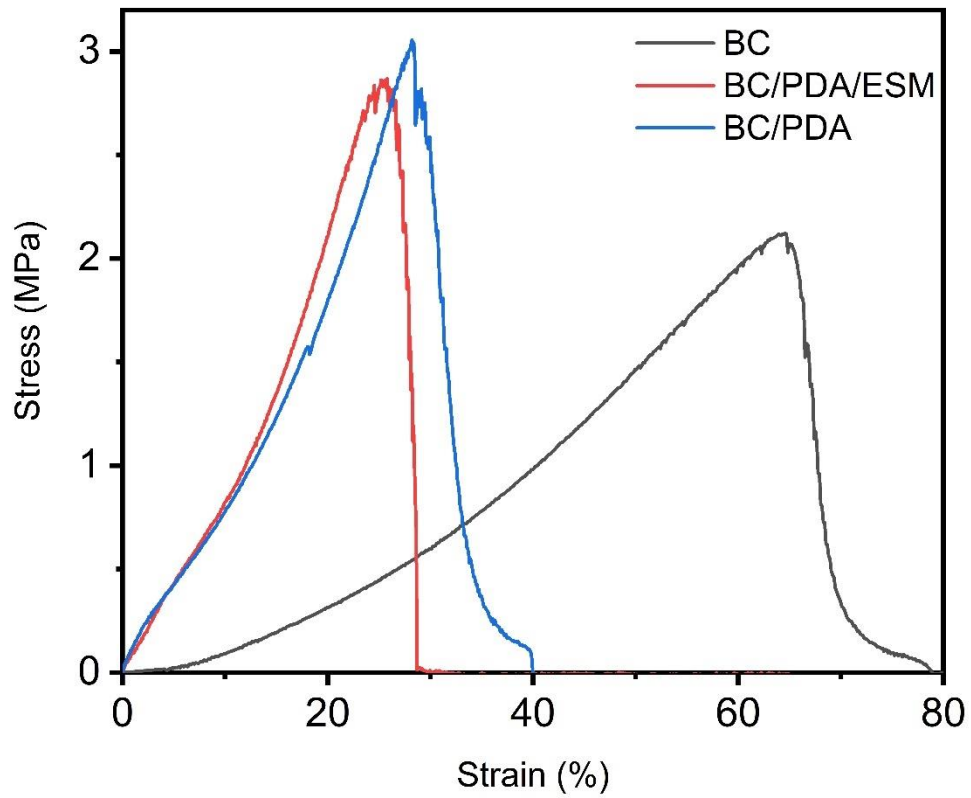
Figure 5.5 Tensile test to determine the mechanical properties of BC/ESM, BC/PDA and BC samples.

Table 5.3 Measurements of mechanical properties of BC, BC/PDA, BC/PDA/ESM in terms of tensile strength and elongation.

Materials	Tensile strength (MPa)	Elongation (%)
BC	2.02 ± 0.30	63.8 ± 1.50
BC/PDA	2.51 ± 1.10	24.50 ± 1.12
BC/PDA/ESM	2.71 ± 1.30	22.41 ± 1.52

In order to test the mechanical properties of wet BC, BC/PDA and BC/PDA/ESM, the tensile test was performed (Figure 5.5) and tensile strength as well as material elongation were measured (Table 5.3). It is evident that all BC based samples show high tensile strength which can be attributed to the existence of the inter-connected nano-network structure of BC nanofibers *via* strong hydrogen bonding. However, BC had the lowest tensile strength combined with the highest elongation, indicating more ductile and flexible mechanical behaviour compared with BC/PDA and BC/PDA/ESM. By the same token, BC/PDA is more ductile and flexible than BC/PDA/ESM nanocomposite. The results can be attributed the presence of phenolic hydroxyl in catechol groups of ESM and PDA which increase the crystallinity of materials, resulting in increased strength[302].

Disk diffusion test
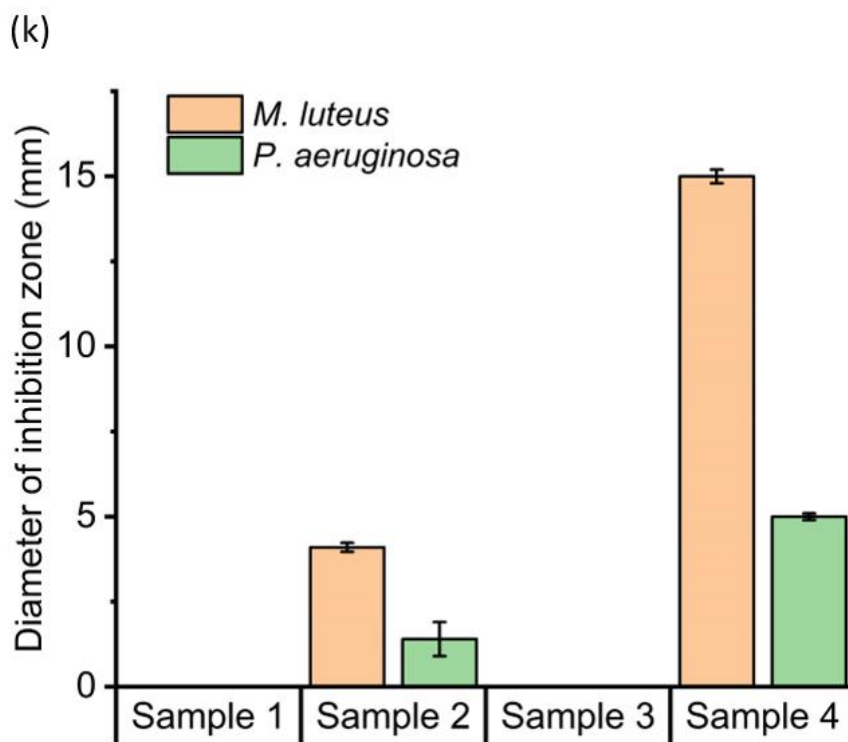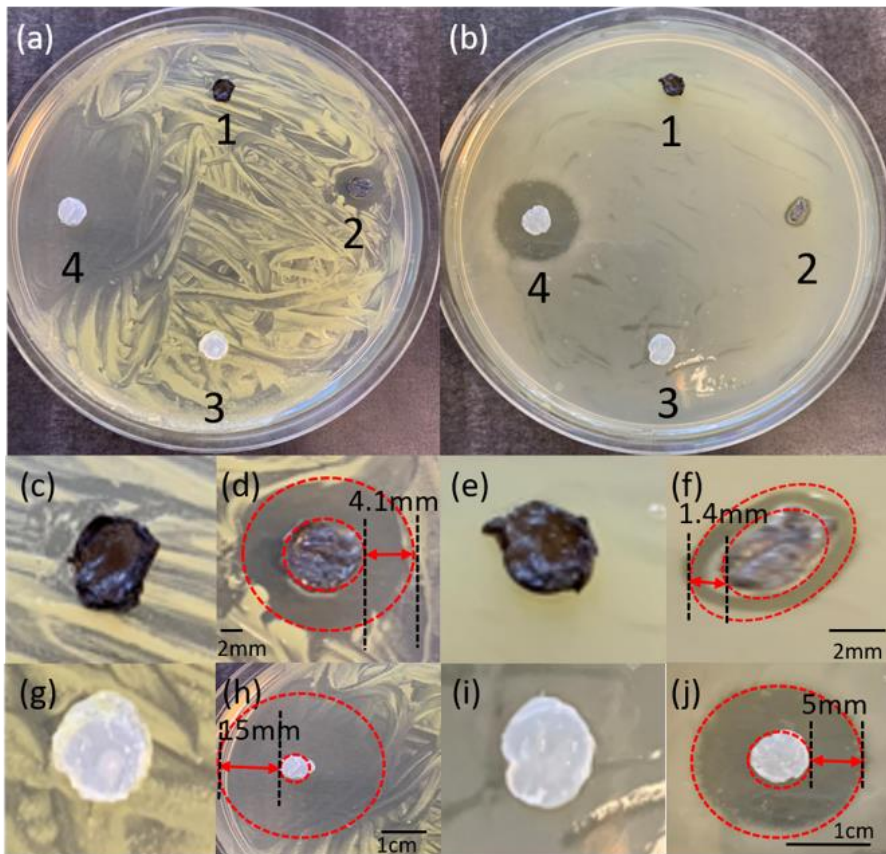
Figure 5.6 Disk diffusion test of BC (sample 3), BC/PDA (sample 1), BC/PDA/ESM (sample 2) and BC/kanamycin (50 mg/ml) (sample 4) against: (a) M. luteus, (b) P. aeruginosa; the measurement of DIZ of: (c) sample 1 against M. luteus, (d) sample 2 against M. luteus, (e) sample 1 against P. aeruginosa, (f) sample 2 against P. aeruginosa, (g) sample 3 against M. luteus, (h) sample 4 against M. luteus (i) sample 3 against P. aeruginosa, (j) sample 4 against P. aeruginosa; (k) summary of DIZ of four samples against two bacteria strains.

The antimicrobial activities of BC/PDA and BC/PDA/ESM were characterized via a disk diffusion test, where plain BC was used as a negative control group. BC/kanamycin (50 mg/ml) was used as a positive control group. Figure 5.6 (a) and (b) show the results of the disk diffusion test against Gram-positive *M. luteus* and Gram-negative *P. aeruginosa*. Antimicrobial activity was measured by the DIZ value shown in Figures 5.6 (c)-(j). Therefore, after 24-hour incubation, BC/PDA and BC did not exhibit any antimicrobial activity against two pathogenic bacteria, whilst BC/PDA/ESM showed good antimicrobial activity against Gram-positive *M. luteus* and slight antimicrobial activity against Gram-negative *P. aeruginosa*. However, compared with positive control groups, the antimicrobial activity of BC/PDA/ESM was less effective especially against Gram-negative bacteria with biofilms. According to work by Ahlborn et.al[303], the main components in eggshell membranes responsible for antimicrobial activity are lysozyme ovo-transferrin and beta-NAGase which are more effective against Gram-positive bacteria. However, this requires further research. It is evident from previous results that BC/AgNP, BC/PDA/ESM have comparable antimicrobial activity against *M. luteus* and less activity towards *P. aeruginosa*. Therefore, BC/PDA/ESM can be used as antimicrobial chronic wound dressings if incorporated

with other stronger anti-bacterial agents to achieve further broad spectrum antimicrobial property.

Ex-vivo stitching test
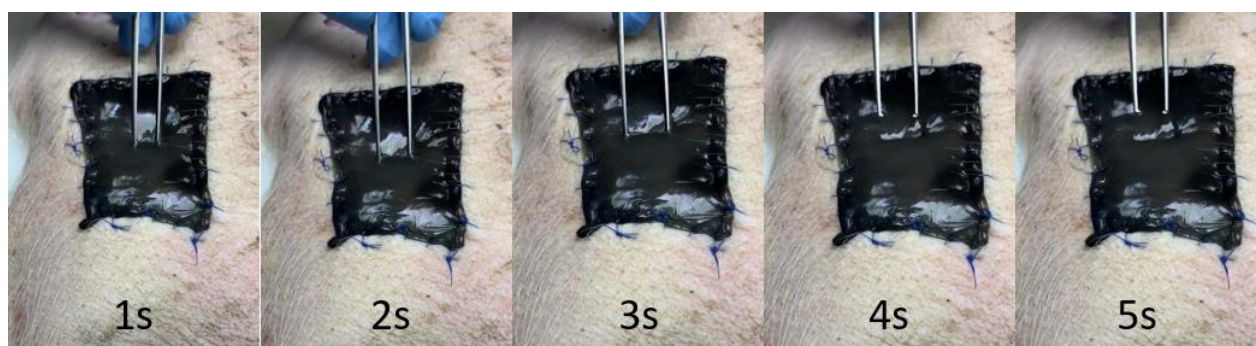
Figure 5.7 Images of the mechanical behaviour of the BC/PDA/ESM membrane by stretching with a hooked sharp tweezer on pig belly skin on a time scale (from 1s to 5s).

In order to further investigate the potential application of BC/PDA/ESM nanocomposite in temporary skin substitute , a wet sample was stitched and tested on a dead pig belly skin on a timescale from 1s to 10s. A sharp tweezer with hook was chosen to investigate the durability. As shown in figure 5.7, the sample can be easily sewed onto the skin. The sample is highly durable and can be firmly stretched by the sharp tweezer without any breakages. The excellent mechanical strength results from the three-dimensional inter-connected nano network structure of cellulose fibres. In addition, the gripping test with the same hooked tweezer was also carried out on the same sample, as shown in figure 5.8. It is evident that when gripped and scraped with the sharp hooked tweezer, the BC/PDA/ESM nanocomposite material still retains original shape without any surface cracks. Therefore, the high durability make BC/PDA/ESM a great candidate as a potential temporary skin substitute material for large non-healing

chronic wounds, though further *in vivo* animal tests should be performed to investigate

the biocompatibility.
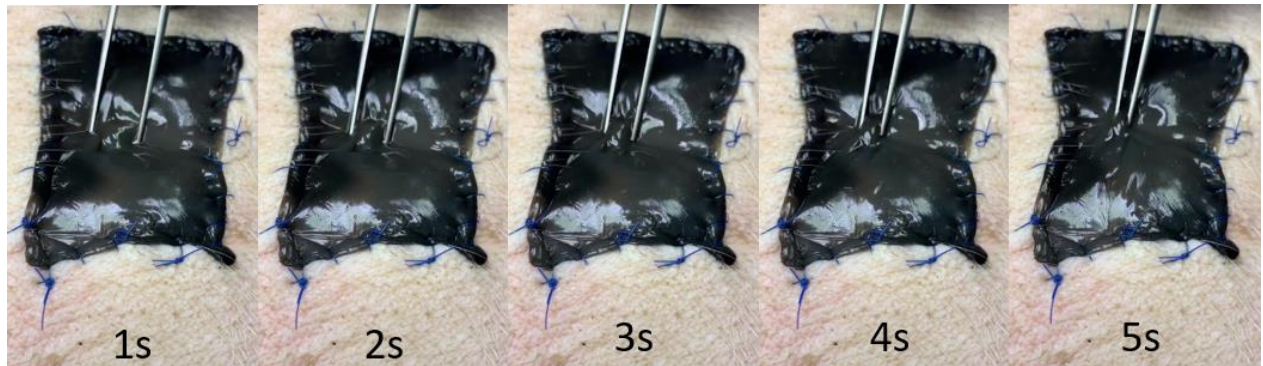
Figure 5.8 Images of the mechanical behaviour of BC/PDA/ESM by gripping with a hooked tweezer on a pig belly skin on a time scale from 1s to 5s.

(3) BC/MGO

SEM and FTIR characterization
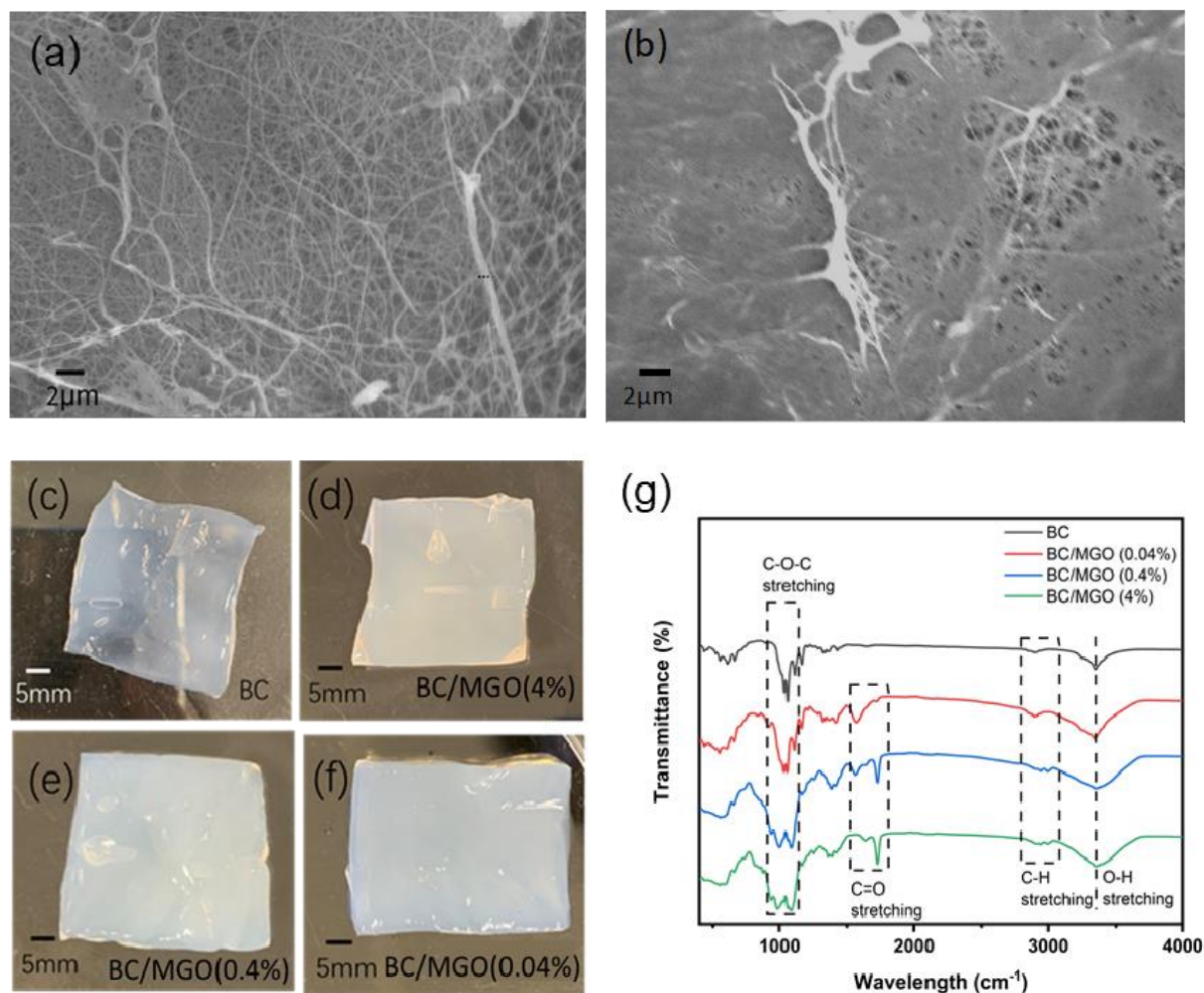
Figure 5.9 Characterization of nanostructure and elemental composition of BC and BC/MGO: (a) SEM image of freeze-dried BC sample. (b) SEM image of BC/MGO nanocomposite; photographs of (c) untreated BC (d) BC/MGO samples (BC/MGO (4%) (e) BC/MGO (0.4%) (f) BC/MGO (0.04%)). (g) FTIR spectrum of BC, BC/MGO (4%), BC/MGO (0.4%), BC/MGO (0.04%).

As demonstrated in the photographs of pristine BC membrane and BC/MGO composite (Figure 5.9, (c)-(f)) both untreated plain BC and BC/MGO membranes were soft and translucent, whilst BC/MGO with a higher MGO content was more yellow. SEM images of MGO/BC confirmed the presence of nano-meter fibrils (circa. 60-200

nm in diameter) and 3D inter-connected structures (Figure 5.9 (b)), in good agreement with the structural characteristics of plain BC (Figure 5.9 (a)). In comparison with the plain BC sample, the MGO/BC sample indicated a change in surface morphology, where MGO acted as a coating filling the voids and covering the fibril network of the original BC. FTIR analysis showed the presence of C-O-C at 980 cm^{-1}, C-H bending at 1088 cm^{-1}[304], C-O stretching and OH stretching at peaks of 1058.75 and 3351.75 cm^{-1}, indicating the chemical structure of the plain BC[305]. In addition, the second line in the FTIR analysis showed the existence of a peak associated with C=O stretching at 1750 cm^{-1} [306], which confirmed the incorporation of MGO into the BC.

AFM characterization

To further investigate and compare the surface morphology between BC and BC/MGO with different MGO coating concentrations, AFM characterization was also performed. As shown in figure 5.10 (a) and (b), the mean diameter of the BC fibres is circa. 50 nm, which was in accordance with other publications [307],[308]. Meanwhile, BC/MGO nanocomposites in figure 5.10 (c)-(h) show similar fibril diameters to the plain BC, however, the surface roughness of the nanocomposites increased with increasing MGO content. In this case, figure 5.10 (g) and (h) reveal the most obvious difference in the surface morphology of BC/MGO nanocomposites from the plain BC, where the roughness is the highest, circa. 114 nm. Furthermore, some knots are observed around the fibre-net, indicating that the incorporation of MGO coating on BC could increase the surface roughness by interpenetrating the nano-network structure, caused by the excellent physical absorption properties of the interconnected nano-network of the plain BC.
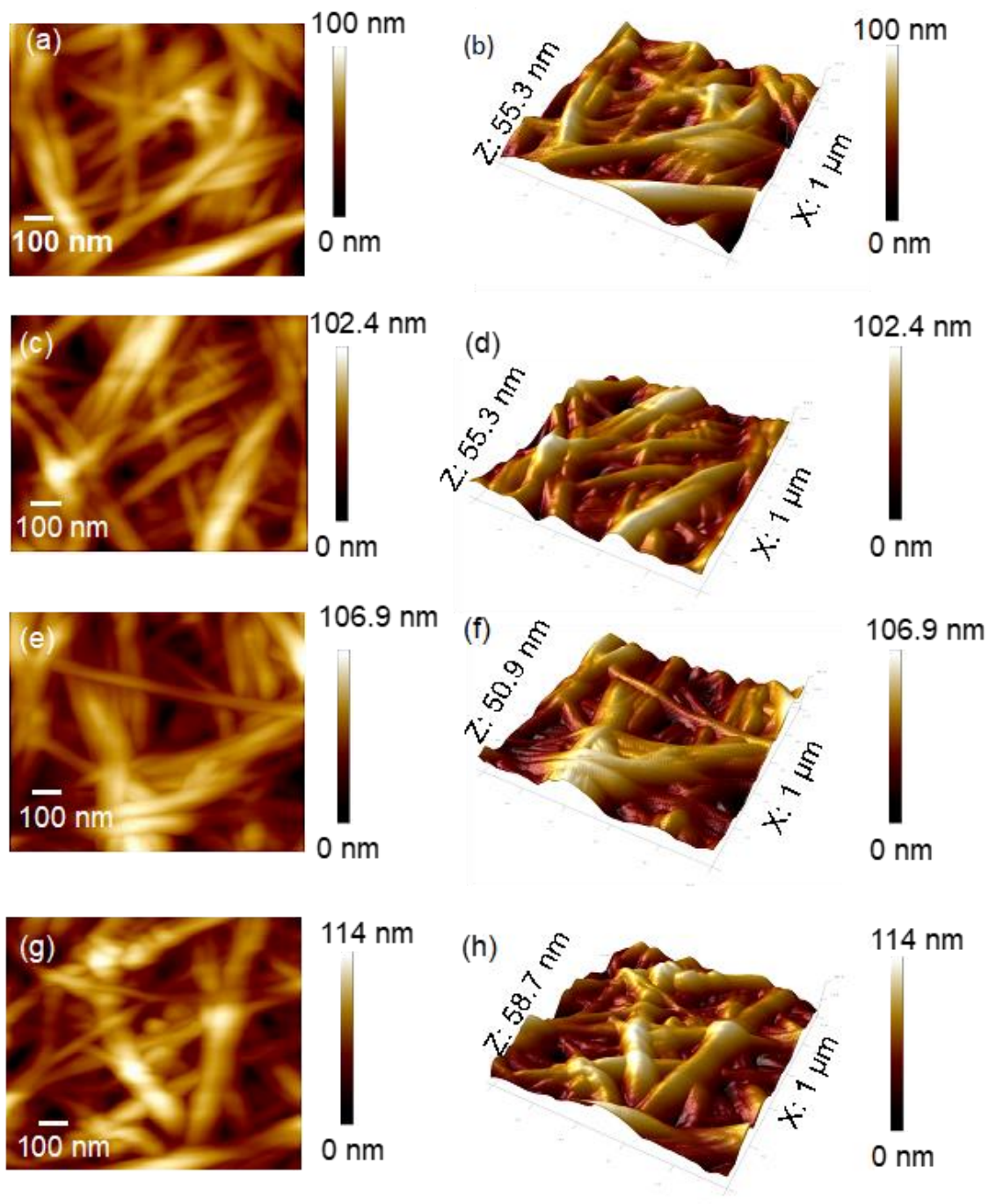
Figure 5.10 AFM images of: (a) BC (c) BC/MGO (0.04%) (e) BC/MGO (0.4%) (g) BC/MGO (4%) and 3D surface images of: (b) BC (d) BC/MGO (0.04%) (f) BC/MGO (0.4%) and (h) BC/MGO (4%).

Thermal stability testing
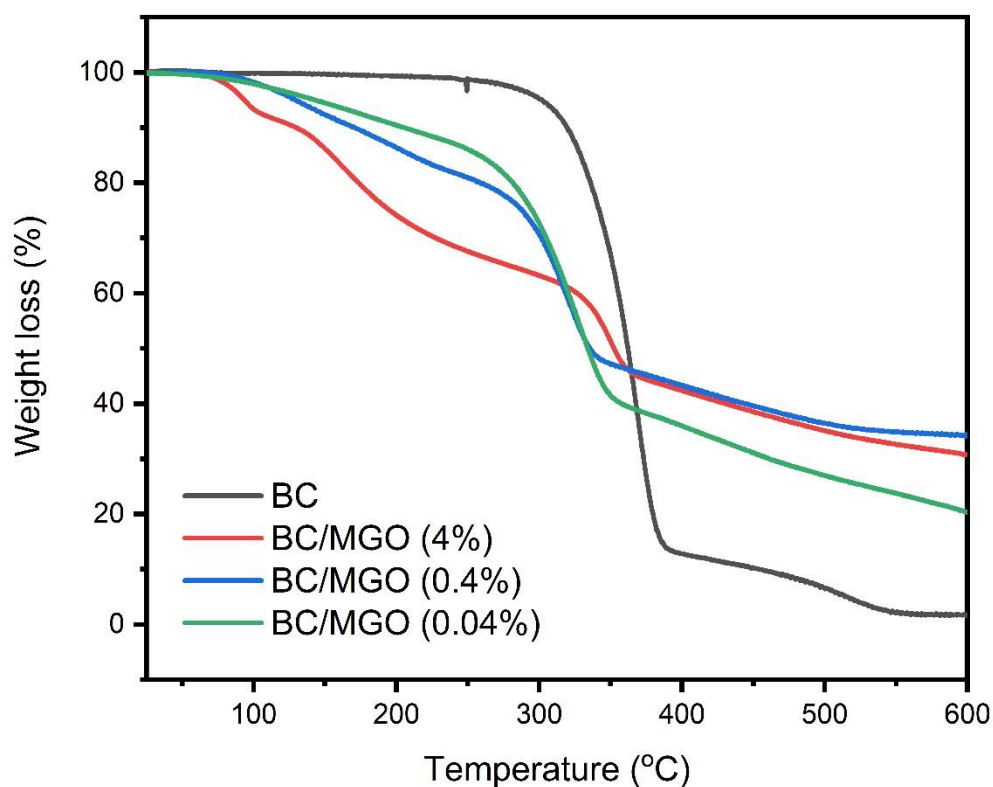
Figure 5.11 TGA curves of BC, BC/MGO (4%), BC/MGO (0.4%), BC/MGO (0.04%).

To understand the thermal decomposition behaviour of BC and BC/MGO composites, TGA was performed. Figure 5.11 shows the weight loss curves (TG) of BC, BC/MGO (4%), BC/MGO (0.4%), and BC/MGO (0.04%), indicating that dehydration occurred below 100°C and depolymerization and decomposition of glucosyl units between 320 to 400°C[309],[310],[311],[312]. When BC coated with MGO was analysed using TGA, the nanocomposite is less stable than plain BC, with degradation at 320-370°C, whilst plain BC degraded at 380 - 400°C. This may be attributed to weaker hydrogen bonding and decreased crystallinity with increasing MGO content.

Tensile testing
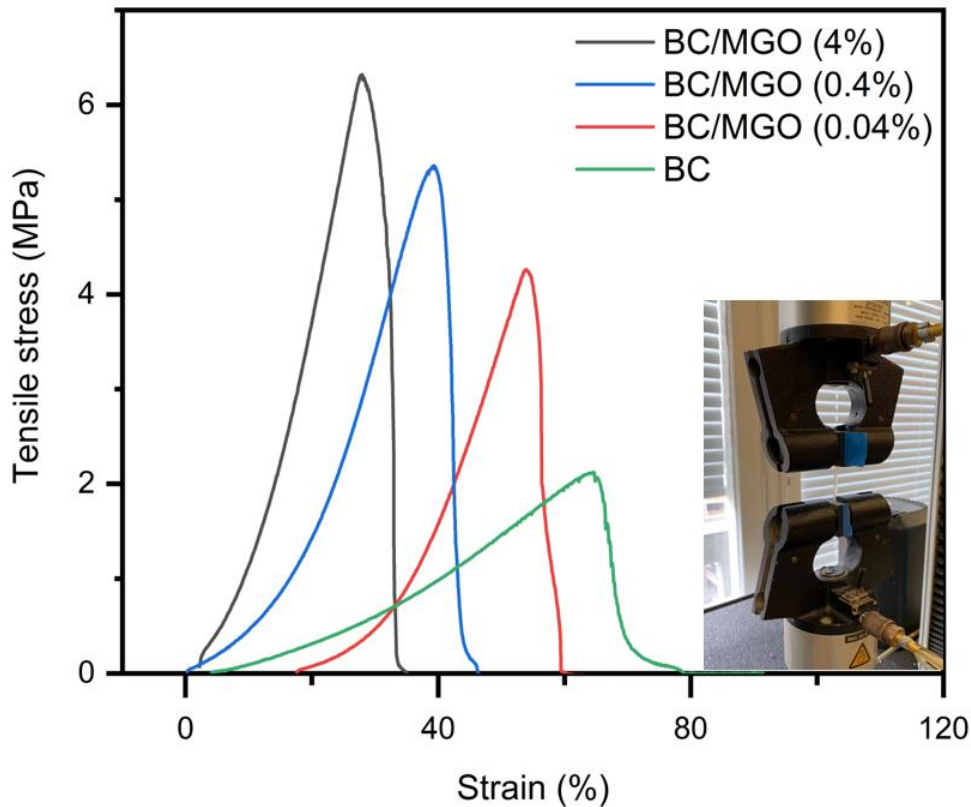
Figure 5.12 Tensile tests to determine the mechanical properties of untreated BC, and treated BC (BC/MGO 4%, BC/MGO 0.4% and BC/MGO 0.04%).

Since mechanical strength is a key property of materials used in wound dressing applications, the tensile strength was tested in untreated BC as well as BC/MGO with various MGO concentrations in the wet state. The tensile properties of the samples were illustrated in figure 5.12 and summarised in table 5.4. BC based samples exhibited high tensile strength due to the interconnected nano-network structure with strong hydrogen bonding interactions[313].Compared with other BC/MGO samples, the untreated BC sample appeared softer, more ductile and flexible. Whereas BC/MGO samples seemed harder and more brittle with increasing MGO concentration.

BC/MGO 4% with the highest coating concentration of MGO exhibited the highest tensile strength but lowest extension, which might be attributed to the presence of the strong carbonyl group due to increased crystallinity of the materials[314]. Overall, all BC/MGO samples exhibited good mechanical properties, which make them promising flexible wound dressing materials.

Table 5.4 Mechanical properties of untreated BC, and BC/MGO (4%), BC/MGO (0.4%) and BC/MGO (0.04%).

Materials	Tensile strength (MPa)	Elongation (%)
Untreated BC	2.02 ± 0.229	63.8 ± 1.453
BC/MGO (4%)	6.32 ± 0.231	29.59 ± 0.768
BC/MGO (0.4%)	5.13 ± 1.640	38.97 ± 1.859
BC/MGO (0.04%)	4.36 ± 1.341	55.33 ± 1.596

Release profile

In order to investigate release behaviours of MGO loaded in BC *via* static impregnation method, the release profile of BC/MGO (4%) has been studied by measuring MGO concentrations collected from the supernatants when after being placed in DI water for different time (0, 0.5, 1, 2, 3, 4, 5, 24, 30 and 48 h), and quantified by a UV/Vis spectrophotometry. The figure 5.13 (a) shows the release profile of BC/MGO (4%) in water for different time intervals. As indicated, when placed in water, the BC/MGO (4%) went through fast release in 5 hours with released MGO concentration up to 1.6%. After 24 h, it experienced slow release and released MGO concentration reached 2.6% in 48 h. The fast release occurred at the beginning due to the MGO residue left on BC surface after fabrication. However, after surface MGO had been released in water, it went into slow release after 24 h. The slow release behaviour of BC can be attributed to its inter-connected nano-network structure trapping part of MGO solution inside. Moreover, the hydrophilicity of BC nanofibrils can result in the wide internal surface area of interstitial space of wet BC pellicle, which allowed physical adsorption of impregnated MGO solution. In order to study whether the static impregnation method reaches the saturation of MGO in samples, the MGO concentration of three samples BC/MGO(4%), BC/MGO(0.4%) and BC/MGO(0.04%) impregnated for 24 and 48 h were measured and quantified by a UV/Vis spectrometry as well. The results in figure 5.13 (b) indicates the three samples can nearly reach the MGO saturation after impregnation for 48 h in static. While after being impregnated for 24 h, all samples can still reach above half of the saturated concentration. The results confirm BC has conducted physical adsorption during the impregnation process and can reach the adsorption saturation after 48 h impregnation time.

(a)
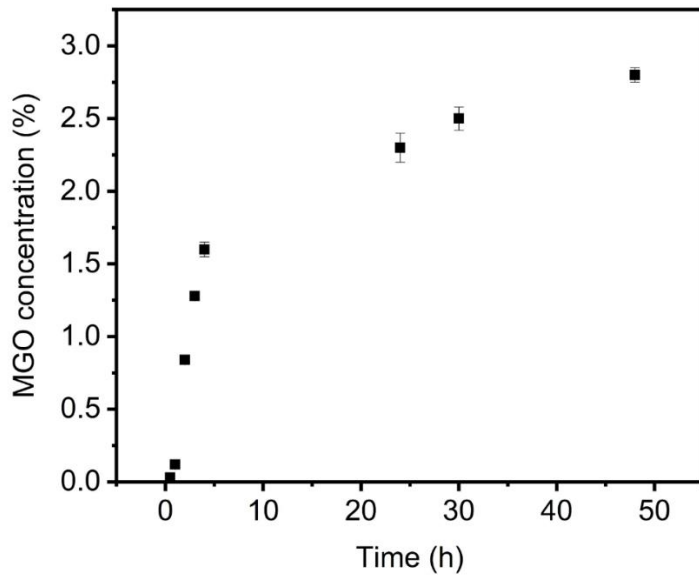
(b)
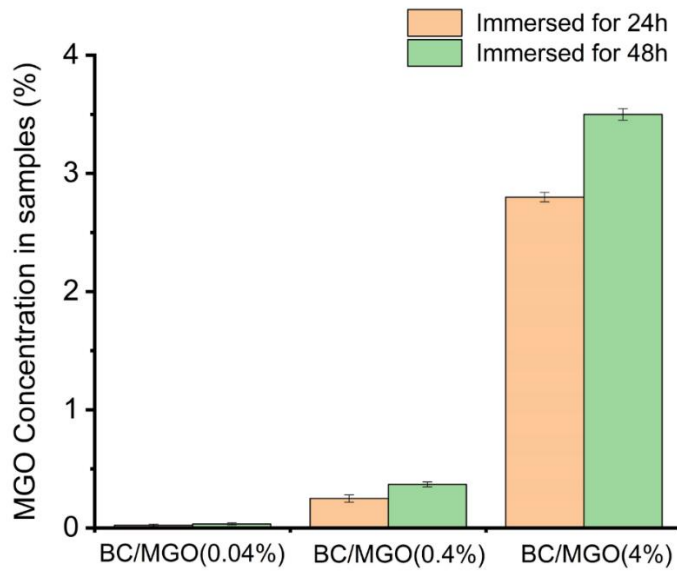
Figure 5.13 (a) cumulative release profiles (mean ± SD, n=3) of BC/MGO(4%) in water, (b) the MGO concentrations measured in samples immersed in different MGO solutions via static impregnation for 24 and 48 h.

Disk diffusion test
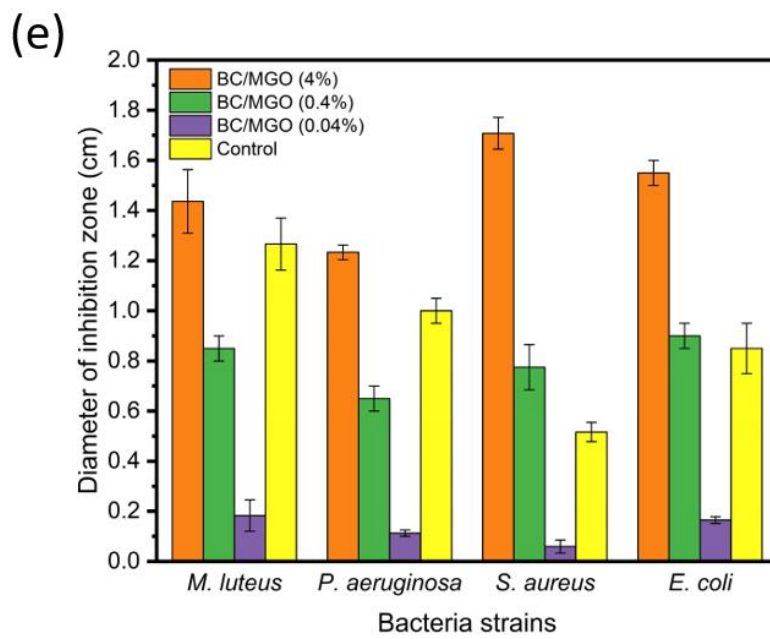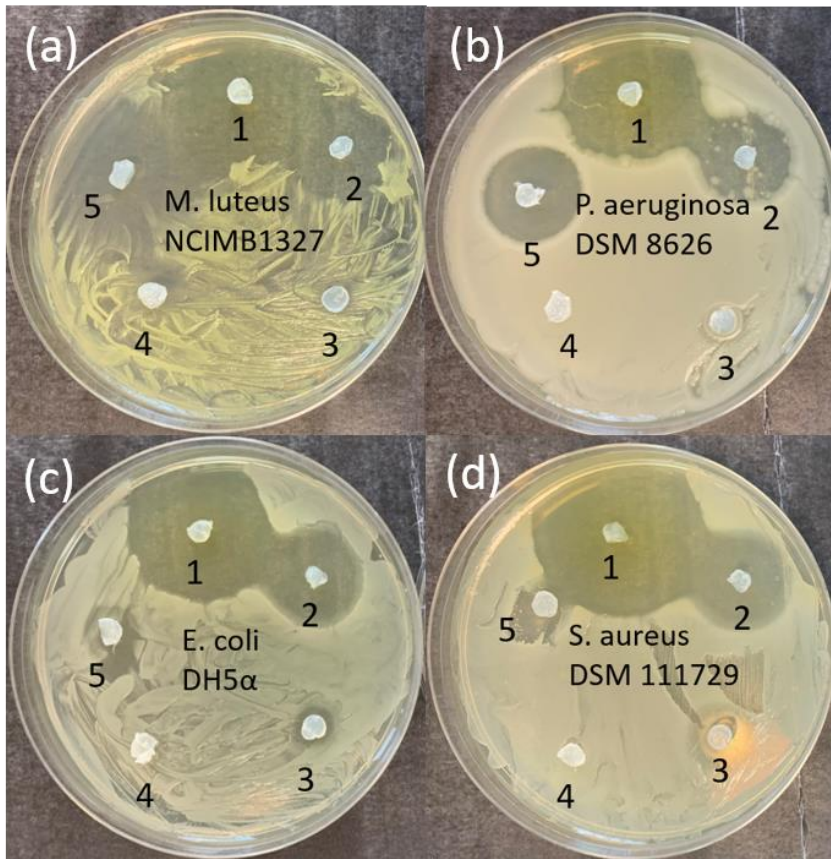
Figure 5.14 Disk Diffusion test of BC/MGO samples against (a) M. luteus, (b) P. aeruginosa, (c) S. aureus, (d) E.coli (sample number 1: BC/MGO (4%), 2:BC/MGO(0.4%), 3:BC/MGO(0.04%), 4: plain BC, 5: antibiotic positive control (kanamycin (50 mg/ml) for (a) and (b), ampicillin (50 mg/ml) for (c) and (d)), (e) Diameter of inhibition zone measured for each sample against different strains of bacteria.

In this work, the antimicrobial property of MGO coated BC nanocomposites against *M. luteus*, *P. aeruginosa*, *S. aureus*, and *E. coli* were investigated using the disk diffusion test (figure 5.14 (a)-(d)). For each plate, a positive control group of two antibiotics, dipped BC and a plain BC control group were tested for comparison. The efficiency of antimicrobial activity was measured by the diameter of clear zones of inhibition (DIZ) around the round-shaped cut samples after 24 h of incubation at 37°C. After 24 h incubation, the DIZ values of MBC4% with the highest MGO concentration were 1.43 ± 0.13 cm, 1.23 ± 0.03 cm, 1.71 ± 0.06 cm, and 1.55 ± 0.05 cm (see figure 5.14 (e)), while the positive control groups had DIZ values of 1.27 ± 0.14 cm, 1.0 ± 0.05 cm, 0.52 ± 0.04 cm and 0.85 ± 0.1 cm. The control groups of plain BC had no zones of inhibition for all the samples, against *M. luteus*, *P. aeruginosa*, *S. aureus*, and *E. coli*, respectively. In addition, it was also obvious from figure 5.14 (e) that BC/MGO nanocomposites were slightly more effective against Gram-positive than Gram-negative strains contained in biofilms while it was still lethal towards multi-antibiotic-resistant *S. aureus* (MRSA). Across all strains of bacteria tested, the antimicrobial activity was more pronounced at increased MGO concentrations. This indicated that MGO coated BC, with at least 0.04% concentration was sufficient to reduce the activity of most pathogenic bacteria which most likely to exist in the mid to late stage of chronic wounds. Table 5.5 summarises recent publications on the antimicrobial properties of BC nanocomposites. Compared with results from existing literature, it is obvious that in non-silver based organic antimicrobial BC composites, our proposed MGO/BC is

greatly efficient against broad-spectrum bacteria. This performance is better than inorganic metal-oxide based BC composites. Although still incomparable with antiseptic or antibiotic based BC composites, the strong and broad-spectrum antibacterial properties of BC/MGO render it a promising antimicrobial wound dressing material or skin substitute for chronic wound care.

Table 5.5 Summary of DIZ in common wound dressing materials proposed in recent literature.

	Materials	Diameter of zone of inhibition (DIZ) (mm)		Type of wounds Applications
		E.coli	*S. aureus*	
Nano-particle based nano-composites	Chitosan/Gelatin/Fe$_3$O$_4$ nano-fibre membrane [315]	21 ± 1	20 ± 2	Normal wounds
	Chitosan/poly(N-vinylpyrrolidone)/TiO$_2$ nanocomposite [316]	30 ± 0	32 ± 0	Infected wounds
	Alginate hydrogel/zinc oxide nanoparticle composite[317]	16 ± 1	18 ± 2	Infected wounds
	Chitosan–hyaluronic acid/nano silver composite sponge[318]	13 ± 2	14 ± 2 10 ± 2 for MRSA	Diabetic wounds
	silver nanoparticle hydrogel[319]	10.4 ± 0.7	10.8 ± 0.7	Burn wounds
Natural antibacterial	*Lawsonia Inermis*-gelatin-starch nano-fibrous dressing[320]	4.45 ± 0.13	3.34	Burn wounds

agents based composites	Hypericum perforatum /chitosan films[321]	2.9 ± 0.1	1.97 ± 0.05	Normal wounds
	Curcumin nanocomposite[322]	19 ± 0	14 ± 0	Infected wounds
	poly(ε-caprolactone)/poly(lactic acid)/Thymol nanofibrous mats[323]	7.8 ± 0	10.4 ± 0	Normal wounds
BC based nano-composites	BC/ tetracycline hydrochloride (TCH)[165]	47.5 ± 0	38.5 ± 0	Infected wounds
	BC/antibiotic fusidic acid (FA)[178]	/	30 ± 0	Infected wounds
	BC/Copper nano-particle[324]	21.3 ± 1.5	20.0 ± 0.8	Long-term infected wounds
	BC/Zinc oxide[325]	27 ± 0	28.6 ± 1.15	Burn wounds
	BC/Silver nano-particle[144]	2.03 ± 0	3.46 ± 0	Normal wounds
Silver-based commercial wound dressings	Silver Sulfadiazine[160]	9.3 ± 0	13 ± 0	Infected wounds
	Acticoat [319]	9.7 ± 0	10.3 ± 0	
The proposed BC/MGO nano-composite	BC/MGO nanocomposite[277]	15.5 ± 0.5	17.1 ± 0.6	Chronic wounds

5.4 Summary

This chapter described the fabrication of inorganic BC/AgNP antimicrobial nanocomposite, organic BC/lysozyme, BC/PDA/ESM and BC/MGO nanocomposite, followed by investigation of the surface morphology, chemical composition, mechanical properties and antimicrobial activities. In addition, all the synthetic procedures were simple, green and cost-effective. The results show that BC/AgNP, BC/lysozyme and BC/PDA/ESM have limited effect on Gram-negative bacteria where BC/lysozyme and BC/PDA/ESM have little or no antimicrobial activity against *P. aeruginosa*. This may be attributed to the extra support provided to the bacterial cell walls of gram-negative bacteria due to the existence of biofilms. Compared with BC/AgNP, BC/lysozyme, BC/PDA/ESM nanocomposites, the BC/MGO with highest concentration (4% MGO) exhibited the great antimicrobial activity against both Gram-positive and Gram-negative pathogenic bacteria, even against MRSA. This makes it the best potential material for antimicrobial chronic wound dressings amongst the four BC nanocomposites proposed here. Furthermore, mechanical properties are another important factor – with all four nanocomposites presented in this chapter maintaining the excellent mechanical strength associated with plain BC due to the 3D inter-connected nano-network structure. From the *in vivo* stitching test of BC/PDA/ESM, little abrasion was observed on the material's surface either by stretching or gripping via sharp hooked tweezers. This also makes it a potential candidate for use as a temporary skin substitute in large diabetic foot ulcers. However, related *in vitro* cell tests including cell attachment, cell proliferation, and cytotoxicity testing are required to further investigate the biocompatibility and biodegradability of these materials. Additionally, an *in vivo* wound healing assay, performed on animals is a necessary further step associated with this research.

Chapter 6 Conclusions and Future Work

6   Conclusions and Future work

6.1 Conclusions

In order to meet the urgent demand for bio-mass based natural materials for smart wound dressing materials, BC and BC-derived nanocomposites were fabricated and characterized according to their different uses. This thesis provides a potential platform for BC and BC based nanocomposite materials used in smart wound dressing applications, which allow acceleration of wound healing and pH monitoring.

The first chapter provides the primary background of chronic wounds, wound types, smart wounds dressings, BC synthesis and properties, BC based antimicrobial wound dressings, and an introduction to the characterisation techniques performed during this project. In this chapter, the recent development of BC and non-BC based chronic wound dressings were investigated and compared according to their fabrication methods, characterization and specific applications. It can be concluded that there still remain challenges for recent technology concerning nature-derived smart chronic wound dressings. For antimicrobial dressings, silver or silver nanoparticle based wound dressings may have hazardous side effects to human health, following long term use. Natural antimicrobial agents provide a better solution but still require further optimisation to improve their efficacy. Smart bandages have the advantages of various wireless products that can facilitate real-time monitoring to improve the wound healing environment but require further investigation into the potential side effects of sensing materials and their reusability and accuracy.

Chapter 2 provides the experimental details and methodology for fabrication of BC and BC based nanocomposites. In this chapter, the fabrication and characterization methods used in this research project are described in detail.

Chapter 3 involves a breakdown of BC grown from four different *Acetobacter xylinus* strains (*G. xylinus* JCM 10150, *K. xylinus* DSM 16663, *K. xylinus* DSM 2325, and *K. xylinus* DSM 2004), which were cultivated in different concentrations of yeast, glucose and carbon medium with pH adjusted to the optimum levels. The four BC samples are characterized in terms of surface morphology, porosity, chemical composition, crystallinity and thermal stability. The results indicate the four BC samples exhibit large surface area, high water-holding capacity, high crystallinity, and great thermal stability, . However, lower glucose concentrations in the BC culture medium results in a reduced degree of crystallinity due to the dense network structure restricting cell motion. *In vitro* biocompatibility cell studies of HDF seeded on BC of different thicknesses demonstrates potentially biocompatibility of BC, especially for BC with lower thickness. It has been found that BC grown from *G. xylinus* JCM10150 and *K. xylinus* DSM16663 requiring low glucose concentration, have exhibited the best water holding capacity, crystallinity, surface area and thermal stability. Therefore, G. xylinus JCM10150 was chosen for p-BC fabrication and K. xylinus DSM16663 was chosen for antimicrobial BC composites.

Chapter 4 proposed a p-BC-based flexible 3D pH sensor for monitoring the pH of chronic wounds pH. The sensor performance was tested in commercial pH buffer solutions and *in vitro* wound simulated fluid, showing a linear potential and sensitivity of -50.4 mV/pH and 28.2 mV/pH, respectively. In spite of the lower pH response in simulated wound fluid, the p-BC/PDMS/PANI nanocomposite showed great potential for integration with chronic wound dressings as smart wound dressings for monitoring the pH levels in a wound bed. Chapter 4 describes the four different types of antimicrobial BC nanocomposites, BC/AgNP, BC/lysozyme, BC/PDA/ESM, and BC/MGO. The results of disk diffusion tests indicate BC/MGO with high concentrations

of MGO (4%), exhibited the greatest, broad-spectrum antimicrobial activity, including against MRSA. The release profile of BC/MGO (4%) has also been investigated and it indicates that BC nanofibrils can trap part of MGO solutions *via* physical adsorption thus resulting in slow release profile after 24 h. In addition, BC/MGO samples can almost reach the MGO saturations after 48 h impregnation in static, which further confirms the adsorption behaviours of BC nanofibrils and made it a great candidate material for static impregnation. This provides a potential platform for BC/MGO to be used in antimicrobial chronic wound dressings. *Ex vivo* stitching tests were carried out for BC/PDA/ESM nanocomposite confirming its potential application as a temporary skin substitute.

The three experimental chapters describe the BC production from four different bacteria strains, novel BC/MGO and BC/PDA/ESM nanocomposites in potential applications of antimicrobial wound dressings and p-BC/PDMS/PANI for wound pH sensors. This PhD project is utilizing BC unique inter-connected nano-network structure to achieve designated functionalities, which confirms BC is a potential element/material in applications for smart wound dressings. However, more experimental works on *in vitro* cell biocompatibility tests, *in vivo* biocompatibility and wound healing tests need to be performed to assess how far it takes to achieve the realistic chronic wounds dressings applications in clinic.

6.2 Future work

For BC production and antimicrobial BC nanocomposites, some of cell work such as cytotoxicity test, cell proliferation test and cell viability test remained incomplete due to limited access to collaborative labs as a consequence of the coronavirus pandemic. Medical products should be thoroughly tested before introduction to human body to

prevent possible negative effects. Therefore, biocompatibility testing of BC and BC nanocomposites is essential for future studies. In order to fully investigate the biocompatibility of BC specimen, further *in vitro* and *in vivo* biocompatibility tests need to be performed. *In vitro* biocompatibility tests may include cell attachment testing, cell viability tests, cell proliferation tests and cytotoxicity testing, to distinguish between quiescent/senescent and actively dividing cells to study the toxicity or irritancy potential of materials. Following completion of these *in vitro* cell tests, *in vivo* tests on animal skin may be performed to be complementary and further probe the biocompatibility on a final product, taking into account the human exposure conditions, the toxicity of chemical compounds and the presence of degradable materials. To test the functionality of novel BC based wound dressings, *in vivo* wound healing assays also need to be performed to further understand the effectiveness of nature-based wound dressings compared with commercial or other antibiotic based/inorganic wound dressings.

Meanwhile, for BC derived flexible pH sensors, the mechanical strength of p-BC carbon aerogels also need to be optimized and pH sensitivity improved in simulated wound fluid where high loads of proteins are prevented from binding extra protons in the protonation process. Long-term stability tests in simulated wound fluid at different pH levels can also be performed to test their functionality during long-term monitoring. In addition, the flexible pH sensors can be incorporated in a complete wireless sensing system with antimicrobial wound dressings for further testing. *In vitro* biocompatibility tests may be performed to investigate if the final composites are compatible with human wound areas without causing allergies.

In conclusion, the need of nature-based materials is on the rise within the developing world due to the threat of chemical contamination or potentially hazardous side effects.

Hence, this research is of great significance because it may allow people to lead healthier lives.

References

[1]   Castleberry, S.A., Almquist, B.D., Li, W., Reis, T., Chow, J., Mayner, S. and Hammond, P.T., 2016. Self-assembled wound dressings silence MMP-9 and improve diabetic wound healing *in vivo. Advanced Materials*, *28*(9), pp.1809-1817.

[2]   Int Wound, J., 2008. Wound Infection in clinical practice: an international consensus. *Int Wound J*, *5*, pp.1-11.

[3]   Dargaville, T.R., Farrugia, B.L., Broadbent, J.A., Pace, S., Upton, Z. and Voelcker, N.H., 2013. Sensors and imaging for wound healing: a review. *Biosensors and Bioelectronics*, *41*, pp.30-42.

[4]   Anastas, P.T., 1999. Green chemistry and the role of analytical methodology development. *Critical reviews in analytical chemistry*, *29*(3), pp.167-175.

[5]   Mustoe, T.A., O'shaughnessy, K. and Kloeters, O., 2006. Chronic wound pathogenesis and current treatment strategies: a unifying hypothesis. *Plastic and reconstructive surgery*, *117*(7S), pp.35S-41S.

[6]   Gottrup, F., 2004. A specialized wound-healing center concept: importance of a multidisciplinary department structure and surgical treatment facilities in the treatment of chronic wounds. *The American journal of surgery*, *187*(5), pp.S38-S43.

[7]   Richmond, N.A., Lamel, S.A., Davidson, J.M., Martins-Green, M., Sen, C.K., Tomic-Canic, M., Vivas, A.C., Braun, L.R. and Kirsner, R.S., 2013. US–N ational I nstitutes of H ealth-funded research for cutaneous wounds in 2012. *Wound Repair and Regeneration*, *21*(6), pp.789-792.

[8]   Eming, S.A., Martin, P. and Tomic-Canic, M., 2014. Wound repair and regeneration: mechanisms, signaling, and translation. *Science translational medicine*, *6*(265), pp.265sr6-265sr6.

[9]   "Mediligence," can be found under http://mediligence.com/rpt/rpt-s249.htm?_ga=1.94828757.831280299.1433739315, n.d.

[10]   Frykberg, R.G. and Banks, J., 2015. Challenges in the treatment of chronic wounds. *Advances in wound care*, *4*(9), pp.560-582.

[11]   Posnett, J. and Franks, P., 2008. The burden of chronic wounds in the UK. *Nursing times*, *104*(3), pp.44-45.

[12]   Olsson, M., Järbrink, K., Divakar, U., Bajpai, R., Upton, Z., Schmidtchen, A. and Car, J., 2019. The humanistic and economic burden of chronic wounds: a systematic review. *Wound Repair and Regeneration*, *27*(1), pp.114-125.

[13]   Gronert, K., 2008. Lipid autacoids in inflammation and injury responses: a matter of privilege. *Molecular interventions*, *8*(1), p.28.

[14]   Diegelmann, R.F. and Evans, M.C., 2004. Wound healing: an overview of acute, fibrotic and delayed healing. *Front biosci*, *9*(1), pp.283-289.

[15]   WoundSource. 2021. *The Four Stages of Wound Healing*. [online] Available at: <https://www.woundsource.com/blog/four-stages-wound-healing> [Accessed 6 July 2021].

[16]   Gerritsen, M.E. and Bloor, C.M., 1993. Endothelial cell gene expression in response to injury. *The FASEB journal*, *7*(6), pp.523-532.

[17]   Banerjee, J. and Sen, C.K., 2015. Skin Wound Healing. In *MicroRNA in Regenerative Medicine* (pp. 631-651). Academic Press.

[18]   Maddocks, S., 2021. *Microbial communities within the chronic wound*. [online] Microbiologysociety.org. Available at: <https://microbiologysociety.org/publication/past-issues/the-microbiome/article/microbial-communities-within-the-chronic-wound.html> [Accessed 6 July 2021].

[19]   Attinger, C. and Wolcott, R., 2012. Clinically addressing biofilm in chronic wounds. *Advances in wound care*, *1*(3), pp.127-132.

[20]   Zhao, G., Usui, M.L., Lippman, S.I., James, G.A., Stewart, P.S., Fleckman, P. and Olerud, J.E., 2013. Biofilms and inflammation in chronic wounds. *Advances in wound care*, *2*(7), pp.389-399.

[21]   Clinton, A. and Carter, T., 2015. Chronic wound biofilms: pathogenesis and potential therapies. *Laboratory medicine*, *46*(4), pp.277-284.

[22]   Parsek, M.R. and Singh, P.K., 2003. Bacterial biofilms: an emerging link to disease pathogenesis. *Annual Reviews in Microbiology*, *57*(1), pp.677-701.

[23]   James, G.A., Swogger, E., Wolcott, R., Pulcini, E.D., Secor, P., Sestrich, J., Costerton, J.W. and Stewart, P.S., 2008. Biofilms in chronic wounds. *Wound Repair and regeneration*, *16*(1), pp.37-44.

[24]   Dhall, S., Do, D., Garcia, M., Wijesinghe, D.S., Brandon, A., Kim, J., Sanchez, A., Lyubovitsky, J., Gallagher, S., Nothnagel, E.A. and Chalfant, C.E., 2014. A novel model of chronic wounds: importance of redox imbalance and biofilm-forming bacteria for establishment of chronicity. *PLoS One*, *9*(10), p.e109848.

[25]   Kadam, S., Nadkarni, S., Lele, J., Sakhalkar, S., Mokashi, P. and Kaushik, K.S., 2019. Bioengineered Platforms for Chronic Wound Infection Studies: How Can

We Make Them More Human-Relevant?. *Frontiers in bioengineering and biotechnology*, *7*, p.418.

[26]   Bowler, P.G., Duerden, B.I. and Armstrong, D.G., 2001. Wound microbiology and associated approaches to wound management. *Clinical microbiology reviews*, *14*(2), pp.244-269.[27]   Kalan, L. and Grice, E.A., 2018. Fungi in the wound microbiome. *Advances in wound care*, *7*(7), pp.247-255.

[28]   Bowers, S. and Franco, E., 2020. Chronic wounds: evaluation and management. *American family physician*, *101*(3), pp.159-166.

[29]   Evans, K., Kim, P.J., Berman, R.S., Bruera, E. and Savarese, D.M., 2017. Overview of treatment of chronic wounds. *UpToDate Inc., Waltham, MA. Last reviewed January.*

[30]   Finlay, I.G., Bowszyc, J., Ramlau, C. and Gwiezdzinski, Z., 1996. The effect of topical 0.75% metronidazole gel on malodorous cutaneous ulcers. *Journal of pain and symptom management*, *11*(3), pp.158-162.

[31]   Masuelli, L., Tumino, G., Turriziani, M., Modesti, A. and Bei, R., 2010. Topical use of sucralfate in epithelial wound healing: clinical evidence and molecular mechanisms of action. *Recent patents on inflammation & allergy drug discovery*, *4*(1), pp.25-36.

[32]   Sharp, D., Gladstone, P., Smith, R.B., Forsythe, S. and Davis, J., 2010. Approaching intelligent infection diagnostics: Carbon fibre sensor for electrochemical pyocyanin detection. *Bioelectrochemistry*, *77*(2), pp.114-119.

[33]   Sharp, D., Forsythe, S. and Davis, J., 2008. Carbon fibre composites: integrated electrochemical sensors for wound management. *Journal of*

biochemistry, 144(1), pp.87-93.

[34] Matzeu, G., Losacco, M., Parducci, E., Pucci, A., Dini, V., Romanelli, M. and Di Francesco, F., 2011, November. Skin temperature monitoring by a wireless sensor. In *IECON 2011-37th Annual Conference of the IEEE Industrial Electronics Society* (pp. 3533-3535). IEEE.

[35] Cui, S.J., Fu, Y., Liu, Y., Kou, X.X., Zhang, J.N., Gan, Y.H., Zhou, Y.H. and Wang, X.D., 2019. Chronic inflammation deteriorates structure and function of collagen fibril in rat temporomandibular joint disc. *International journal of oral science, 11*(1), pp.1-8.

[36] Pace, S., Vasani, R.B., Zhao, W., Perrier, S. and Voelcker, N.H., 2014. Photonic porous silicon as a pH sensor. *Nanoscale research letters, 9*(1), pp.1-7.

[37] Meier, R.J., Schreml, S., Wang, X.D., Landthaler, M., Babilas, P. and Wolfbeis, O.S., 2011. Simultaneous photographing of oxygen and pH in vivo using sensor films. *Angewandte Chemie International Edition, 50*(46), pp.10893-10896.

[38] Han, G. and Ceilley, R., 2017. Chronic wound healing: a review of current management and treatments. *Advances in therapy, 34*(3), pp.599-610.

[39] Hogg, S., 2013. *Essential microbiology.* John Wiley & Sons.

[40] Simões, D., Miguel, S.P., Ribeiro, M.P., Coutinho, P., Mendonça, A.G. and Correia, I.J., 2018. Recent advances on antimicrobial wound dressing: A review. *European Journal of Pharmaceutics and Biopharmaceutics, 127*, pp.130-141.

[41] Patrick, G.L., 2013. *An introduction to medicinal chemistry*. Oxford university press.

[42] Etebu, E. and Arikekpar, I., 2016. Antibiotics: Classification and mechanisms of action with emphasis on molecular perspectives. *Int. J. Appl. Microbiol. Biotechnol. Res*, *4*(2016), pp.90-101.

[43] Hong, W., Zeng, J. and Xie, J., 2014. Antibiotic drugs targeting bacterial RNAs. *Acta Pharmaceutica Sinica B*, *4*(4), pp.258-265.

[44] Aldred, K.J., Kerns, R.J. and Osheroff, N., 2014. Mechanism of quinolone action and resistance. *Biochemistry*, *53*(10), pp.1565-1574.

[45] Ranghar, S., Sirohi, P., Verma, P. and Agarwal, V., 2014. Nanoparticle-based drug delivery systems: promising approaches against infections. *Brazilian Archives of Biology and Technology*, *57*, pp.209-222.

[46] Salouti, M. and Ahangari, A., 2014. *Nanoparticle based drug delivery systems for treatment of infectious diseases* (Vol. 552). InTech.

[47] Yang, Y., Qin, Z., Zeng, W., Yang, T., Cao, Y., Mei, C. and Kuang, Y., 2017. Toxicity assessment of nanoparticles in various systems and organs. *Nanotechnology Reviews*, *6*(3), pp.279-289.

[48] Santos, C.L., Albuquerque, A.J.R., Sampaio, F.C. and Keyson, D., 2013. Nanomaterials with antimicrobial properties: applications in health sciences. *Microbial pathogens and strategies for combating them: science, technology and education. Volume*, *4*(2).

[49] Essa, M.M., Manickavasagan, A. and Sukumar, E., 2012. *Natural products and their active compounds on disease prevention*. Nova Science Publishers,

Inc..[50]   Davis, S.C. and Perez, R., 2009. Cosmeceuticals and natural products: wound healing. *Clinics in dermatology*, *27*(5), pp.502-506.

[51]   Sato, T. and Miyata, G., 2000. The nutraceutical benefit, part iii: honey. *Nutrition (Burbank, Los Angeles County, Calif.)*, *16*(6), pp.468-469.

[52]   Cutting, K.F., 2007. Honey and contemporary wound care: an overview. *Ostomy Wound Management*, *53*(11), p.49.

[53]   Molan, P.C., 2006. The evidence supporting the use of honey as a wound dressing. *The international journal of lower extremity wounds*, *5*(1), pp.40-54.

[54]   Molan, P.C., 1992. The antibacterial activity of honey: 1. The nature of the antibacterial activity. *Bee world*, *73*(1), pp.5-28.

[55]   Seow, Y.X., Yeo, C.R., Chung, H.L. and Yuk, H.G., 2014. Plant essential oils as active antimicrobial agents. *Critical reviews in food science and nutrition*, *54*(5), pp.625-644.

[56]   Arkoun, M., Daigle, F., Heuzey, M.C. and Ajji, A., 2017. Mechanism of action of electrospun chitosan-based nanofibers against meat spoilage and pathogenic bacteria. *Molecules*, *22*(4), p.585.

[57]   Mardirossian, M., Grzela, R., Giglione, C., Meinnel, T., Gennaro, R., Mergaert, P. and Scocchi, M., 2014. The host antimicrobial peptide Bac71-35 binds to bacterial ribosomal proteins and inhibits protein synthesis. *Chemistry & biology*, *21*(12), pp.1639-1647.

[58]   Huan, Y., Kong, Q., Mou, H. and Yi, H., 2020. Antimicrobial peptides: classification, design, application and research progress in multiple fields. *Frontiers in microbiology*, *11*, p.2559.

[59] Lam, S.J., O'Brien-Simpson, N.M., Pantarat, N., Sulistio, A., Wong, E.H.H., Chen, Y.Y., Lenzo, J.C., Holden, J.A., Blencowe, A., Reynolds, E.C. and Qiao, G.G., 2016. Combating multidrug-resistant Gram-negative bacteria with structurally nanoengineered antimicrobial peptide polymers. Nat Microbiol [Internet]. 2016; 1 (11): 16162.

[60] Tripathy, A., Sen, P., Su, B. and Briscoe, W.H., 2017. Natural and bioinspired nanostructured bactericidal surfaces. *Advances in colloid and interface science*, *248*, pp.85-104.

[61] Queen, D., Evans, J.H., Gaylor, J.D.S., Courtney, J.M. and Reid, W.H., 1987. An in vitro assessment of wound dressing conformability. *Biomaterials*, *8*(5), pp.372-376.

[62] Wright, T.E., Payne, W.G., Ko, F., Ladizinsky, D., Bowlby, N., Neeley, R., Mannari, B. and Robson, M.C., 2003. The effects of an oxygen-generating dressing on tissue infection and wound healing. *J Appl Res Fall*, *3*(4), pp.363-70.

[63] Brett, D.W., 2006. A review of moisture-control dressings in wound care. *Journal of Wound Ostomy & Continence Nursing*, *33*, pp.S3-S8.

[64] Berthier, E., Young, E.W. and Beebe, D., 2012. Engineers are from PDMS-land, Biologists are from Polystyrenia. *Lab on a Chip*, *12*(7), pp.1224-1237.

[65] van de Stolpe, A. and den Toonder, J., 2013. Workshop meeting report Organs-on-Chips: human disease models. *Lab on a chip*, *13*(18), pp.3449-3470.

[66] Chan, C.Y., Huang, P.H., Guo, F., Ding, X., Kapur, V., Mai, J.D., Yuen, P.K.

and Huang, T.J., 2013. Accelerating drug discovery via organs-on-chips. *Lab on a Chip*, *13*(24), pp.4697-4710.

[67]   Ratner, B.D., Hoffman, A.S., Schoen, F.J. and Lemons, J.E., 2004. *Biomaterials science: an introduction to materials in medicine*. Elsevier.

[68]   Hong, K.S., Wang, J., Sharonov, A., Chandra, D., Aizenberg, J. and Yang, S., 2006. Tunable microfluidic optical devices with an integrated microlens array. *Journal of Micromechanics and Microengineering*, *16*(8), p.1660.

[69]   Dessy, L.A., Serratore, F., Corrias, F., Parisi, P., Mazzocchi, M. and Carlesimo, B., 2015. Retention of polyurethane foam fragments during VAC therapy: a complication to be considered. *International wound journal*, *12*(2), pp.132-136.

[70]   Guelcher, S.A., Brown, K.V., Li, B., Guda, T., Lee, B.H. and Wenke, J.C., 2011. Dual-purpose bone grafts improve healing and reduce infection. *Journal of orthopaedic trauma*, *25*(8), pp.477-482.

[71]   Blume, P.A., Walters, J., Payne, W., Ayala, J. and Lantis, J., 2008. Comparison of negative pressure wound therapy using vacuum-assisted closure with advanced moist wound therapy in the treatment of diabetic foot ulcers: a multicenter randomized controlled trial. *Diabetes care*, *31*(4), pp.631-636.

[72]   Huang, C., Leavitt, T., Bayer, L.R. and Orgill, D.P., 2014. Effect of negative pressure wound therapy on wound healing. *Current problems in surgery*, *51*(7), pp.301-331.

[73]   Lee, E., Zhang, H., Jackson, J.K., Lim, C.J. and Chiao, M., 2016. Janus films

with stretchable and waterproof properties for wound care and drug delivery applications. *RSC advances*, *6*(83), pp.79900-79909.

[74]   Zhang, Y., Ishida, M., Kazoe, Y., Sato, Y. and Miki, N., 2009. Water-vapor permeability control of PDMS by the dispersion of collagen powder. *IEEJ transactions on electrical and electronic engineering*, *4*(3), pp.442-449.

[75]   Merkel, T.C., Bondar, V.I., Nagai, K., Freeman, B.D. and Pinnau, I., 2000. Gas sorption, diffusion, and permeation in poly (dimethylsiloxane). *Journal of Polymer Science Part B: Polymer Physics*, *38*(3), pp.415-434.

[76]   Zhou, L., Xu, T., Yan, J., Li, X., Xie, Y. and Chen, H., 2020. Fabrication and characterization of matrine-loaded konjac glucomannan/fish gelatin composite hydrogel as antimicrobial wound dressing. *Food Hydrocolloids*, *104*, p.105702.

[77]   Eghbalifam, N., Shojaosadati, S.A., Hashemi-Najafabadi, S. and Khorasani, A.C., 2020. Synthesis and characterization of antimicrobial wound dressing material based on silver nanoparticles loaded gum Arabic nanofibers. *International journal of biological macromolecules*, *155*, pp.119-130.

[78]   Cheng, H., Shi, Z., Yue, K., Huang, X., Xu, Y., Gao, C., Yao, Z., Zhang, Y.S. and Wang, J., 2021. Sprayable hydrogel dressing accelerates wound healing with combined reactive oxygen species-scavenging and antibacterial abilities. *Acta Biomaterialia*, *124*, pp.219-232.

[79]   Lam, S.J., O'Brien-Simpson, N.M., Pantarat, N., Sulistio, A., Wong, E.H., Chen, Y.Y., Lenzo, J.C., Holden, J.A., Blencowe, A., Reynolds, E.C. and Qiao, G.G., 2016. Combating multidrug-resistant Gram-negative bacteria with structurally nanoengineered antimicrobial peptide polymers. *Nature*

microbiology, *1*(11), pp.1-11.

[80] Nakatsuji, T., Chen, T.H., Narala, S., Chun, K.A., Two, A.M., Yun, T., Shafiq, F., Kotol, P.F., Bouslimani, A., Melnik, A.V. and Latif, H., 2017. Antimicrobials from human skin commensal bacteria protect against Staphylococcus aureus and are deficient in atopic dermatitis. *Science translational medicine*, *9*(378).

[81] Mao, Y., Hoffman, T., Singh-Varma, A., Duan-Arnold, Y., Moorman, M., Danilkovitch, A. and Kohn, J., 2017. Antimicrobial peptides secreted from human cryopreserved viable amniotic membrane contribute to its antibacterial activity. *Scientific reports*, *7*(1), pp.1-8.

[82] Thangavel, P., Ramachandran, B., Chakraborty, S., Kannan, R., Lonchin, S. and Muthuvijayan, V., 2017. Accelerated healing of diabetic wounds treated with L-glutamic acid loaded hydrogels through enhanced collagen deposition and angiogenesis: an in vivo study. *Scientific reports*, *7*(1), pp.1-15.

[83] Tsao, C.T., Chang, C.H., Lin, Y.Y., Wu, M.F., Wang, J.L., Han, J.L. and Hsieh, K.H., 2010. Antibacterial activity and biocompatibility of a chitosan–γ-poly (glutamic acid) polyelectrolyte complex hydrogel. *Carbohydrate Research*, *345*(12), pp.1774-1780.

[84] Tripathy, A., Sen, P., Su, B. and Briscoe, W.H., 2017. Natural and bioinspired nanostructured bactericidal surfaces. *Advances in colloid and interface science*, *248*, pp.85-104.

[85] Hasan, J., Raj, S., Yadav, L. and Chatterjee, K., 2015. Engineering a nanostructured "super surface" with superhydrophobic and superkilling properties. *RSC advances*, *5*(56), pp.44953-44959.

[86] Bhadra, C.M., Truong, V.K., Pham, V.T., Al Kobaisi, M., Seniutinas, G., Wang, J.Y., Juodkazis, S., Crawford, R.J. and Ivanova, E.P., 2015. Antibacterial titanium nano-patterned arrays inspired by dragonfly wings. *Scientific reports*, *5*(1), pp.1-12.

[87] Kim, S., Jung, U.T., Kim, S.K., Lee, J.H., Choi, H.S., Kim, C.S. and Jeong, M.Y., 2015. Nanostructured multifunctional surface with antireflective and antimicrobial characteristics. *ACS applied materials & interfaces*, *7*(1), pp.326-331.

[88] Winter, G.D., 1962. Formation of the scab and the rate of epithelization of superficial wounds in the skin of the young domestic pig. *Nature*, *193*(4812), pp.293-294.

[89] Zhou, J., Loftus, A.L., Mulley, G. and Jenkins, A.T.A., 2010. A thin film detection/response system for pathogenic bacteria. *Journal of the American Chemical Society*, *132*(18), pp.6566-6570.

[90] Jankowska, D., Schulenburg, C., Faccio, G., Maniura-Weber, K. and Richter, M., 2016. Biosensors for monitoring of enzymatic wound healing processes. In *Front. Bioeng. Biotechnol. Conference Abstract: 10th World Biomaterials Congress. doi: 10.3389/conf. FBIOE* (Vol. 2629).

[91] Kim, D.H., Wang, S., Keum, H., Ghaffari, R., Kim, Y.S., Tao, H., Panilaitis, B., Li, M., Kang, Z., Omenetto, F. and Huang, Y., 2012. Thin, flexible sensors and actuators as 'instrumented'surgical sutures for targeted wound monitoring and therapy. *Small*, *8*(21), pp.3263-3268.

[92] Farooqui, M.F. and Shamim, A., 2016. Low cost inkjet printed smart bandage for wireless monitoring of chronic wounds. *Scientific reports*, *6*(1), pp.1-13.

[93]   Ochoa, M., Rahimi, R., Zhou, J., Jiang, H., Yoon, C.K., Maddipatla, D., Narakathu, B.B., Jain, V., Oscai, M.M., Morken, T.J. and Oliveira, R.H., 2020. Integrated sensing and delivery of oxygen for next-generation smart wound dressings. *Microsystems & Nanoengineering*, *6*(1), pp.1-16.

[94]   Schneider, L.A., Korber, A., Grabbe, S. and Dissemond, J., 2007. Influence of pH on wound-healing: a new perspective for wound-therapy?. *Archives of dermatological research*, *298*(9), pp.413-420.

[95]   Schreml, S., Meier, R.J., Wolfbeis, O.S., Landthaler, M., Szeimies, R.M. and Babilas, P., 2011. 2D luminescence imaging of pH in vivo. *Proceedings of the National Academy of Sciences*, *108*(6), pp.2432-2437.

[96]   Sharpe, J.R., Booth, S., Jubin, K., Jordan, N.R., Lawrence-Watt, D.J. and Dheansa, B.S., 2013. Progression of wound pH during the course of healing in burns. *Journal of Burn Care & Research*, *34*(3), pp.e201-e208.

[97]   Ochoa, M., Rahimi, R. and Ziaie, B., 2013. Flexible sensors for chronic wound management. *IEEE reviews in biomedical engineering*, *7*, pp.73-86.

[98]   Korostynska, O., Arshak, K., Gill, E. and Arshak, A., 2007. Materials and techniques for in vivo pH monitoring. *IEEE Sensors Journal*, *8*(1), pp.20-28.

[99]   Rahimi, R., Ochoa, M., Parupudi, T., Zhao, X., Yazdi, I.K., Dokmeci, M.R., Tamayol, A., Khademhosseini, A. and Ziaie, B., 2016. A low-cost flexible pH sensor array for wound assessment. *Sensors and Actuators B: Chemical*, *229*, pp.609-617.

[100]   Vu, H., Nair, A., Tran, L., Pal, S., Senkowsky, J., Hu, W. and Tang, L., 2020. A Device to Predict Short-Term Healing Outcome of Chronic Wounds. *Advances*

in wound care, *9*(6), pp.312-324.

[101] Sharifuzzaman, M., Chhetry, A., Zahed, M.A., Yoon, S.H., Park, C.I., Zhang, S., Barman, S.C., Sharma, S., Yoon, H. and Park, J.Y., 2020. Smart bandage with integrated multifunctional sensors based on MXene-functionalized porous graphene scaffold for chronic wound care management. *Biosensors and Bioelectronics*, *169*, p.112637.

[102] Esa, F., Tasirin, S.M. and Abd Rahman, N., 2014. Overview of bacterial cellulose production and application. *Agriculture and Agricultural Science Procedia*, *2*, pp.113-119.

[103] Chen, P., Cho, S.Y. and Jin, H.J., 2010. Modification and applications of bacterial celluloses in polymer science. *Macromolecular Research*, *18*(4), pp.309-320.

[104] Saibuatong, O.A. and Phisalaphong, M., 2010. Novo aloe vera–bacterial cellulose composite film from biosynthesis. *Carbohydrate Polymers*, *79*(2), pp.455-460.

[105] Dahman, Y., Jayasuriya, K.E. and Kalis, M., 2010. Potential of biocellulose nanofibers production from agricultural renewable resources: preliminary study. *Applied biochemistry and biotechnology*, *162*(6), pp.1647-1659.

[106] Castro, C., Zuluaga, R., Putaux, J.L., Caro, G., Mondragon, I. and Gañán, P., 2011. Structural characterization of bacterial cellulose produced by Gluconacetobacter swingsii sp. from Colombian agroindustrial wastes. *Carbohydrate Polymers*, *84*(1), pp.96-102.

[107] Keshk, S.M., 2014. Bacterial cellulose production and its industrial

applications. *J Bioprocess Biotech*, *4*(150), p.2.

[108] Eicorn, S.J., 2001. Review Current International Research into Cellulosic Fibers and Composites. *Journal Of Material Science*, *36*, pp.2107-2131.

[109] Klemm, D., Schumann, D., Udhardt, U. and Marsch, S., 2001. Bacterial synthesized cellulose—artificial blood vessels for microsurgery. *Progress in polymer science*, *26*(9), pp.1561-1603.

[110] Rambo, C.R., Recouvreux, D.O.S., Carminatti, C.A., Pitlovanciv, A.K., Antônio, R.V. and Porto, L.M., 2008. Template assisted synthesis of porous nanofibrous cellulose membranes for tissue engineering. *Materials Science and Engineering: C*, *28*(4), pp.549-554.

[111]   Bielecki, S., Krystynowicz, A., Turkiewicz, M. and Kalinowska, H., 2005. Bacterial cellulose. *Polysaccharides and polyamides in the food industry: properties, production, and patents*, pp.31-84.

[112]   Ruan, C., Zhu, Y., Zhou, X., Abidi, N., Hu, Y. and Catchmark, J.M., 2016. Effect of cellulose crystallinity on bacterial cellulose assembly. *Cellulose*, *23*(6), pp.3417-3427.

[113] Shah, N., Ul-Islam, M., Khattak, W.A. and Park, J.K., 2013. Overview of bacterial cellulose composites: a multipurpose advanced material. *Carbohydrate polymers*, *98*(2), pp.1585-1598.

[114] Kucińska-Lipka, J., Gubanska, I. and Janik, H., 2015. Bacterial cellulose in the field of wound healing and regenerative medicine of skin: recent trends and future prospectives. *Polymer Bulletin*, *72*(9), pp.2399-2419.

[115] Czaja, W., Krystynowicz, A., Bielecki, S. and Brown Jr, R.M., 2006. Microbial

cellulose—the natural power to heal wounds. *Biomaterials*, *27*(2), pp.145-151.

[116] Ross, P., Mayer, R. and Benziman, M., 1991. Cellulose biosynthesis and function in bacteria. *Microbiology and Molecular Biology Reviews*, *55*(1), pp.35-58.

[117] Klemm, D., Heublein, B., Fink, H.P. and Bohn, A., 2005. Cellulose: fascinating biopolymer and sustainable raw material. *Angewandte chemie international edition*, *44*(22), pp.3358-3393.

[118] Szot, C.S., Buchanan, C.F., Gatenholm, P., Rylander, M.N. and Freeman, J.W., 2011. Investigation of cancer cell behavior on nanofibrous scaffolds. *Materials Science and Engineering: C*, *31*(1), pp.37-42.

[119]   Von Burkersroda, F., Schedl, L. and Göpferich, A., 2002. Why degradable polymers undergo surface erosion or bulk erosion. *Biomaterials*, *23*(21), pp.4221-4231.

[120]   Torgbo, S. and Sukyai, P., 2020. Biodegradation and thermal stability of bacterial cellulose as biomaterial: The relevance in biomedical applications. *Polymer Degradation and Stability*, *179*, p.109232.

[121]   Chen, Y.M., Xi, T.F., Zheng, Y.F., Zhou, L. and Wan, Y.Z., 2011. In vitro structural changes of nano-bacterial cellulose immersed in phosphate buffer solution. In *Journal of Biomimetics, Biomaterials and Tissue Engineering* (Vol. 10, pp. 55-66). Trans Tech Publications Ltd.

[122]   Gajjar, C.R. and King, M.W., 2014. *Resorbable Fiber-Forming Polymers for Biotextile Applications* (pp. 1-5). New York, NY, USA:: Springer.

[123] Jozala, A.F., de Lencastre-Novaes, L.C., Lopes, A.M., de Carvalho Santos-

Ebinuma, V., Mazzola, P.G., Pessoa-Jr, A., Grotto, D., Gerenutti, M. and Chaud, M.V., 2016. Bacterial nanocellulose production and application: a 10-year overview. *Applied microbiology and biotechnology*, *100*(5), pp.2063-2072.

[124] Tanskul, S., Amornthatree, K. and Jaturonlak, N., 2013. A new cellulose-producing bacterium, Rhodococcus sp. MI 2: Screening and optimization of culture conditions. *Carbohydrate polymers, 92*(1), pp.421-428.

[125] Mohammadkazemi, F., Azin, M. and Ashori, A., 2015. Production of bacterial cellulose using different carbon sources and culture media. *Carbohydrate polymers, 117*, pp.518-523.

[126] Lynd, L.R., Weimer, P.J., Van Zyl, W.H. and Pretorius, I.S., 2002. Microbial cellulose utilization: fundamentals and biotechnology. *Microbiology and molecular biology reviews*, *66*(3), pp.506-577.

[127] Conley, K., Godbout, L., Whitehead, M.T. and van de Ven, T.G., 2016. Origin of the twist of cellulosic materials. *Carbohydrate polymers*, *135*, pp.285-299.

[128] Thompson, D.N. and Hamilton, M.A., 2001. Production of bacterial cellulose from alternate feedstocks. In *Twenty-Second Symposium on Biotechnology for Fuels and Chemicals* (pp. 503-513). Humana Press, Totowa, NJ.

[129] Rehim, S.A., Singhal, M. and Chung, K.C., 2014. Dermal skin substitutes for upper limb reconstruction: current status, indications, and contraindications. *Hand clinics*, *30*(2), pp.239-252.

[130] Cakar, F., Özer, I., Aytekin, A.Ö. and Şahin, F., 2014. Improvement production of bacterial cellulose by semi-continuous process in molasses medium. *Carbohydrate polymers*, *106*, pp.7-13.

[131] Hsieh, J.T., Wang, M.J., Lai, J.T. and Liu, H.S., 2016. A novel static cultivation of bacterial cellulose production by intermittent feeding strategy. *Journal of the Taiwan Institute of Chemical Engineers*, *63*, pp.46-51.

[132] Chen, S.Q., Mikkelsen, D., Lopez-Sanchez, P., Wang, D., Martinez-Sanz, M., Gilbert, E.P., Flanagan, B.M. and Gidley, M.J., 2017. Characterisation of bacterial cellulose from diverse Komagataeibacter strains and their application to construct plant cell wall analogues. *Cellulose*, *24*(3), pp.1211-1226.

[133] Watanabe, K., Tabuchi, M., Morinaga, Y. and Yoshinaga, F., 1998. Structural features and properties of bacterial cellulose produced in agitated culture. *Cellulose*, *5*(3), pp.187-200.

[134] Yoshinaga, F., Tonouchi, N. and Watanabe, K., 1997. Research progress in production of bacterial cellulose by aeration and agitation culture and its application as a new industrial material. *Bioscience, biotechnology, and biochemistry*, *61*(2), pp.219-224.

[135] Chen, Y.M., Xi, T., Zheng, Y., Guo, T., Hou, J., Wan, Y. and Gao, C., 2009. In vitro cytotoxicity of bacterial cellulose scaffolds used for tissue-engineered bone. *Journal of bioactive and compatible polymers*, *24*(1_suppl), pp.137-145.

[136] Grande, C.J., Torres, F.G., Gomez, C.M. and Bañó, M.C., 2009. Nanocomposites of bacterial cellulose/hydroxyapatite for biomedical applications. *Acta Biomaterialia*, *5*(5), pp.1605-1615.

[137] Zhang, C., Cao, J., Zhao, S., Luo, H., Yang, Z., Gama, M., Zhang, Q., Su, D. and Wan, Y., 2020. Biocompatibility evaluation of bacterial cellulose as a scaffold material for tissue-engineered corneal stroma. *Cellulose*, *27*(5), pp.2775-2784.

[138] Sanchavanakit, N., Sangrungraungroj, W., Kaomongkolgit, R., Banaprasert, T., Pavasant, P. and Phisalaphong, M., 2006. Growth of human keratinocytes and fibroblasts on bacterial cellulose film. *Biotechnology progress*, *22*(4), pp.1194-1199.

[139] Torres, F.G., Commeaux, S. and Troncoso, O.P., 2012. Biocompatibility of bacterial cellulose based biomaterials. *Journal of functional biomaterials*, *3*(4), pp.864-878.

[140]   Scully, C., Bagan, J.V., Black, M., Carrozzo, M., Eisen, D., Escudier, M., Farthing, P., Kuffer, R., Lo Muzio, L., Mignogna, M. and Porter, S.R., 2005. Number 1 Epithelial biology. *Oral diseases*, *11*(2), pp.58-71.

[141]   Gumbiner, B.M., 1996. Cell adhesion: the molecular basis of tissue architecture and morphogenesis. *Cell*, *84*(3), pp.345-357.

[142]   Klemm, D., Kramer, F., Moritz, S., Lindström, T., Ankerfors, M., Gray, D. and Dorris, A., 2011. Nanocelluloses: a new family of nature-based materials. *Angewandte Chemie International Edition*, *50*(24), pp.5438-5466.

[143]   Martins, D., de Carvalho Ferreira, D., Gama, M. and Dourado, F., 2020. Dry Bacterial Cellulose and Carboxymethyl Cellulose formulations with interfacial-active performance: processing conditions and redispersion. *Cellulose*, *27*, pp.6505-6520.

[144] Maneerung, T., Tokura, S. and Rujiravanit, R., 2008. Impregnation of silver nanoparticles into bacterial cellulose for antimicrobial wound dressing. *Carbohydrate polymers*, *72*(1), pp.43-51.

[145] Lin, Q., Zheng, Y., Ren, L., Wu, J., Wang, H., An, J. and Fan, W., 2014.

Preparation and characteristic of a sodium alginate/carboxymethylated bacterial cellulose composite with a crosslinking semi-interpenetrating network. *Journal of Applied Polymer Science*, *131*(3).

[146] Chen, H.H., Lin, S.B., Hsu, C.P. and Chen, L.C., 2013. Modifying bacterial cellulose with gelatin peptides for improved rehydration. *Cellulose*, *20*(4), pp.1967-1977.

[147] Kim, J., Cai, Z., Lee, H.S., Choi, G.S., Lee, D.H. and Jo, C., 2011. Preparation and characterization of a bacterial cellulose/chitosan composite for potential biomedical application. *Journal of Polymer Research*, *18*(4), pp.739-744.

[148] Nakayama, A., Kakugo, A., Gong, J.P., Osada, Y., Takai, M., Erata, T. and Kawano, S., 2004. High mechanical strength double-network hydrogel with bacterial cellulose. *Advanced Functional Materials*, *14*(11), pp.1124-1128.

[149] Shi, Z., Zang, S., Jiang, F., Huang, L., Lu, D., Ma, Y. and Yang, G., 2012. In situ nano-assembly of bacterial cellulose–polyaniline composites. *Rsc Advances*, *2*(3), pp.1040-1046.

[150] Müller, D., Mandelli, J.S., Marins, J.A., Soares, B.G., Porto, L.M., Rambo, C.R. and Barra, G.M.O., 2012. Electrically conducting nanocomposites: preparation and properties of polyaniline (PAni)-coated bacterial cellulose nanofibers (BC). *Cellulose*, *19*(5), pp.1645-1654.

[151] Cai, Z. and Kim, J., 2010. Bacterial cellulose/poly (ethylene glycol) composite: characterization and first evaluation of biocompatibility. *Cellulose*, *17*(1), pp.83-91.

[152] Feng, Y., Zhang, X., Shen, Y., Yoshino, K. and Feng, W., 2012. A

mechanically strong, flexible and conductive film based on bacterial cellulose/graphene nanocomposite. *Carbohydrate Polymers*, *87*(1), pp.644-649.

[153] Luo, H., Xiong, G., Huang, Y., He, F., Wang, Y. and Wan, Y., 2008. Preparation and characterization of a novel COL/BC composite for potential tissue engineering scaffolds. *Materials Chemistry and Physics*, *110*(2-3), pp.193-196.

[154] Hu, W., Chen, S., Li, X., Shi, S., Shen, W., Zhang, X. and Wang, H., 2009. In situ synthesis of silver chloride nanoparticles into bacterial cellulose membranes. *Materials Science and Engineering: C*, *29*(4), pp.1216-1219.

[155] Pinto, R.J., Daina, S., Sadocco, P., Neto, C.P. and Trindade, T., 2013. Antibacterial activity of nanocomposites of copper and cellulose. *BioMed research international*, *2013*.

[156] Zhang, T., Wang, W., Zhang, D., Zhang, X., Ma, Y., Zhou, Y. and Qi, L., 2010. Biotemplated synthesis of gold nanoparticle–bacteria cellulose nanofiber nanocomposites and their application in biosensing. *Advanced Functional Materials*, *20*(7), pp.1152-1160.

[157] Ul-Islam, M., Khan, T. and Park, J.K., 2012. Nanoreinforced bacterial cellulose–montmorillonite composites for biomedical applications. *Carbohydrate polymers*, *89*(4), pp.1189-1197.

[158] Khalid, A., Khan, R., Ul-Islam, M., Khan, T. and Wahid, F., 2017. Bacterial cellulose-zinc oxide nanocomposites as a novel dressing system for burn wounds. *Carbohydrate polymers*, *164*, pp.214-221.

[159] Lamboni, L., Li, Y., Liu, J. and Yang, G., 2016. Silk sericin-functionalized bacterial cellulose as a potential wound-healing biomaterial. *Biomacromolecules*, *17*(9), pp.3076-3084.

[160] Lee, A.R.C., Leem, H., Lee, J. and Park, K.C., 2005. Reversal of silver sulfadiazine-impaired wound healing by epidermal growth factor. *Biomaterials*, *26*(22), pp.4670-4676.

[161] Cho, K.H., Park, J.E., Osaka, T. and Park, S.G., 2005. The study of antimicrobial activity and preservative effects of nanosilver ingredient. *Electrochimica Acta*, *51*(5), pp.956-960.

[162] Temgire, M.K. and Joshi, S.S., 2004. Optical and structural studies of silver nanoparticles. *Radiation physics and Chemistry*, *71*(5), pp.1039-1044.

[163] Evans, B.R., O'Neill, H.M., Malyvanh, V.P., Lee, I. and Woodward, J., 2003. Palladium-bacterial cellulose membranes for fuel cells. *Biosensors and Bioelectronics*, *18*(7), pp.917-923.

[164] Wiegand, C., Moritz, S., Hessler, N., Kralisch, D., Wesarg, F., Müller, F.A., Fischer, D. and Hipler, U.C., 2015. Antimicrobial functionalization of bacterial nanocellulose by loading with polihexanide and povidone-iodine. *Journal of Materials Science: Materials in Medicine*, *26*(10), pp.1-14.

[165] Shao, W., Liu, H., Wang, S., Wu, J., Huang, M., Min, H. and Liu, X., 2016. Controlled release and antibacterial activity of tetracycline hydrochloride-loaded bacterial cellulose composite membranes. *Carbohydrate polymers*, *145*, pp.114-120.

[166] Shah, N., Ul-Islam, M., Khattak, W.A. and Park, J.K., 2013. Overview of

bacterial cellulose composites: a multipurpose advanced

material. *Carbohydrate polymers*, *98*(2), pp.1585-1598.

[167]   Azeredo, H., Barud, H., Farinas, C.S., Vasconcellos, V.M. and Claro,

A.M., 2019. Bacterial cellulose as a raw material for food and food packaging

applications. *Frontiers in Sustainable Food Systems*, *3*, p.7.

[168]   Maneerung, T., Tokura, S. and Rujiravanit, R., 2008. Impregnation of

silver nanoparticles into bacterial cellulose for antimicrobial wound

dressing. *Carbohydrate polymers*, *72*(1), pp.43-51.

[169]   Tang, W., Jia, S., Jia, Y. and Yang, H., 2010. The influence of fermentation

conditions and post-treatment methods on porosity of bacterial cellulose

membrane. *World Journal of Microbiology and Biotechnology*, *26*(1), pp.125-

131.

[170]   Ul-Islam, M., Khan, T. and Park, J.K., 2012. Water holding and release

properties of bacterial cellulose obtained by in situ and ex situ

modification. *Carbohydrate Polymers*, *88*(2), pp.596-603.

[171]   Korsmeyer, R.W., Gurny, R., Doelker, E., Buri, P. and Peppas, N.A.,

1983. Mechanisms of solute release from porous hydrophilic

polymers. *International journal of pharmaceutics*, *15*(1), pp.25-35.

[172]   Ritger, P.L. and Peppas, N.A., 1987. A simple equation for description of

solute release II. Fickian and anomalous release from swellable

devices. *Journal of controlled release*, *5*(1), pp.37-42.

[173]   Huang, L., Chen, X., Nguyen, T.X., Tang, H., Zhang, L. and Yang, G.,

2013. Nano-cellulose 3D-networks as controlled-release drug carriers. *Journal*

of Materials Chemistry B, *1*(23), pp.2976-2984.

[174]   Trovatti, E., Silva, N.H., Duarte, I.F., Rosado, C.F., Almeida, I.F., Costa, P., Freire, C.S., Silvestre, A.J. and Neto, C.P., 2011. Biocellulose membranes as supports for dermal release of lidocaine. *Biomacromolecules*, *12*(11), pp.4162-4168.

[175] Zhang, P., Chen, L., Zhang, Q. and Hong, F.F., 2016. Using in situ dynamic cultures to rapidly biofabricate fabric-reinforced composites of chitosan/bacterial nanocellulose for antibacterial wound dressings. *Frontiers in microbiology*, *7*, p.260.

[176] Fernandes, S.C., Sadocco, P., Alonso-Varona, A., Palomares, T., Eceiza, A., Silvestre, A.J., Mondragon, I. and Freire, C.S., 2013. Bioinspired antimicrobial and biocompatible bacterial cellulose membranes obtained by surface functionalization with aminoalkyl groups. *ACS applied materials & interfaces*, *5*(8), pp.3290-3297.

[177] Jebel, F.S. and Almasi, H., 2016. Morphological, physical, antimicrobial and release properties of ZnO nanoparticles-loaded bacterial cellulose films. *Carbohydrate polymers*, *149*, pp.8-19.

[178] Liyaskina, E., Revin, V., Paramonova, E., Nazarkina, M., Pestov, N., Revina, N. and Kolesnikova, S., 2017. Nanomaterials from bacterial cellulose for antimicrobial wound dressing. In *Journal of Physics: Conference Series* (Vol. 784, No. 1, p. 012034). IOP Publishing.

[179] Padrao, J., Gonçalves, S., Silva, J.P., Sencadas, V., Lanceros-Méndez, S., Pinheiro, A.C., Vicente, A.A., Rodrigues, L.R. and Dourado, F., 2016. Bacterial cellulose-lactoferrin as an antimicrobial edible packaging. *Food*

Hydrocolloids, *58*, pp.126-140.

[180] Shao, W., Liu, H., Liu, X., Wang, S., Wu, J., Zhang, R., Min, H. and Huang, M., 2015. Development of silver sulfadiazine loaded bacterial cellulose/sodium alginate composite films with enhanced antibacterial property. *Carbohydrate polymers*, *132*, pp.351-358.

[181] Pal, S., Nisi, R., Stoppa, M. and Licciulli, A., 2017. Silver-functionalized bacterial cellulose as antibacterial membrane for wound-healing applications. *ACS omega*, *2*(7), pp.3632-3639.

[182] Sampaio, L.M., Padrão, J., Faria, J., Silva, J.P., Silva, C.J., Dourado, F. and Zille, A., 2016. Laccase immobilization on bacterial nanocellulose membranes: Antimicrobial, kinetic and stability properties. *Carbohydrate polymers*, *145*, pp.1-12.

[183] Parish, L.C., 2011. Andrews' Diseases of the Skin: Clinical Dermatology. *JAMA*, *306*(2), pp.213-213.

[184] Semnani, D., 2017. Geometrical characterization of electrospun nanofibers. In *Electrospun Nanofibers* (pp. 151-180). Woodhead Publishing.

[185]   Ray, S.S., 2013. *Environmentally friendly polymer nanocomposites: types, processing and properties*. Elsevier.

[186] Birkner, N. and Wang, Q., 2014. How an FTIR Spectrometer Operates. *UC Davis ChemWiki*.

[187] Sabarinathan, C., 2012. MuthuS., AliM. N.,"Experimental Study on Tensile Behavior of Multi Wall Carbon Nanotube Reinforced Epoxy Composites". *Journal of Applied Sciences Research*, *8*(7).

[188]   *What is Compression Testing?,* Available at: *https://www.instron.com/en-gb/our-company/library/test-types/compression-test?region=United%20Kingdom* (Accessed: 13th July 2021).

[189] Nina, H. and Andrew, R.B., 2011. BET Surface Area Analysis of Nanoparticles. *Rice University, Houston TX*.

[190] Unapumnuk, K., Keener, T.C., Lu, M. and Khang, S.J., 2006. Pyrolysis behavior of tire-derived fuels at different temperatures and heating rates. *Journal of the Air & Waste Management Association*, *56*(5), pp.618-627.

[191] Tomoda, B.T., Yassue-Cordeiro, P.H., Ernesto, J.V., Lopes, P.S., Péres, L.O., da Silva, C.F. and de Moraes, M.A., 2020. Chapter 3—Characterization of biopolymer membranes and films: Physicochemical, mechanical, barrier, and biological properties. *Biopolymer Membranes and Films; Elsevier Inc.: Amsterdam, The Netherlands*, pp.67-95.

[192] Bibi, S., Bremner, D.H., Macdougall-Heasman, M., Reid, R., Simpson, K., Tough, A., Waddell, S., Stewart, I.J. and Matthews, K.H., 2015. A preliminary investigation to group disparate batches of licit and illicit diazepam tablets using differential scanning calorimetry. *Analytical methods*, *7*(20), pp.8597-8604.

[193] Rai, S.N., Pan, J., Cambon, A., Chaires, J.B. and Garbett, N.C., 2013. Group classification based on high-dimensional data: application to differential scanning calorimetry plasma thermogram analysis of cervical cancer and control samples. *Open Access Medical Statistics*, *3*, pp.1-9.

[194] Madhav, H., Singh, N. and Jaiswar, G., 2019. Thermoset, bioactive, metal–polymer composites for medical applications. In *Materials for biomedical*

engineering (pp. 105-143). Elsevier.

[195] Di Gianfrancesco, A., 2017. Technologies for chemical analyses, microstructural and inspection investigations. In *Materials for ultra-supercritical and advanced ultra-supercritical power plants* (pp. 197-245). Woodhead Publishing.

[196] Alexander, L., 1971. X-ray diffraction methods in polymer science. *Journal of Materials Science*, *6*(1), pp.93-93.

[197] Segal, L.G.J.M.A., Creely, J.J., Martin Jr, A.E. and Conrad, C.M., 1959. An empirical method for estimating the degree of crystallinity of native cellulose using the X-ray diffractometer. *Textile research journal*, *29*(10), pp.786-794.

[198] Majd, E.S., Goldberg, M. and Stanislawski, L., 2003. *In vitro* effects of ascorbate and Trolox on the biocompatibility of dental restorative materials. *Biomaterials*, *24*(1), pp.3-9.

[199] Cheong, H.I., Johnson, J., Cormier, M. and Hosseini, K., 2008. *In vitro* cytotoxicity of eight β-blockers in human corneal epithelial and retinal pigment epithelial cell lines: Comparison with epidermal keratinocytes and dermal fibroblasts. *Toxicology in Vitro*, *22*(4), pp.1070-1076.

[200] Mosmann, T., 1983. Rapid colorimetric assay for cellular growth and survival: application to proliferation and cytotoxicity assays. *Journal of immunological methods*, *65*(1-2), pp.55-63.

[201] Keong, L.C. and Halim, A.S., 2009. In vitro models in biocompatibility assessment for biomedical-grade chitosan derivatives in wound management. *International journal of molecular sciences*, *10*(3), pp.1300-

1313.

[202] Kawahara, R., Sahatiya, P., Badhulika, S. and Uno, S., 2018. based potentiometric pH sensor using carbon electrode drawn by pencil. *Japanese Journal of Applied Physics*, *57*(4S), p.04FM08.

[203] Galdino, F.E., Smith, J.P., Kwamou, S.I., Kampouris, D.K., Iniesta, J., Smith, G.C., Bonacin, J.A. and Banks, C.E., 2015. Graphite screen-printed electrodes applied for the accurate and reagentless sensing of pH. *Analytical chemistry*, *87*(23), pp.11666-11672.

[204] "How to measure pH," can be found under https://www.awe-ltd.co.uk/knowledge-base/ph/how-to-measure-ph.html, n.d.

[205]   Mosmann, T., 1983. Rapid colorimetric assay for cellular growth and survival: application to proliferation and cytotoxicity assays. *Journal of immunological methods*, *65*(1-2), pp.55-63.

[206]   Dyamenahalli, K., Famili, A. and Shandas, R., 2015. Characterization of shape-memory polymers for biomedical applications. In *Shape memory polymers for biomedical applications* (pp. 35-63). Woodhead Publishing.

[207] Li, Z., Wang, L., Chen, S., Feng, C., Chen, S., Yin, N., Yang, J., Wang, H. and Xu, Y., 2015. Facilely green synthesis of silver nanoparticles into bacterial cellulose. *Cellulose*, *22*(1), pp.373-383.[208]   Garza-Cervantes, J.A., Mendiola-Garza, G., de Melo, E.M., Dugmore, T.I., Matharu, A.S. and Morones-Ramirez, J.R., 2020. Antimicrobial activity of a silver-microfibrillated cellulose biocomposite against susceptible and resistant bacteria. *Scientific reports*, *10*(1), pp.1-7.

[209] Bayazidi, P., Almasi, H. and Asl, A.K., 2018. Immobilization of lysozyme on bacterial cellulose nanofibers: Characteristics, antimicrobial activity and morphological properties. *International journal of biological macromolecules*, *107*, pp.2544-2551.

[210] Liu, M., Luo, G., Wang, Y., Xu, R., Wang, Y., He, W., Tan, J., Xing, M. and Wu, J., 2017. Nano-silver-decorated microfibrous eggshell membrane: processing, cytotoxicity assessment and optimization, antibacterial activity and wound healing. *Scientific reports*, *7*(1), pp.1-14.

[211] International Organization for Standardization. Technical Committee ISO/TC 24. Particle characterization including sieving, Subcommittee SC 4, Particle characterization, 2010. *Determination of the Specific Surface Area of Solids by Gas Adsorption: BET Method*. ISO.

[212] Krasteva, P.V., Bernal-Bayard, J., Travier, L., Martin, F.A., Kaminski, P.A., Karimova, G., Fronzes, R. and Ghigo, J.M., 2017. Insights into the structure and assembly of a bacterial cellulose secretion system. *Nature communications*, *8*(1), pp.1-10.

[213] Wang, S.S., Han, Y.H., Chen, J.L., Zhang, D.C., Shi, X.X., Ye, Y.X., Chen, D.L. and Li, M., 2018. Insights into bacterial cellulose biosynthesis from different carbon sources and the associated biochemical transformation pathways in Komagataeibacter sp. W1. *Polymers*, *10*(9), p.963.[214]Gorgieva, S. and Trček, J., 2019. Bacterial cellulose: Production, modification and perspectives in biomedical applications. *Nanomaterials*, *9*(10), p.1352.

[215] Bandyopadhyay, S., Saha, N. and Sáha, P., 2018. Characterization of bacterial cellulose produced using media containing waste apple juice. *Applied*

Biochemistry and Microbiology, *54*(6), pp.649-657.

[216] Trček, J. and Barja, F., 2015. Updates on quick identification of acetic acid

bacteria with a focus on the 16S–23S rRNA gene internal transcribed spacer

and the analysis of cell proteins by MALDI-TOF mass

spectrometry. *International journal of food microbiology*, *196*, pp.137-144.

[217] Škraban, J., Cleenwerck, I., Vandamme, P., Fanedl, L. and Trček, J., 2018.

Genome sequences and description of novel exopolysaccharides producing

species Komagataeibacter pomaceti sp. nov. and reclassification of

Komagataeibacter kombuchae (Dutta and Gachhui 2007) Yamada et al., 2013

as a later heterotypic synonym of Komagataeibacter hansenii (Gosselé et al.

1983) Yamada et al., 2013. *Systematic and applied microbiology*, *41*(6),

pp.581-592.

[218] Castro, C., Zuluaga, R., Álvarez, C., Putaux, J.L., Caro, G., Rojas, O.J.,

Mondragon, I. and Gañán, P., 2012. Bacterial cellulose produced by a new

acid-resistant strain of Gluconacetobacter genus. *Carbohydrate*

polymers, *89*(4), pp.1033-1037.

[219] Castro, C., Cleenwerck, I., Trček, J., Zuluaga, R., De Vos, P., Caro, G.,

Aguirre, R., Putaux, J.L. and Ganan, P., 2013. Gluconacetobacter

medellinensis sp. nov., cellulose-and non-cellulose-producing acetic acid

bacteria isolated from vinegar. *International journal of systematic and*

evolutionary microbiology, *63*(3), pp.1119-1125.

[220] Bae, S.O. and Shoda, M., 2005. Production of bacterial cellulose by

Acetobacter xylinum BPR2001 using molasses medium in a jar

fermentor. *Applied microbiology and biotechnology*, *67*(1), pp.45-51.

[221] Son, H.J., Heo, M.S., Kim, Y.G. and Lee, S.J., 2001. Optimization of fermentation conditions for the production of bacterial cellulose by a newly isolated Acetobacter. *Biotechnology and applied biochemistry*, *33*(1), pp.1-5.

[222] Aydın, Y.A. and Aksoy, N.D., 2014. Isolation and characterization of an efficient bacterial cellulose producer strain in agitated culture: Gluconacetobacter hansenii P2A. *Applied microbiology and biotechnology*, *98*(3), pp.1065-1075.

[223] Semjonovs, P., Ruklisha, M., Paegle, L., Saka, M., Treimane, R., Skute, M., Rozenberga, L., Vikele, L., Sabovics, M. and Cleenwerck, I., 2017. Cellulose synthesis by Komagataeibacter rhaeticus strain P 1463 isolated from Kombucha. *Applied microbiology and biotechnology*, *101*(3), pp.1003-1012.

[224] Lu, Z., Zhang, Y., Chi, Y., Xu, N., Yao, W. and Sun, B., 2011. Effects of alcohols on bacterial cellulose production by Acetobacter xylinum 186. *World Journal of Microbiology and Biotechnology*, *27*(10), pp.2281-2285.

[225] Keshk, S.M., 2014. Vitamin C enhances bacterial cellulose production in Gluconacetobacter xylinus. *Carbohydrate polymers*, *99*, pp.98-100.

[226] Lin, S.P., Calvar, I.L., Catchmark, J.M., Liu, J.R., Demirci, A. and Cheng, K.C., 2013. Biosynthesis, production and applications of bacterial cellulose. *Cellulose*, *20*(5), pp.2191-2219.

[227] Pogorelova, N., Rogachev, E., Digel, I., Chernigova, S. and Nardin, D., 2020. Bacterial cellulose nanocomposites: morphology and mechanical properties. *Materials*, *13*(12), p.2849.

[228] Vicente, A.T., Araújo, A., Gaspar, D., Santos, L., Marques, A.C., Mendes, M.J.,

Pereira, L., Fortunato, E. and Martins, R., 2017. Optoelectronics and bio devices on paper powered by solar cells. In *Nanostructured solar cells*. IntechOpen.

[229] Indrianingsih, A.W., Rosyida, V.T., Jatmiko, T.H., Prasetyo, D.J., Poeloengasih, C.D., Apriyana, W., Nisa, K., Nurhayati, S., Darsih, C., Pratiwi, D. and Suwanto, A., 2017, December. Preliminary study on biosynthesis and characterization of bacteria cellulose films from coconut water. In *IOP Conference Series: Earth and Environmental Science* (Vol. 101, No. 1, p. 012010). IOP Publishing.

[230] Krystynowicz, A., Czaja, W., Wiktorowska-Jezierska, A., Gonçalves-Miśkiewicz, M., Turkiewicz, M. and Bielecki, S., 2002. Factors affecting the yield and properties of bacterial cellulose. *Journal of Industrial Microbiology and Biotechnology*, *29*(4), pp.189-195.

[231] Barud, H.S., Barrios, C., Regiani, T., Marques, R.F., Verelst, M., Dexpert-Ghys, J., Messaddeq, Y. and Ribeiro, S.J., 2008. Self-supported silver nanoparticles containing bacterial cellulose membranes. *Materials Science and Engineering: C*, *28*(4), pp.515-518.

[232] Czaja, W., Romanovicz, D. and Malcolm Brown, R., 2004. Structural investigations of microbial cellulose produced in stationary and agitated culture. *Cellulose*, *11*(3), pp.403-411.

[233] Tercjak, A., Gutierrez, J., Barud, H.S., Domeneguetti, R.R. and Ribeiro, S.J., 2015. Nano-and macroscale structural and mechanical properties of in situ synthesized bacterial cellulose/PEO-b-PPO-b-PEO biocomposites. *ACS applied materials & interfaces*, *7*(7), pp.4142-4150.

[234] Wang, S.S., Han, Y.H., Ye, Y.X., Shi, X.X., Xiang, P., Chen, D.L. and Li, M., 2017. Physicochemical characterization of high-quality bacterial cellulose produced by Komagataeibacter sp. strain W1 and identification of the associated genes in bacterial cellulose production. *RSC advances*, *7*(71), pp.45145-45155.

[235] Wada, M., Sugiyama, J. and Okano, T., 1993. Native celluloses on the basis of two crystalline phase (Iα/Iβ) system. *Journal of Applied Polymer Science*, *49*(8), pp.1491-1496.

[236] Watanabe, K., Tabuchi, M., Morinaga, Y. and Yoshinaga, F., 1998. Structural features and properties of bacterial cellulose produced in agitated culture. *Cellulose*, *5*(3), pp.187-200.

[237] Zeng, X., Liu, J., Chen, J., Wang, Q., Li, Z. and Wang, H., 2011. Screening of the common culture conditions affecting crystallinity of bacterial cellulose. *Journal of Industrial Microbiology and Biotechnology*, *38*(12), pp.1993-1999.

[238] Shibazaki, H., Saito, M., Kuga, S. and Okano, T., 1998. Native cellulose II production by Acetobacter xylinum under physical constraints. *Cellulose*, *5*(3), pp.165-173.

[239] Yassine, F., Bassil, N., Chokr, A., El Samrani, A., Serghei, A., Boiteux, G. and El Tahchi, M., 2016. Two-step formation mechanism of Acetobacter cellulosic biofilm: synthesis of sparse and compact cellulose. *Cellulose*, *23*(2), pp.1087-1100.

[240] Yang, Z., Peng, H., Wang, W. and Liu, T., 2010. Crystallization behavior of poly (ε-caprolactone)/layered double hydroxide nanocomposites. *Journal of*

applied polymer science, *116*(5), pp.2658-2667.

[241] Carrillo, F., Colom, X., Sunol, J.J. and Saurina, J., 2004. Structural FTIR analysis and thermal characterisation of lyocell and viscose-type fibres. *European Polymer Journal*, *40*(9), pp.2229-2234.

[242] Rani, M.U., Rastogi, N.K. and Anu Appaiah, K.A., 2011. Statistical optimization of medium composition for bacterial cellulose production by Gluconacetobacter hansenii UAC09 using coffee cherry husk extract-an agro-industry waste. *Journal of microbiology and biotechnology*, *21*(7), pp.739-745.

[243] Ashori, A., Sheykhnazari, S., Tabarsa, T., Shakeri, A. and Golalipour, M., 2012. Bacterial cellulose/silica nanocomposites: Preparation and characterization. *Carbohydrate Polymers*, *90*(1), pp.413-418.

[244] Amin, M.C.I.M., Ahmad, N., Halib, N. and Ahmad, I., 2012. Synthesis and characterization of thermo-and pH-responsive bacterial cellulose/acrylic acid hydrogels for drug delivery. *Carbohydrate Polymers*, *88*(2), pp.465-473.

[245] Pa'e, N., Salehudin, M.H., Hassan, N.D., Marsin, A.M. and Muhamad, I.I., 2018. Thermal behavior of bacterial cellulose-based hydrogels with other composites and related instrumental analysis. *Cellulose-Based Superabsorbent Hydrogels. Polymers and Polymeric Composites: A Reference Series; Mondal, MIH, Ed*, pp.763-787.

[246] George, J., Ramana, K.V., Sabapathy, S.N., Jagannath, J.H. and Bawa, A.S., 2005. Characterization of chemically treated bacterial (Acetobacter xylinum) biopolymer: Some thermo-mechanical properties. *International journal of biological macromolecules*, *37*(4), pp.189-194.

[247] Surma-Ślusarska, B., Presler, S. and Danielewicz, D., 2008. Characteristics of bacterial cellulose obtained from Acetobacter xylinum culture for application in papermaking. *Fibres & Textiles in Eastern Europe*, *16*(4), pp.108-111.

[248]   Torres, F.G., Commeaux, S. and Troncoso, O.P., 2012. Biocompatibility of bacterial cellulose based biomaterials. *Journal of Functional Biomaterials*, *3*(4), pp.864-878.

[249]   Marquez, J.P., Elson, E.L. and Genin, G.M., 2010. Whole cell mechanics of contractile fibroblasts: relations between effective cellular and extracellular matrix moduli. *Philosophical Transactions of the Royal Society A: Mathematical, Physical and Engineering Sciences*, *368*(1912), pp.635-654.

[250]   Freyman, T.M., Yannas, I.V., Yokoo, R. and Gibson, L.J., 2002. Fibroblast contractile force is independent of the stiffness which resists the contraction. *Experimental cell research*, *272*(2), pp.153-162.

[251] Yang, M. and Choy, K.L., 2021. A nature-derived, flexible and three dimensional (3D) nano-composite for chronic wounds pH monitoring. *Materials Letters*, *288*, p.129335.

[252] Yu, Z.L., Xin, S., You, Y., Yu, L., Lin, Y., Xu, D.W., Qiao, C., Huang, Z.H., Yang, N., Yu, S.H. and Goodenough, J.B., 2016. Ion-catalyzed synthesis of microporous hard carbon embedded with expanded nanographite for enhanced lithium/sodium storage. *Journal of the American Chemical Society*, *138*(45), pp.14915-14922.

[253] Yu, Z.L., Qin, B., Ma, Z.Y., Huang, J., Li, S.C., Zhao, H.Y., Li, H., Zhu, Y.B., Wu, H.A. and Yu, S.H., 2019. Superelastic hard carbon nanofiber aerogels. *Advanced Materials*, *31*(23), p.1900651.

[254] Fitzer, E., Kochling, K.H., Boehm, H.P. and Marsh, H., 1995. Recommended terminology for the description of carbon as a solid (IUPAC Recommendations 1995). *Pure and Applied Chemistry*, *67*(3), pp.473-506.

[255] Punjiya, M., Mostafalu, P. and Sonkusale, S., 2014, October. Low-cost paper-based electrochemical sensors with CMOS readout IC. In *2014 IEEE Biomedical Circuits and Systems Conference (BioCAS) Proceedings* (pp. 324-327). IEEE.

[256] Mostafalu, P., Tamayol, A., Rahimi, R., Ochoa, M., Khalilpour, A., Kiaee, G., Yazdi, I.K., Bagherifard, S., Dokmeci, M.R., Ziaie, B. and Sonkusale, S.R., 2018. Smart bandage for monitoring and treatment of chronic wounds. *Small*, *14*(33), p.1703509.

[257] Punjiya, M., Rezaei, H., Zeeshan, M.A. and Sonkusale, S., 2017, June. A flexible pH sensing smart bandage with wireless CMOS readout for chronic wound monitoring. In *2017 19th International Conference on Solid-State Sensors, Actuators and Microsystems (TRANSDUCERS)* (pp. 1700-1702). IEEE.

[258] Gill, E., Arshak, A., Arshak, K. and Korostynska, O., 2007. pH sensitivity of novel PANI/PVB/PS3 composite films. *Sensors*, *7*(12), pp.3329-3346.

[259] Huang, W.S., Humphrey, B.D. and MacDiarmid, A.G., 1986. Polyaniline, a novel conducting polymer. Morphology and chemistry of its oxidation and reduction in aqueous electrolytes. *Journal of the Chemical Society, Faraday Transactions 1: Physical Chemistry in Condensed Phases*, *82*(8), pp.2385-2400.

[260] Gill, E., Arshak, A., Arshak, K. and Korostynska, O., 2007. pH sensitivity of novel PANI/PVB/PS3 composite films. *Sensors, 7*(12), pp.3329-3346.

[261] Luthra, V., Singh, R., Gupta, S.K. and Mansingh, A., 2003. Mechanism of dc conduction in polyaniline doped with sulfuric acid. *Current Applied Physics, 3*(2-3), pp.219-222.

[262] Stejskal, J. and Gilbert, R.G., 2002. Polyaniline. Preparation of a conducting polymer (IUPAC technical report). *Pure and applied chemistry, 74*(5), pp.857-867.

[263] Deshmukh, K., Ahamed, M.B., Deshmukh, R.R., Pasha, S.K., Bhagat, P.R. and Chidambaram, K., 2017. Biopolymer composites with high dielectric performance: interface engineering. In *Biopolymer composites in electronics* (pp. 27-128). Elsevier.

[264] Liang, H.W., Guan, Q.F., Song, L.T., Yao, H.B., Lei, X. and Yu, S.H., 2012. Highly conductive and stretchable conductors fabricated from bacterial cellulose. *NPG Asia Materials, 4*(6), pp.e19-e19.

[265] Lai, F., Miao, Y.E., Zuo, L., Zhang, Y. and Liu, T., 2016. Carbon aerogels derived from bacterial cellulose/polyimide composites as versatile adsorbents and supercapacitor electrodes. *ChemNanoMat, 2*(3), pp.212-219.[266] Wang, X., Kong, D., Zhang, Y., Wang, B., Li, X., Qiu, T., Song, Q., Ning, J., Song, Y. and Zhi, L., 2016. All-biomaterial supercapacitor derived from bacterial cellulose. *Nanoscale, 8*(17), pp.9146-9150.

[267] Wang, B., Li, X., Luo, B., Yang, J., Wang, X., Song, Q., Chen, S. and Zhi, L., 2013. Pyrolyzed bacterial cellulose: a versatile support for lithium ion battery anode materials. *Small, 9*(14), pp.2399-2404.

268] Yang, H., Li, Y., Long, P., Han, J., Cao, C., Yao, F. and Feng, W., 2018. Amorphous red phosphorus incorporated with pyrolyzed bacterial cellulose as a free-standing anode for high-performance lithium ion batteries. *RSC advances*, 8(31), pp.17325-17333.

[269] Ibrahim, M. and Koglin, E., 2005. Spectroscopic study of polyaniline emeraldine base: modelling approach. *Acta Chim Slov*, *52*(2), pp.159-63.

[270] Srinivasan, P. and Gottam, R., 2018. Infrared spectra: useful technique to identify the conductivity level of emeraldine form of polyaniline and indication of conductivity measurement either two or four probe technique. *Material Science Research India*, *15*(3), pp.209-217.

[271] Noby, H., El-Shazly, A.H., Elkady, M.F. and Ohshima, M., 2018. Novel preparation of self-assembled HCl-doped polyaniline nanotubes using compressed CO2-assisted polymerization. *Polymer*, *156*, pp.71-75.

[272] Mata, A., Fleischman, A.J. and Roy, S., 2005. Characterization of polydimethylsiloxane (PDMS) properties for biomedical micro/nanosystems. *Biomedical microdevices*, *7*(4), pp.281-293.[273] Silva, F.A., Chagas-Silva, F.A., Florenzano, F.H. and Pissetti, F.L., 2016. Poly (dimethylsiloxane) and poly [vinyltrimethoxysilane-co-2-(dimethylamino) ethyl methacrylate] based cross-linked organic-inorganic hybrid adsorbent for copper (II) removal from aqueous solutions. *Journal of the Brazilian Chemical Society*, *27*(12), pp.2181-2191.

[274] Pissetti, F.L., Yoshida, I.V., Gushikem, Y. and Kholin, Y.V., 2008. Metal ions adsorption from ethanol solutions on ethylenediamine-modified poly (dimethylsiloxane) elastomeric network. *Colloids and Surfaces A:*

Physicochemical and Engineering Aspects, *328*(1-3), pp.21-27.

[275] Salvo, P., Calisi, N., Melai, B., Dini, V., Paoletti, C., Lomonaco, T., Pucci, A., Di Francesco, F., Piaggesi, A. and Romanelli, M., 2017. Temperature-and pH-sensitive wearable materials for monitoring foot ulcers. *International journal of nanomedicine*, *12*, p.949.

[276] Trengove, N.J., Langton, S.R. and Stacey, M.C., 1996. Biochemical analysis of wound fluid from nonhealing and healing chronic leg ulcers. *Wound Repair and Regeneration*, *4*(2), pp.234-239.

[277] Yang, M., Ward, J. and Choy, K.L., 2020. Nature-Inspired Bacterial Cellulose/Methylglyoxal (BC/MGO) Nanocomposite for Broad-Spectrum Antimicrobial Wound Dressing. *Macromolecular bioscience*, *20*(8), p.2000070.

[278] Guarderas, F., Leavell, Y., Sengupta, T., Zhukova, M. and Megraw, T.L., 2016. Assessment of chicken-egg membrane as a dressing for wound healing. *Advances in skin & wound care*, *29*(3), pp.131-134.

[279] Baláž, M., 2014. Eggshell membrane biomaterial as a platform for applications in materials science. *Acta biomaterialia*, *10*(9), pp.3827-3843.

[2807] Chen, L., Kang, J. and Sukigara, S., 2014. Preparation and characterization of polyurethane/soluble eggshell membrane nanofibers. *Bio-medical materials and engineering*, *24*(6), pp.1979-1989.

[2817] Messersmith, P.B., 2008. Multitasking in tissues and materials. *Science*, *319*(5871), pp.1767-1768.

[2828] Lee, H., Dellatore, S.M., Miller, W.M. and Messersmith, P.B., 2007. Mussel-inspired surface chemistry for multifunctional coatings. *science*, *318*(5849),

pp.426-430.

[283] Liu, M., Zeng, G., Wang, K., Wan, Q., Tao, L., Zhang, X. and Wei, Y., 2016. Recent developments in polydopamine: an emerging soft matter for surface modification and biomedical applications. *Nanoscale*, *8*(38), pp.16819-16840.

[284] Gethin, G. and Cowman, S., 2005. Case series of use of Manuka honey in leg ulceration. *International Wound Journal*, *2*(1), pp.10-15.

[285] Johnson, D.W., van Eps, C., Mudge, D.W., Wiggins, K.J., Armstrong, K., Hawley, C.M., Campbell, S.B., Isbel, N.M., Nimmo, G.R. and Gibbs, H., 2005. Randomized, controlled trial of topical exit-site application of honey (Medihoney) versus mupirocin for the prevention of catheter-associated infections in hemodialysis patients. *Journal of the American Society of Nephrology*, *16*(5), pp.1456-1462.

[286] Rafter, L., Reynolds, T.I.M., Collier, M., Rafter, M. and WEST, M., 2017. A clinical evaluation of Algivon® Plus manuka honey dressings for chronic wounds. *Wounds UK*, *13*(4).

[287] Jenkins, R., Burton, N. and Cooper, R., 2011. Effect of manuka honey on the expression of universal stress protein A in meticillin-resistant Staphylococcus aureus. *International journal of antimicrobial agents*, *37*(4), pp.373-376.

[288] Leong, A.G., Herst, P.M. and Harper, J.L., 2012. Indigenous New Zealand honeys exhibit multiple anti-inflammatory activities. *Innate immunity*, *18*(3), pp.459-466.

[289] Adams, C.J., Manley-Harris, M. and Molan, P.C., 2009. The origin of methylglyoxal in New Zealand manuka (Leptospermum scoparium)

honey. *Carbohydrate research*, *344*(8), pp.1050-1053.

[290] Bulman, S.E., Tronci, G., Goswami, P., Carr, C. and Russell, S.J., 2017. Antibacterial properties of nonwoven wound dressings coated with Manuka honey or methylglyoxal. *Materials*, *10*(8), p.954.

[291] Mavric, E., Wittmann, S., Barth, G. and Henle, T., 2008. Identification and quantification of methylglyoxal as the dominant antibacterial constituent of Manuka (Leptospermum scoparium) honeys from New Zealand. *Molecular nutrition & food research*, *52*(4), pp.483-489.

[292] Fidaleo, M., Zuorro, A. and Lavecchia, R., 2010. Methylglyoxal: a new weapon against staphylococcal wound infections?. *Chemistry letters*, *39*(4), pp.322-323.

[293] Ghosh, S., Chakraborty, P., Saha, P., Acharya, S. and Ray, M., 2014. Polymer based nanoformulation of methylglyoxal as an antimicrobial agent: efficacy against resistant bacteria. *RSC Advances*, *4*(44), pp.23251-23261.

[294] Rabie, E., Serem, J.C., Oberholzer, H.M., Gaspar, A.R.M. and Bester, M.J., 2016. How methylglyoxal kills bacteria: An ultrastructural study. *Ultrastructural pathology*, *40*(2), pp.107-111.

[295] Fürsatz, M., Skog, M., Sivlér, P., Palm, E., Aronsson, C., Skallberg, A., Greczynski, G., Khalaf, H., Bengtsson, T. and Aili, D., 2018. Functionalization of bacterial cellulose wound dressings with the antimicrobial peptide ε-poly-L-Lysine. *Biomedical Materials*, *13*(2), p.025014.

[296] Araújo, I.M., Silva, R.R., Pacheco, G., Lustri, W.R., Tercjak, A., Gutierrez, J., Júnior, J.R., Azevedo, F.H., Figuêredo, G.S., Vega, M.L. and Ribeiro, S.J.,

2018. Hydrothermal synthesis of bacterial cellulose–copper oxide nanocomposites and evaluation of their antimicrobial activity. *Carbohydrate polymers*, *179*, pp.341-349.

[297] Adepu, S. and Khandelwal, M., 2018. Broad-spectrum antimicrobial activity of bacterial cellulose silver nanocomposites with sustained release. *Journal of Materials Science*, *53*(3), pp.1596-1609.

[298] Wu, J., Zheng, Y., Wen, X., Lin, Q., Chen, X. and Wu, Z., 2014. Silver nanoparticle/bacterial cellulose gel membranes for antibacterial wound dressing: investigation in vitro and in vivo. *Biomedical materials, 9*(3), p.035005.

[299] Hughey, V.L. and Johnson, E.A., 1987. Antimicrobial activity of lysozyme against bacteria involved in food spoilage and food-borne disease. *Applied and Environmental Microbiology*, *53*(9), pp.2165-2170.

[300] Centeno, S.A. and Shamir, J., 2008. Surface enhanced Raman scattering (SERS) and FTIR characterization of the sepia melanin pigment used in works of art. *Journal of Molecular Structure*, *873*(1-3), pp.149-159.

[301] Zangmeister, R.A., Morris, T.A. and Tarlov, M.J., 2013. Characterization of polydopamine thin films deposited at short times by autoxidation of dopamine. *Langmuir*, *29*(27), pp.8619-8628.

[302] Filippidi, E., Cristiani, T.R., Eisenbach, C.D., Waite, J.H., Israelachvili, J.N., Ahn, B.K. and Valentine, M.T., 2017. Toughening elastomers using mussel-inspired iron-catechol complexes. *Science, 358*(6362), pp.502-505.

[303] Ahlborn, G. and Sheldon, B.W., 2006. Identifying the components in eggshell

membrane responsible for reducing the heat resistance of bacterial pathogens. *Journal of food protection*, *69*(4), pp.729-738.

[304] Auta, R., Adamus, G., Kwiecien, M., Radecka, I. and Hooley, P., 2017. Production and characterization of bacterial cellulose before and after enzymatic hydrolysis. *African Journal of Biotechnology*, *16*(10), pp.470-482.

[305] Choi, Y.J., Ahn, Y., Kang, M.S., Jun, H.K., Kim, I.S. and Moon, S.H., 2004. Preparation and characterization of acrylic acid-treated bacterial cellulose cation-exchange membrane. *Journal of Chemical Technology & Biotechnology: International Research in Process, Environmental & Clean Technology*, *79*(1), pp.79-84.

[306] Islam, S., Mir, A.R., Arfat, M.Y., Alam, K. and Ali, A., 2017. Studies on glycoxidatively modified human IgG: Implications in immuno-pathology of type 2 diabetes mellitus. *International journal of biological macromolecules*, *104*, pp.19-29.

[307] Lee, K.Y. and Bismarck, A., 2012. Susceptibility of never-dried and freeze-dried bacterial cellulose towards esterification with organic acid. *Cellulose*, *19*(3), pp.891-900.

[308] Mautner, A., Lee, K.Y., Tammelin, T., Mathew, A.P., Nedoma, A.J., Li, K. and Bismarck, A., 2015. Cellulose nanopapers as tight aqueous ultra-filtration membranes. *Reactive and Functional Polymers*, *86*, pp.209-214.

[309] Roman, M. and Winter, W.T., 2004. Effect of sulfate groups from sulfuric acid hydrolysis on the thermal degradation behavior of bacterial cellulose. *Biomacromolecules*, *5*(5), pp.1671-1677.

[310] George, J., Ramana, K.V. and Bawa, A.S., 2011. Bacterial cellulose nanocrystals exhibiting high thermal stability and their polymer nanocomposites. *International Journal of Biological Macromolecules*, *48*(1), pp.50-57.

[311] Gea, S., Reynolds, C.T., Roohpour, N., Wirjosentono, B., Soykeabkaew, N., Bilotti, E. and Peijs, T., 2011. Investigation into the structural, morphological, mechanical and thermal behaviour of bacterial cellulose after a two-step purification process. *Bioresource technology*, *102*(19), pp.9105-9110.

[312] Jia, Y., Wang, X., Huo, M., Zhai, X., Li, F. and Zhong, C., 2017. Preparation and characterization of a novel bacterial cellulose/chitosan bio-hydrogel. *Nanomaterials and Nanotechnology*, *7*, p.1847980417707172.

[313] Yan, Z., Chen, S., Wang, H., Wang, B. and Jiang, J., 2008. Biosynthesis of bacterial cellulose/multi-walled carbon nanotubes in agitated culture. *Carbohydrate Polymers*, *74*(3), pp.659-665.

[314] Xiong, J., Ni, K., Liao, X., Zhu, J., An, Z., Yang, Q., Huang, Y. and Li, G., 2016. Investigation of chemi-crystallization and free volume changes of high-density polyethylene weathered in a subtropical humid zone. *Polymer International*, *65*(12), pp.1474-1481.

[315] Cai, N., Li, C., Han, C., Luo, X., Shen, L., Xue, Y. and Yu, F., 2016. Tailoring mechanical and antibacterial properties of chitosan/gelatin nanofiber membranes with Fe3O4 nanoparticles for potential wound dressing application. *Applied Surface Science*, *369*, pp.492-500.

[316] Archana, D., Singh, B.K., Dutta, J. and Dutta, P.K., 2013. In vivo evaluation of chitosan–PVP–titanium dioxide nanocomposite as wound dressing

material. *Carbohydrate polymers*, *95*(1), pp.530-539.

[317] Mohandas, A., Sudheesh Kumar, P.T., Raja, B., Lakshmanan, V.K. and Jayakumar, R., 2015. Exploration of alginate hydrogel/nano zinc oxide composite bandages for infected wounds. *International journal of nanomedicine*, *10*(Suppl 1), p.53.

[318] Anisha, B.S., Biswas, R., Chennazhi, K.P. and Jayakumar, R., 2013. Chitosan–hyaluronic acid/nano silver composite sponges for drug resistant bacteria infected diabetic wounds. *International journal of biological macromolecules*, *62*, pp.310-320.

[319] Boonkaew, B., Barber, P.M., Rengpipat, S., Supaphol, P., Kempf, M., He, J., John, V.T. and Cuttle, L., 2014. Development and characterization of a novel, antimicrobial, sterile hydrogel dressing for burn wounds: single-step production with gamma irradiation creates silver nanoparticles and radical polymerization. *Journal of pharmaceutical sciences*, *103*(10), pp.3244-3253.

[320] Hadisi, Z., Nourmohammadi, J. and Nassiri, S.M., 2018. The antibacterial and anti-inflammatory investigation of Lawsonia Inermis-gelatin-starch nano-fibrous dressing in burn wound. *International journal of biological macromolecules*, *107*, pp.2008-2019.

[321] Güneş, S. and Tıhmınlıoğlu, F., 2017. Hypericum perforatum incorporated chitosan films as potential bioactive wound dressing material. *International journal of biological macromolecules*, *102*, pp.933-943.

[322] Venkatasubbu, G.D. and Anusuya, T., 2017. Investigation on Curcumin nanocomposite for wound dressing. *International journal of biological macromolecules*, *98*, pp.366-378.

[323] Karami, Z., Rezaeian, I., Zahedi, P. and Abdollahi, M., 2013. Preparation and performance evaluations of electrospun poly (ε-caprolactone), poly (lactic acid), and their hybrid (50/50) nanofibrous mats containing thymol as an herbal drug for effective wound healing. *Journal of applied polymer science*, *129*(2), pp.756-766.

[324] He, W., Huang, X., Zheng, Y., Sun, Y., Xie, Y., Wang, Y. and Yue, L., 2018. In situ synthesis of bacterial cellulose/copper nanoparticles composite membranes with long-term antibacterial property. *Journal of Biomaterials Science, Polymer Edition*, *29*(17), pp.2137-2153.

[325] Khalid, A., Khan, R., Ul-Islam, M., Khan, T. and Wahid, F., 2017. Bacterial cellulose-zinc oxide nanocomposites as a novel dressing system for burn wounds. *Carbohydrate polymers*, *164*, pp.214-221.